# MODELING, ANALYSIS, AND EXPERIMENTAL INVESTIGATIONS OF GRINDING PROCESSES

by

ZHICHAO LI

B. Eng., Tianjin University of Technology & Education, 1999
M.S., Tianjin University, 2002

AN ABSTRACT OF A DISSERTATION

submitted in partial fulfillment of the requirements for the degree

DOCTOR OF PHILOSOPHY

Department of Industrial and Manufacturing Systems Engineering
College of Engineering

KANSAS STATE UNIVERSITY
Manhattan, Kansas

2006

# Abstract

Grinding is one of the important operations employed in modern manufacturing industry to remove materials and achieve desired geometry and surface finish. Simultaneous double side grinding (SDSG) and ultrasonic vibration assisted grinding (UVAG) are two typical cost-effective grinding processes which are utilized to grind semiconductor materials and high performance ceramic materials, respectively.

The objectives of this research are to investigate several technical issues in modern grinding processes by using theoretical, numerical, and experimental research approaches. Those technical issues are related to SDSG and UVAG, which have been chosen as two typical grinding processes for this research.

This thesis reviews the literature on SDSG (covering process applications, modeling of grinding marks, and modeling of wafer shapes) and UVAG (covering process applications, edge chipping, and coolant effects, etc). The theoretical research work of this thesis is conducted by developing mathematical models for grinding marks and wafers shapes in SDSG of silicon wafers. These developed models are then used to study the effects of SDSG parameters on the curvature of the grinding marks, the distance between adjacent grinding marks, and the wafer shapes.

The numerical research work of this thesis is done by conducting a three dimensional (3-D) finite element analysis (FEA) of UVAG process. A 3-D FEA model is developed to study the edge chipping commonly observed in UVAG of ceramics. Edge chippings not only compromises geometric accuracy but also possibly causes an increase in machining cost. A solution to reduce the edge chipping is proposed based upon the FEA simulations and validated by pilot experiments.

Several experimental studies are conducted to provide new knowledge for the UVAG process. Firstly, a novel coolant delivery system is explored for UVAG machine system. Secondly, UVAG is introduced into machining of fiber-reinforced ceramic matrix composites (CMC). Results of a feasibility study and a designed experimental investigation show that UVAG is a promising process for CMC machining. Finally, an experimental study on cutting

forces during UVAG of zirconia/alumina composites is conducted. The feasibility to machine different zirconia/alumina composites using UVAG is also investigated and discussed.

The findings in this thesis will provide theoretical and practical guidance for modern grinding processes especially for SDSG and UVAG.

# MODELING, ANALYSIS, AND EXPERIMENTAL INVESTIGATIONS OF GRINDING PROCESSES

by

ZHICHAO LI

B. Eng., Tianjin University of Technology & Education, 1999
M.S., Tianjin University, 2002

A DISSERTATION

submitted in partial fulfillment of the requirements for the degree

DOCTOR OF PHILOSOPHY

Department of Industrial and Manufacturing Systems Engineering
College of Engineering

KANSAS STATE UNIVERSITY
Manhattan, Kansas

2006

Approved by:

Major Professor
Dr. Zhijian Pei

# Abstract

Grinding is one of the important operations employed in modern manufacturing industry to remove materials and achieve desired geometry and surface finish. Simultaneous double side grinding (SDSG) and ultrasonic vibration assisted grinding (UVAG) are two typical cost-effective grinding processes which are utilized to grind semiconductor materials and high performance ceramic materials, respectively.

The objectives of this research are to investigate several technical issues in modern grinding processes by using theoretical, numerical, and experimental research approaches. Those technical issues are related to SDSG and UVAG, which have been chosen as two typical grinding processes for this research.

This thesis reviews the literature on SDSG (covering process applications, modeling of grinding marks, and modeling of wafer shapes) and UVAG (covering process applications, edge chipping, and coolant effects, etc). The theoretical research work of this thesis is conducted by developing mathematical models for grinding marks and wafers shapes in SDSG of silicon wafers. These developed models are then used to study the effects of SDSG parameters on the curvature of the grinding marks, the distance between adjacent grinding marks, and the wafer shapes.

The numerical research work of this thesis is done by conducting a three dimensional (3-D) finite element analysis (FEA) of UVAG process. A 3-D FEA model is developed to study the edge chipping commonly observed in UVAG of ceramics. Edge chippings not only compromises geometric accuracy but also possibly causes an increase in machining cost. A solution to reduce the edge chipping is proposed based upon the FEA simulations and validated by pilot experiments.

Several experimental studies are conducted to provide new knowledge for the UVAG process. Firstly, a novel coolant delivery system is explored for UVAG machine system. Secondly, UVAG is introduced into machining of fiber-reinforced ceramic matrix composites (CMC). Results of a feasibility study and a designed experimental investigation show that UVAG is a promising process for CMC machining. Finally, an experimental study on cutting

forces during UVAG of zirconia/alumina composites is conducted. The feasibility to machine different zirconia/alumina composites using UVAG is also investigated and discussed.

The findings in this thesis will provide theoretical and practical guidance for modern grinding processes especially for SDSG and UVAG.

# Table of Contents

# List of Figures

# List of Tables

# Acknowledgements

I would like to express my gratitude to all those who gave me the possibility to complete this thesis. I am deeply indebted to my supervisor, Professor Zhijian Pei, from the Industrial & Manufacturing Systems Engineering Department. His help, stimulating suggestions, and encouragement helped me in all the time of my research during the past three years.

My sincere thanks also go to Professor Talat S. Rahman from the Physics Department for being the chairperson of the examining committee. Meanwhile, I would like to thank other members of my supervisory committee: Professor E. Stanley Lee from the Industrial & Manufacturing Systems Engineering Department, and Professor Liang-wu Cai from the Mechanical and Nuclear Engineering Department. Their suggestions and advices are tremendously helpful to me. I would like to express my thanks to Dr. Graham R. Fisher, from MEMC Electronic Materials, Inc., not only for being one of my supervisory committee members but also for his generous help and support to my research work.

I also would like to thank our department head, Professor Bradley A. Kramer for all his help and support to my research work and all the other department staff for their assistance and the research facilities provided.

In addition, I would like to thank all my friends: Dr. Wangping Sun and Ms. Lian Li, Mr. Budong Yang and Ms. Lin Xu for their warmhearted help to my research work and life in Kansas; Ms. Jian (Jessie) Wu, Ms. Xiaohong (Tina) Zhang, Ms. Weike (Vicky) Lu, and Ms. Jinghua (Amy) Liu for their assistance to the SDSG part of my research.

I also appreciate the generous help to the UVAG part of my research from Dr. Yue (June) Jiao, Dr. Jianmei (Jenny) Zhang, Mr. Timothy Deines, Mr. Weimin (Cavin) Zeng, Mr. Nikhil Churi, Mr. Ping Hu, and Mr. Yu (Richard) Chen.

Finally, I will never forget my beloved parents as well as my younger sister for their incredible encouragements and supports to me.

# CHAPTER 1 - Introduction

## 1.1 Background

Machining plays a central role in modern manufacturing. It was reported that machining cost amounts to more than 15% of the total value of products in the entire manufacturing industry (Merchant, 1998). As one of the most important manufacturing processes, grinding accounts for about 20-25% of the total expenditures on machining operations (Malkin, 1989).

Grinding means the machining processes which utilize hard abrasive particles as the cutting medium (Malkin, 1989). It is traditionally regarded as a final machining process in the production of components which require smooth surfaces and fine tolerance (Malkin, 1989; Shaw, 1996). As cutting tools for the grinding process, grinding wheels are generally composed of two materials – "tiny abrasive particles called grains or grits to do the cutting and a softer bonding agent to hold the countless abrasive grains together in a solid mass" (Malkin, 1989).

According to the wheel shape and kinematics of the workpiece and grinding wheel, there are different types of grinding operations like surface grinding and cylindrical grinding. Nowadays, grinding has been widely introduced into various surface finishing or stock removal processes of different materials including semiconductor materials, ceramics, and glasses, etc.

## 1.2 Motivations, Objectives, and Significance of This Research

Despite its industrial importance, grinding is the least understood in practice of all the machining processes in common use due to its process complexity (Malkin, 1989; Shaw, 1996). In the past 50 years, the grinding process has been the subject of extensive research (Malkin, 1989). However, as the grinding process finds more and more applications in industry, there is always a need to understand grinding mechanisms in various grinding processes of different materials.

In this research work, two modern grinding processes are chosen to conduct a comprehensive study with three approaches - theoretical modeling, finite element analysis, and experimental investigations. One process is simultaneous double side grinding (SDSG); the other is ultrasonic vibration assisted grinding (UVAG).

SDSG is used to flatten silicon wafers on which 90% integrated circuits (ICs) are built (Van Zant, 2000). About 150 million silicon wafers of different sizes are manufactured each year worldwide (Tricard et al., 1998). In 2005, the worldwide revenues generated by silicon wafers were $ 8.3 billion (Online staff, 2005).

UVAG is a promising grinding process for advanced ceramics and ceramic composites, which have been often utilized to replace conventional materials to improve performance of a component. A general perception in the industry is that machining costs are too high and are probably the major hindrance to the greater success of ceramics and ceramic composites (Freitag and Richerson, 1998; Online staff, 2000).

UVAG combines the material removal mechanisms of diamond grinding and ultrasonic machining (USM). It was invented in 1960s to overcome the disadvantages of USM like slow material removal rate (MRR), low accuracy, and high tool wear. Compared with USM, UVAG is about 10 times faster; it is easier to drill deep and small holes with UVAG than with USM, and the hole accuracy could be improved (Cleave, 1976). Other advantages of this process include superior surface finish, low tool pressure and low tool wear rate (Graff, 1975; Petrukha et al., 1970; Pei, 1995). UVAG has been proved as a promising process for cost-effective machining of ceramics.

SDSG and UVAG show great potentials to meet the demands for cost-effective machining of high quality silicon wafers, ceramics, and ceramic composites. However, there are some technical issues in SDSG of silicon wafers waiting to be addressed, such as the following:

1) How can the grinding marks be reduced or eliminated?
2) How can the good flatness (or good wafer shape) be achieved?

Also, there still exist some challenges for UVAG, such as the following:

1) How can the edge chipping be reduced or eliminated?
2) How can the ceramic composites be machined efficiently?

The research on the above issues will have great effects on SDSG and UVAG. For example, reduction or elimination of the grinding marks in SDSG will reduce the production time in subsequent polishing processes; with the help of a mathematic model capable of predicting the wafer shape, an easy and speedy adjustment for the grinding wheels will be feasible to achieve flatter wafers; reduction or elimination of the edge chipping in UVAG will reduce the cost and time in the following grinding process to eliminate the edge chipping on

ceramic components. These potential benefits will be very helpful to enhance the competitiveness of the wafer manufacturers as well as ceramic component manufacturers.

## 1.3 Research Approaches

Three research approaches (theoretical, numerical, and experimental) are employed to study two grinding processes (SDSG and UVAG). As for the theoretical research work, two mathematical models are developed to investigate grinding marks and wafer shapes in SDSG of silicon wafers. As for the numerical research work, a finite element analysis (FEA) with experimental validation is conducted to investigate the edge chipping in UVAG of ceramics. When it comes to the experimental research work, several experimental investigations are conducted to study the effects of coolant in UVAG and the applications of UVAG in machining of ceramic matrix composites (CMC).

## 1.4 Outline of This Dissertation

The thesis is divided into nine chapters. Following this chapter, Chapter 2 reviews the literature related to SDSG of silicon wafers and UVAG of ceramics.

The theoretical modeling part of the thesis is comprised of Chapter 3 and Chapter 4. Chapter 3 establishes a mathematical model to investigate the effects of SDSG parameters on the grinding marks. Chapter 4 develops a mathematical model to predict the wafer shape in SDSG, which is then used to systematically study the effects of SDSG parameters on the wafer shape.

The finite element analysis part of the thesis is presented in Chapter 5. A three-dimensional (3-D) FEA model for UVAG is developed to investigate the effects of three parameters (cutting depth, support length, and pretightening load) on the maximum stresses in the region where the edge chipping initiates. The model is then used to study the relationship between the edge chipping thickness and the support length. A possible solution to reduce the edge chipping thickness through increasing the support length is proposed and verified by experiments.

Chapters 6, 7, and 8 are the experimental investigation part. Chapter 6 introduces the air-operated double diaphragm pump (AODDP) into the UVAG coolant system**.** Chapter 7 discusses the feasibility of using UVAG to machine fiber-reinforced CMC materials. A designed

experimental study on UVAG of CMC is also conducted. Chapter 8 investigates the viability of UVAG for different zirconia/alumina composites.

Finally, the achievements and contributions of this research are summarized in Chapter 9.

# CHAPTER 2 - Literature Review

## 2.1 A Brief History of SDSG

SDSG was first used for double side grinding of small metal workpieces of simple shapes in 1930s to 1950s (Rodemeyer, 1930; Junker, 1936; Carlson et al., 1953). In 1960s to 1970s, it was used to flatten workpieces made of various types of materials and having different dimensions and shapes (Hannon, 1965; Rimmer et al., 1968; Zerbola, 1975; Cook, 1976). From 1980s to the middle of 1990s, additional capabilities of flexibility, precision, and fast changeovers were provided to SDSG (Ueda, 1982; Oppelt, 1984; Ahejew, 1984; Dunn, 1984; Ogawa, 1984; Nishio, 1988; Wang, 1990; Fetouh and Malarz, 1988; Dunn, 1980; Doubman and Cox, 1997; Eade, 1988; Paquin, 1995).

SDSG was introduced into semiconductor industry in 1990s (Tameyoshi, 1999; Toshio, 1998; Ikeda et al., 1999; Ikeda et al., 2000; Koichi and Yasuto, 1999; Hasegawa and Kobayashi, 1997). Applications to both 200 mm (Kerstan and Pietsch, 2000; Pietsch and Kerstan, 2001; Hashii and Watanabe, 2004; Toshio, 1998; Koichi and Yasuto, 1999) and 300 mm (Kerstan and Pietsch, 2000; Pietsch and Kerstan, 2001; Pietsch and Kerstan, 2005; Hashii and Watanabe, 2004; Toshio, 1998; Koichi and Yasuto, 1999) silicon wafers were reported. Use of grinding wheels whose diameters are equal or greater than the wafer diameter (Nobuto and Akihide, 1997; Ikeda et al., 2003; Okura, 2002; Shizuki et al., 2002; Saitoh and Masahiko, 2004) and use of grinding wheels whose diameters were less than the wafer diameter and greater than the wafer radius (Kerstan and Pietsch, 2000; Pietsch and Kerstan, 2001; Pietsch and Kerstan, 2005; Tameyoshi, 1999; Toshio, 1998; Ikeda et al., 1999; Ikeda et al., 2000; Koichi and Yasuto, 1999; Abe, 2000; Yutaka, 2003; Kato et al., 2004; Nishi et al., 2001; Akira et al., 2003; Aiko et al., 2004; Abe, 1997) were reported.

## 2.2 SDSG in Silicon Wafer Manufacturing

### *2.2.1 Silicon Wafer Manufacturing*

**Figure 2.1 A Typical Manufacturing Process Flow for Silicon Wafers (Quirk and Serda, 2001; Bawa et al., 1995; Fukami et al., 1997; Pei et al., 1999; Piestch and Kerstan, 2001; Wolf and Tauber, 2000)**

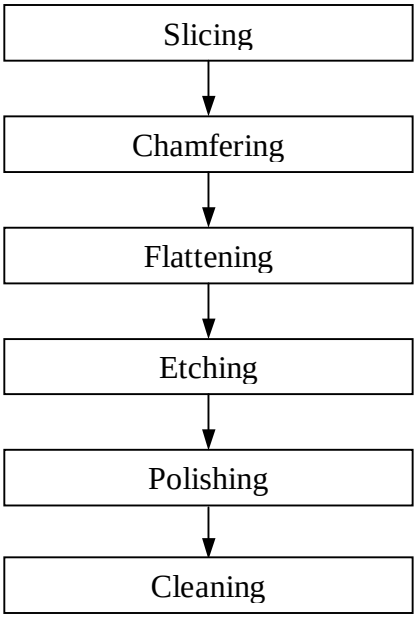


A sequence of processes is needed to turn a silicon ingot into silicon wafers. As shown in Figure 2.1, it typically consists of the following processes (Quirk and Serda, 2001; Bawa et al., 1995; Fukami et al., 1997; Pei and Billingsley, 1999; Piestch and Kerstan, 2001; Wolf and Tauber, 2000):

1) slicing, to slice a silicon ingot into wafers of thin disk shape using an internal diamond sawing method or wire sawing method;
2) edge profiling or chamfering, to chamfer the peripheral edge portion of the wafer to reduce the risk of wafer damage in further processing;
3) flattening (lapping or grinding), to achieve a high degree of flatness and parallelism of the wafer;
4) etching, to chemically remove the damage induced by slicing and flattening without introducing further mechanical damage;

5) polishing, to obtain a mirror surface on the wafer;
6) cleaning, to remove the polishing agent or dust particles from the wafer surface.

### *2.2.2 Pros and Cons of Three Flattening Processes*

**Figure 2.2 Illustration of Lapping Process**

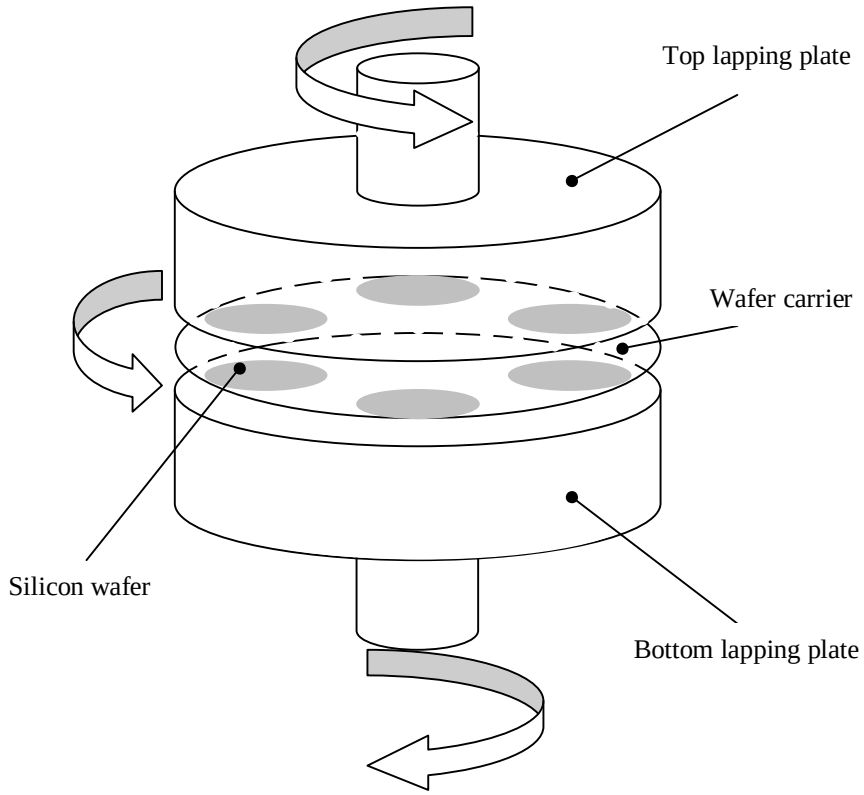


Three processes can be used to flatten the sliced wafers: lapping, single side grinding (SSG), and simultaneous double side grinding (SDSG). The lapping operation is illustrated in Figure 2.2. A batch of wafers (for example, 20 wafers) are manually loaded into a lapping machine. The loaded wafers are then lapped by the abrasive slurry, typically a mixture of alumina and glycerine (Wolf and Tauber, 2000) injected between two lapping plates rotating in opposite directions. Lapping can effectively remove or reduce the wire-sawing induced waviness (Liu et al., 2002). However, the lapping operation would generate subsurface damages in silicon wafers, which need to be removed by its subsequent processes. There are several disadvantages for lapping operation (Piestch and Kerstan, 2001; Liu et al., 2002; Pei et al., 2003; Vandamme et al., 2001):

1) Low material removal rate;
2) High cost of consumables (abrasive slurry);
3) It causes batch-to-batch wafer thickness variation;
4) Wafer loading and unloading is done manually, not only increasing labor costs, but also causing frequent wafer breakage; and
5) Less benign to the environment due to the use of abrasive slurry.

**Figure 2.3 Illustration of SSG Process**

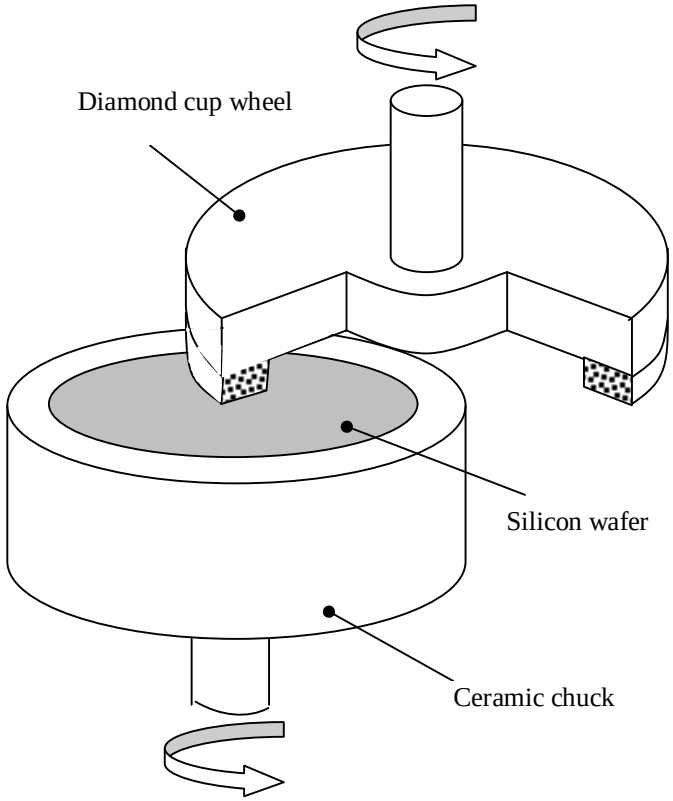


In SSG, as shown in Figure 2.3, a silicon wafer is held on a porous ceramic chuck by means of vacuum. The grinding wheel is a diamond cup wheel. The grinding wheel and the wafer rotate about their own rotation axes simultaneously, and the wheel is fed towards the wafer along its axis (Pei and Billingsley, 1999; Liu et al., 2002; Pei et al., 2003). After the wafer front side is ground, the grinder flips the wafer over and continues to grind the back side. The advantages of SSG over lapping include (Pietsch and Kerstan, 2001; Liu et al., 2002; Pei et al, 2003; Vandamme et al., 2001):

1) It uses fixed-abrasive grinding wheels instead of abrasive slurry so the cost of consumables per wafer is lower;
2) Fixed-abrasive grinding wheels are more benign to the environment than lapping slurry;
3) It has higher throughput (the number of wafers processed within the unit of time);
4) It is fully automatic; and

SSG has its own drawbacks. It cannot effectively remove the waviness induced by the wire sawing process (Liu et al., 2002; Pei et al, 2003; Kato et al., 1997; Yasunaga et al., 1997; Shinetsu, 1997; Kassir and Walsh, 1999; Xin et al., 2002). Furthermore, any imperfection in the chuck will copy its deficiencies to the ground wafers (Kerstan and Peitsch, 2000).

**Figure 2.4 Illustration of SDSG Process**

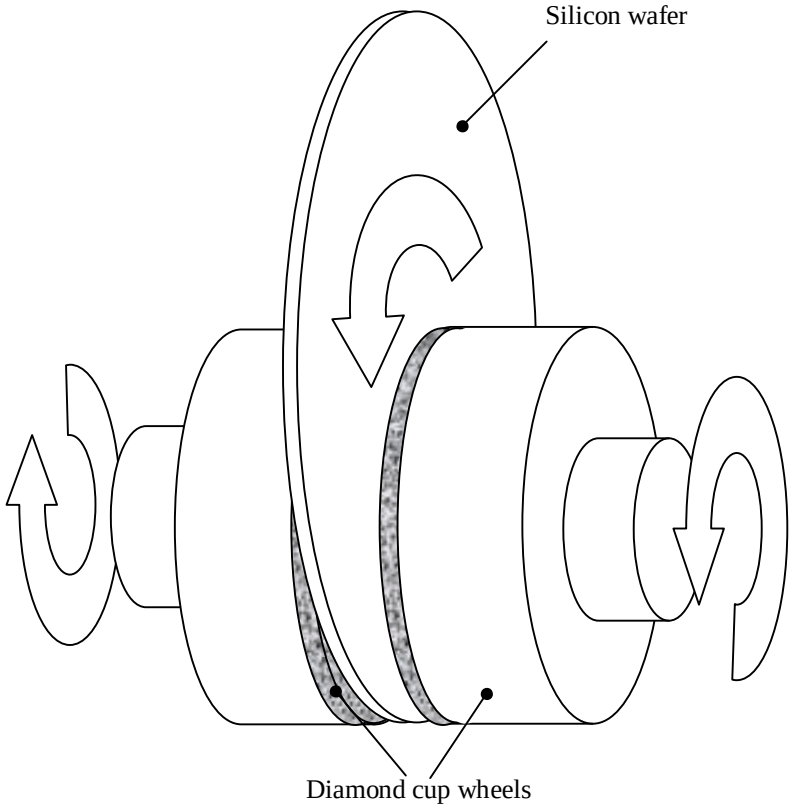


Figure 2.4 illustrates the SDSG process. A pair of diamond cup wheels are located on the opposite sides of a rotating silicon wafer. The two wheels rotate in opposite directions (Pietsch

and Kerstan, 2001; Pietsch and Kerstan, 2005). Both sides of the rotating silicon wafer are ground simultaneously by the two wheels, which are synchronously fed towards the wafer.

SDSG possesses the advantages of both lapping and SSG. Since SDSG share the same material removal mechanism (grinding) as SSG, it has the same advantages as those of SSG (like lower consumable cost, higher throughput, environmentally benign, and fully automatic). Furthermore, both sides of the wafer are ground by a pair of wheels simultaneously in SDSG, very similar to lapping where both sides of the wafer are machined simultaneously (Pietsch and Kerstan, 2001; Pietsch and Kerstan, 2005; Dudley, 1986; Marinescu et al, 2002). Therefore, SDSG is believed to be as effective as lapping in waviness reduction. Since no chuck is used in SDSG, it does not have the chuck-related problems as in SSG (Kerstan and Pietsch, 2000; Pietsch and Kerstan, 2001).

**Table 2.1 Comparison of Three Processes for Flattening Silicon Wafers (Kerstan and Pietsch, 2000; Fukami et al., 1997; Pietsch and Kerstan, 2001; Wolf and Tauber, 2000; Liu et al., 2002; Pei et al., 2003; Vandamme et al., 2001; Kato et al., 1997; Yasunaga et al., 1997; Shinetsu, 1997; Kassir and Walsh, 1999; Xin et al., 2002; Pietsch and Kerstan, 2005)**

| Process | Lapping | SSG | SDSG |
|---|---|---|---|
| Waviness removal | Excellent | Poor | Good |
| Throughput | Low | Medium | High |
| Consumable cost/wafer | High | Low | Low |
| Subsurface damages | High | Low | Low |
| Automation | Low | High | High |
| Environmental benignity | Poor | Good | Good |

Table 2.1 compares lapping, SSG, and SDSG in five aspects: ability to remove or reduce wire-sawing induced waviness; throughput; consumable cost per wafer; level of automation; and environmental benignity. It can be seen that SDSG is better in almost every aspect. More information can be found in the literature about lapping (Dudley, 1986; Marinescu et al., 2002), SSG (Pei and Strasbaugh, 2001; Pei, 2002; Sun et al., 2005), and SDSG (Kerstan and Pietsch, 2000; Pietsch and Kerstan, 2001; Pietsch and Kerstan, 2005).

### *2.2.3 Proposed Applications of SDSG*

**Figure 2.5 Process Flows Using SDSG and Lapping (after (Hashii and Watanabe, 2004))**

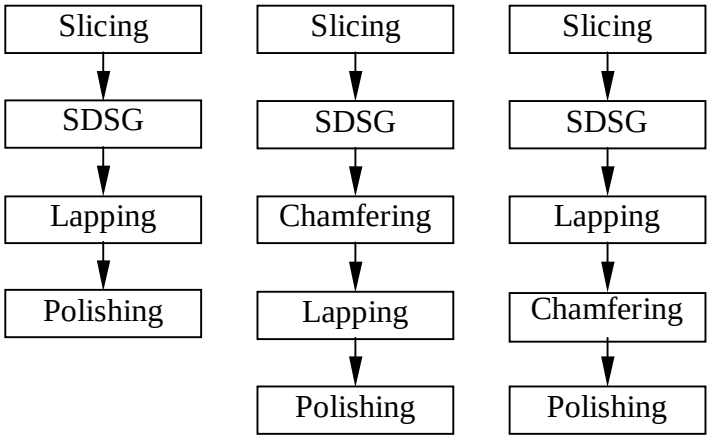


Figure 2.5 shows three proposed process flows using SDSG and lapping to flatten silicon wafers. The SDSG process is used to improve the wafer flatness and roughness and remove a layer of residual stress on the wafer surfaces induced by slicing (Hashii and Watanabe, 2004). The lapping process is used to remove minute surface undulations (with a height of a few tens of nm and period of a few mm) incurred during SDSG (Hashii and Watanabe, 2004).

**Figure 2.6 Process Flows Using SDSG, Lapping, and SSG (after (Hashii and Watanabe, 2004))**

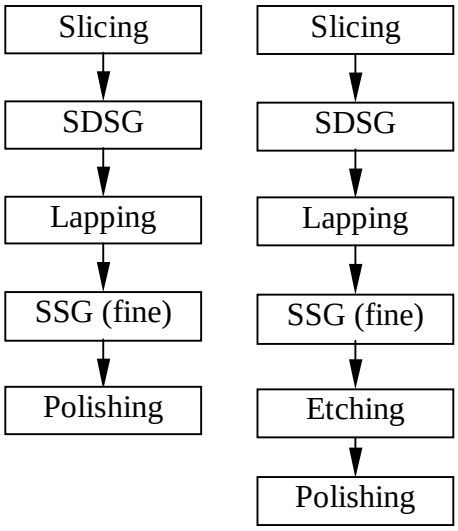

**Figure 2.7 Process Flow Using SDSG and SSG (after (Hashii and Watanabe, 2004; Hashii et al., 2002; Watanabe, 2003))**

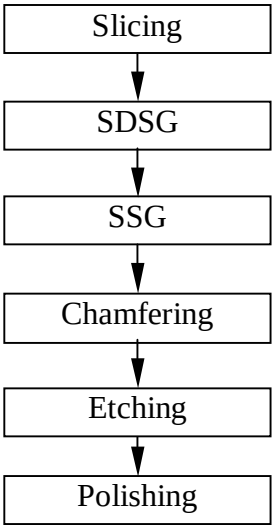


For the two process flows shown in Figure 2.6, the wafer is flattened using SDSG, lapping, and SSG (Hashii and Watanabe, 2004). The SDSG and lapping processes serve the same purposes as those in the process flows shown in Figure 2.5. The SSG process is used to remove the layer of residual stress on the wafer surfaces induced by lapping (Hashii and Watanabe, 2004).

Figure 2.7 shows a process flow using SDSG and SSG to flatten silicon wafers (Hashii and Watanabe, 2004; Hashii et al., 2002; Watanabe, 2003). The SDSG process is used to remove the slicing-induced waviness and the layer of residual stress on the wafer surfaces generated during slicing (Hashii and Watanabe, 2004; Hashii et al., 2002). The SSG process is used to further improve the flatness and roughness (Hashii and Watanabe, 2004; Hashii et al., 2002). It was reported that the roughness and flatness of the wafers can be improved due to the introduction of SDSG into those process flows shown in Figs. 2.5-7 (Hashii and Watanabe, 2004; Hashii et al., 2002; Watanabe, 2003). High precision wafers without minute undulations could be obtained by conducting lapping and polishing after SDSG (Hashii and Watanabe, 2004). Also, the amount of waste caused by the abrasive slurry in the lapping operation can be reduced to about one quarter in some process flows (Hashii and Watanabe, 2004).

**Figure 2.8 Process Flows Using SDSG Twice (after (Kuroki and Maeda, 2000; Kato et al., 2001))**

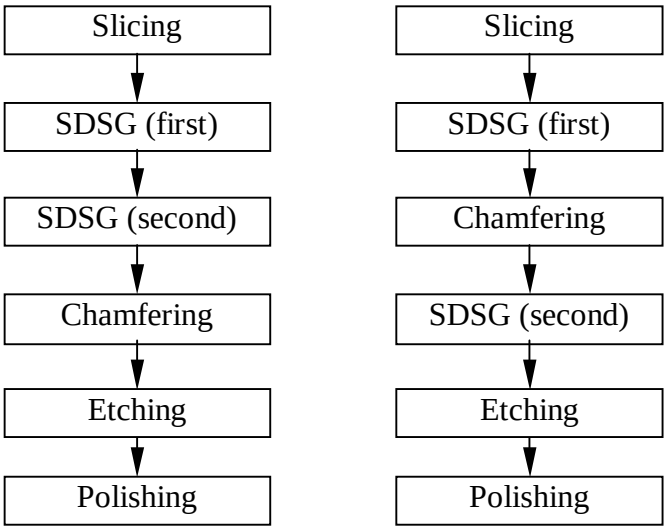


The process flows shown in Figure 2.8 use the SDSG process twice. The first SDSG was conducted after the slicing process to flatten the sliced wafers by coarse grinding (Kuroki and Maeda, 2000; Kato et al., 2001). The second SDSG was then performed (before or after chamfering) to fine grind both sides of the wafer to improve the flatness and remove the layer of residual stress on the wafer surfaces incurred during the first SDSG process (Kuroki and Maeda, 2000).

## 2.3 Models of Grinding Marks for SDSG Process

### *2.3.1 The Model for Cylindrical Face Grinding by Shih and Lee (1999)*

**Figure 2.9 Illustration for Cylindrical Face Grinding (after (Shih and Lee, 1999))**

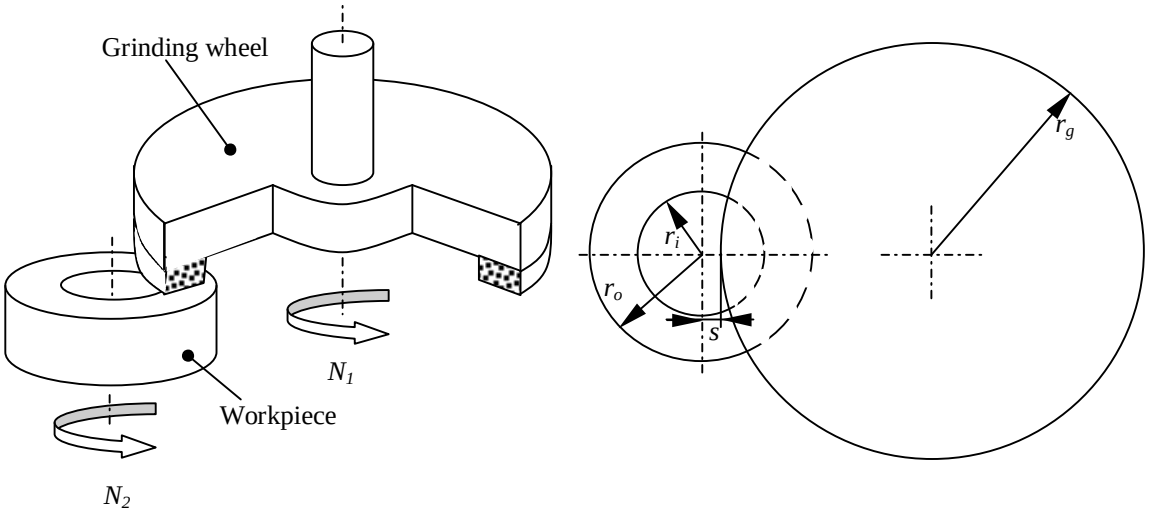

Shih and Lee (1999) developed a mathematical model to calculate and plot the grinding trajectories (curvature of grinding marks) in cylindrical face grinding. Figure 2.9 illustrates the cylindrical face grinding. The workpiece has the shape of a hollow cylinder and its inner and outer radii are designated by $r_i$ and $r_o$, respectively. The grinding wheel (with a radius of $r_g$) was modeled as a ring of rotating abrasives and the ring was offset by a distance ($s$) from the centerline of the workpiece. Both the workpiece and grinding wheel rotate about their own axes. Please note that the kinematics in the cylindrical face grinding becomes the same as that in wafer grinding when both the inner radius of the workpiece and the offset become zero (i.e. $r_i = 0$ and $s = 0$).

**Figure 2.10 The mechanism Generating Two Sets of Grinding Trajectories (after (Shih and Lee, 1999))**

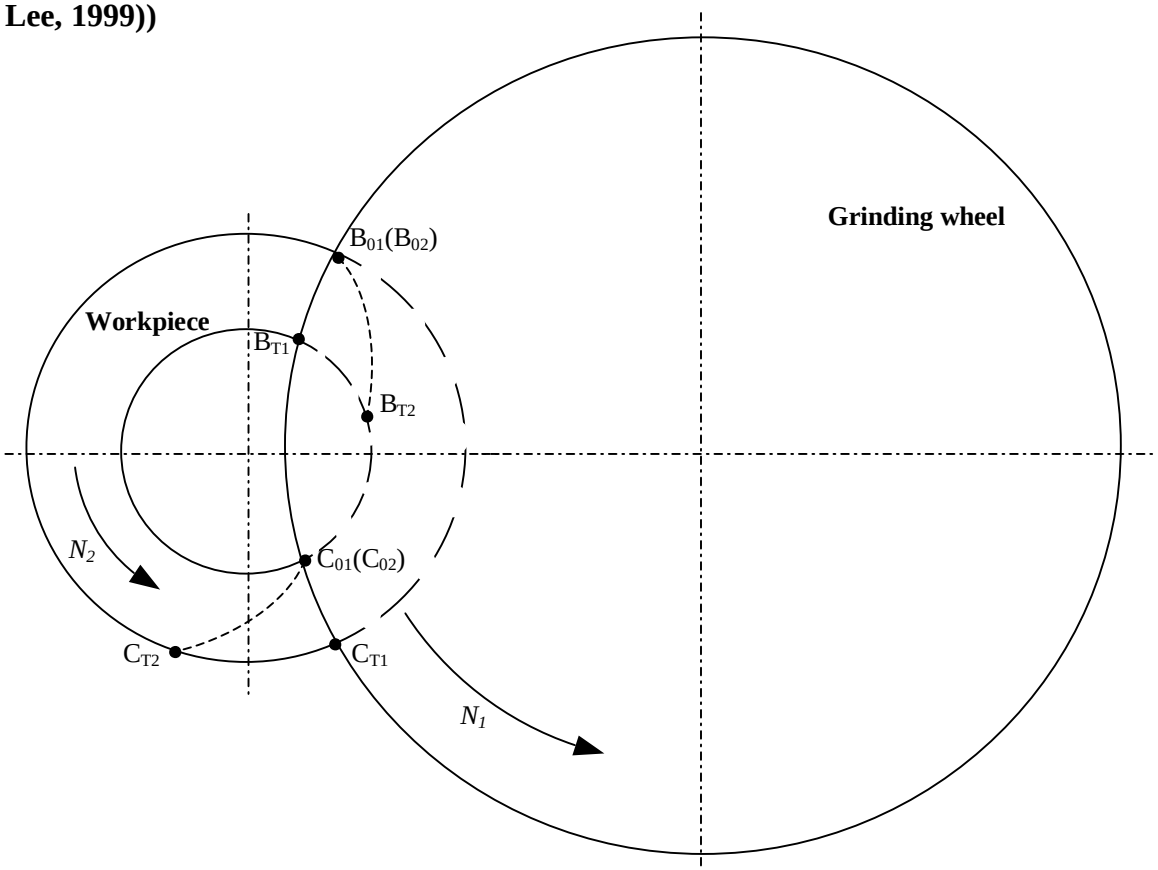


The fundamental assumption in their model can be stated as follows with the help of Figure 2.10. At time $t = 0$, the abrasive grit $B_{01}$ on the grinding wheel is in contact with the outer diameter of the workpiece $B_{02}$, and the abrasive grit $C_{01}$ on the grinding wheel is in contact with the inner diameter of the workpiece $C_{02}$. At time $t = T$, these two abrasive grits rotate from $B_{01}$ to

$B_{T1}$ and from $C_{01}$ to $C_{T1}$, respectively. Because the workpiece is also rotating, abrasive grits B and C generate two curved grinding trajectories on the workpiece from $B_{02}$ to $B_{T2}$ and from $C_{02}$ to $C_{T2}$ , respectively. Please note that this assumption is different from the assumptions (that grinding marks are generated by a single abrasive grit on the grinding wheel, or by the most protrusive portion of the grinding wheel) used by other researchers (Chidambaram, 2003; Tso and Teng, 2001; Zhou et al., 2003) in developing their grinding mark models.

Two sets of equations were developed to present the two grinding trajectories respectively. In the derivation, the effect of workpiece rotation is modeled by rotating the center of the grinding wheel an angle (in the opposite direction to the rotation direction of the workpiece) around the center of the workpiece.

Shih and Lee have studied the effects of the ratio of the grinding wheel rotation speed ($N_1$) versus the workpiece rotation speed ($N_2$) and the grinding wheel diameter on the grinding trajectories. However, they did not report any results about the effects of these parameters on the distance between adjacent grinding marks.

### *2.3.2 The Model for Single Side Grinding of Silicon Wafers by Chidambaram et al. (2003)*

**Figure 2.11 Illustration for Single Side Grinding of Silicon Wafers (Chidambaram et al., 2003)**

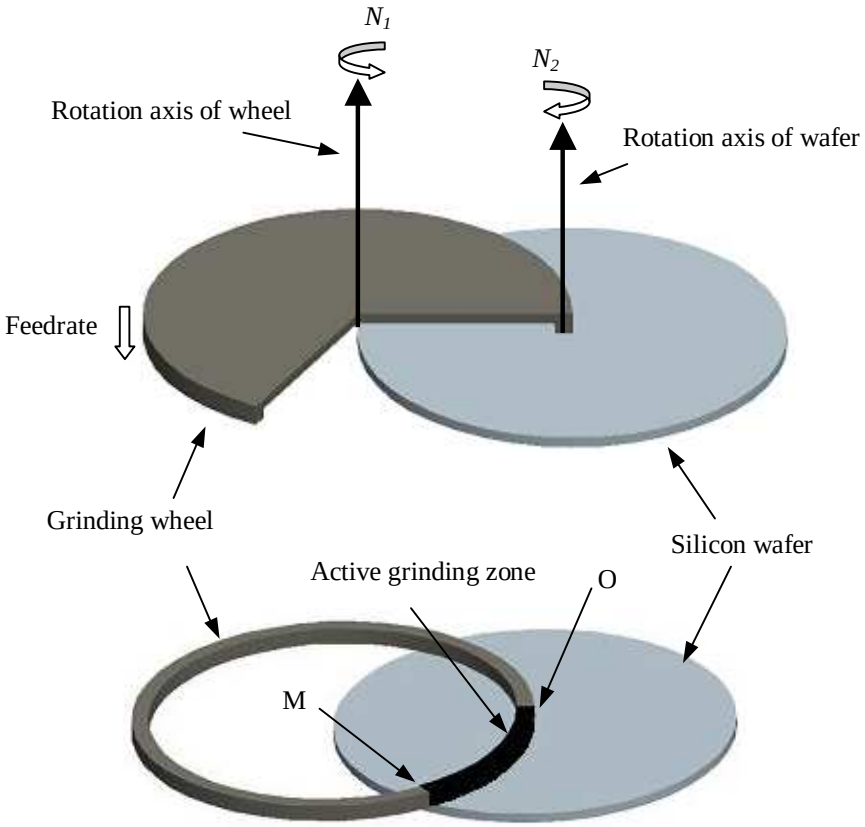

Figure 2.11 illustrates the single side grinding of silicon wafers. The grinding wheel is a diamond cup wheel. The wafer is held on a porous ceramic chuck by means of vacuum. The rotation axis for the grinding wheel is offset by a distance of the wheel radius relative to the rotation axis for the wafer. During grinding, the grinding wheel and the wafer rotate about their own rotation axes simultaneously, and the wheel is fed towards the wafer along its axis. The ceramic chuck is typically ground to a conic shape with a very small slope. When the wafer is held onto the chuck, it elastically deforms to the chuck's conic shape, thus ensuring that the grinding wheel only contacts half of the wafer. This contact area is marked as "Active grinding zone."

Chidambaram et al. (2003) developed a model based on the assumption that the grinding wheel behaves like a single-point tool. The grinding wheel removes the wafer material from the edge to the center along the arch MO, as shown in Figure 2.11. They first derived the equations to present the locus of a grinding mark when the wafer was kept stationary. In order to compensate the rotation of the wafer to obtain the grinding mark on the wafer, an offset was added to each point on this locus.

Using the model developed, they have studied the effects of process parameters (wheel rotation speed, wafer rotation speed, and wheel radius) on both the curvature of the grinding marks and the distance between adjacent grinding lines.

### *2.3.3 The Model for Single Side Grinding of Silicon Wafers by Tso and Teng (2001)*

Tso and Teng (2001) claimed that they have developed equations for the locus of a scratch (a grinding mark) for single side grinding of silicon wafers. However, no details of such equations and their deviations were given in their paper.

They presented a comparison of scratch patterns between computer simulation and experimental results as the speed ratio ($N_1/N_2$) of the grinding wheel versus silicon wafer changes. Both experimental results and computer simulations showed that, as the speed ratio increased, the grinding lines became more curved. However, they did not show any changes in the number of grinding lines for different speed ratios. Furthermore, the effects of other parameters were not reported.

### *2.3.4 The Model for Single Side Grinding of Silicon Wafers by Zhou et al. (2003)*

Zhou et al. (2003) presented a general equation in matrix forms for the grinding marks in SSG of silicon wafers without detailed deviations. A diamond grain which is initially located at the wheel periphery was chosen for grinding of silicon wafers with 300 mm diameter. The cutting path patterns of the diamond grain were studied at different speed ratio ($N_1/N_2$). In their study, the tilts of the wafer axis were considered so that the grinding marks were generated in three-dimensional coordinates.

They presented cutting path patterns for three different speed ratios ($N_1/N_2$ = 2, 30, and 37.5). They observed that, when $N_1/N_2$ = 2, the cutting path formed was a straight line. Another conclusion they got was that the cutting path pattern (grinding marks) is only determined by the speed ratio, not the individual rotation speed. However, they did not report the effects of other process parameters on the grinding marks.

### *2.3.5 The Research Work for SDSG of Silicon Wafers by Pietsch and Kerstan (2005)*

**Figure 2.12 Illustration of SDSG Grinding Marks (after (Pietsch and Kerstan, 2001; Pietsch and Kerstan, 2005))**

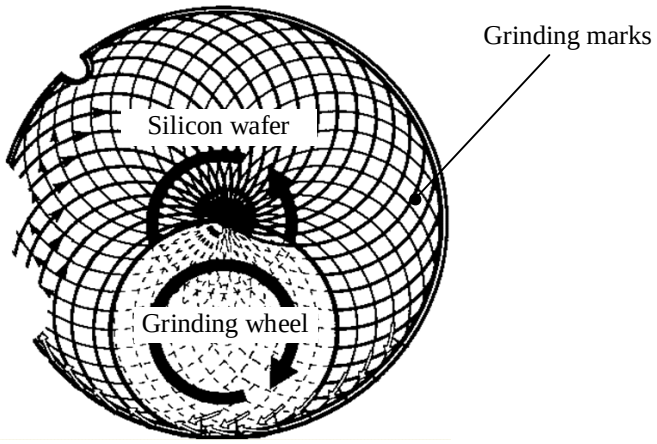


Defining grinding marks as the cutting paths (or trajectories) swept by a diamond abrasive bonded on the wheel, Pietsch and Kerstan presented a simulation graph (shown in Figure 2.12) of the grinding marks for SDSG of silicon wafers without giving detailed equations. They reported that a “criss-cross” grinding marks were visible on the wafer surfaces processed by SDSG, different from the radial grinding marks on the wafer surfaces processed by SSG.

However, they did not report any systematic study about the effects of SDSG process parameters on the grinding marks.

**Table 2.2 Summary of Research Progress in the Grinding Marks**

| Authors (Ref.) | Process | Distance between adjacent grinding marks | Curvature of grinding marks | Systematic study on effects of process parameters |
|---|---|---|---|---|
| Shih and Lee (1999) | Cylindrical surface grinding of harden steel workpiece | × | √ | √* |
| Chidambaram et al. (2003) | SSG of 200 mm silicon wafers | √ | √ | √ |
| Tso and Teng (2001) | SSG of 300 mm silicon wafers | √ | × | √** |
| Zhou et al. (2003) | SSG of 300 mm silicon wafers | √ | × | × |
| Pietsch and Kerstan (2005) | SDSG of 300 mm silicon wafers | × | × | × |

*Study on the curvature of grinding marks.
**Study on the distance between adjacent grinding lines.

Table 2.2 summarizes the aforementioned investigations into the grinding marks. It indicates that no mathematical models were ever developed to systematically study the grinding marks in SDSG of silicon wafers.

## 2.4 Models of Wafer Shape for SDSG Process

### *2.4.1 The Model for the Part Face Profile in Cylindrical Face Grinding of Metal Parts by Shih and Lee (1999)*

**Figure 2.13 Illustration for Cylindrical Face Grinding with Tilt Spindle (after (Shih and Lee, 1999))**

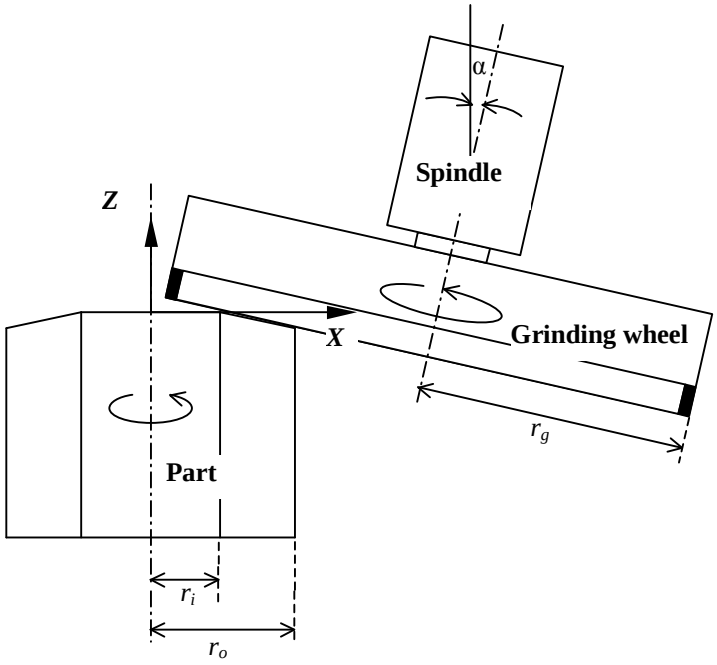


Shih and Lee (1999) developed a mathematical model to calculate the face profile of steel parts in cylindrical face grinding. An illustration of the cylindrical face grinding is shown in Figure 2.13. The part has the shape of a hollow cylinder and its inner and outer radii are designated by $r_i$ and $r_o$, respectively. The grinding wheel (with a radius of $r_g$) was modeled as a ring of rotating abrasives and the ring was offset by a distance from the rotation axis of the part. Both the part and grinding wheel rotate about their own axes.

The *Z* axis coincided with the rotation axis of the part. The part material was removed by the ring of rotating abrasives and a convex or concave surface was generated by tilting the wheel spindle a small angle (α) relative to the *Z* axis. A series of equations were developed to present the part face profile. Several grinding experiments were conducted to validate the model and the experimental results agreed well with those predicted by the mathematical model.

In Shih and Lee's model, the grinding wheel only has a "pitch" angle (will be defined and discussed in Chapter 4) relative to the part. For grinding of silicon wafers, the grinding wheel typically have both "roll" (will be defined and discussed in Chapter 4) and "pitch" angles relative to the wafer. Furthermore, they did not report any systematical study about the effects of those parameters (the "roll" angle and the "pitch" angle) on the part surface profile.

### *2.4.2 The Model for the Wafer Shape in Single Side Grinding of Silicon Wafers by Sun et al. (2004)*

Sun et al. (2004) developed a model to predict the wafer shape in SSG of silicon wafers. They have studied the relations between the wafer shape and the setup parameters using the model developed, and discussed the practical applications of the model. Both two-dimensional (2D) and three-dimensional (3D) wafer shapes based upon different setup parameters were presented.

### *2.4.3 The Model for the Wafer Shape in Single Side Grinding of Silicon Wafers by Tso and Teng (2001)*

**Figure 2.14 Geometry for Developing the Wafer Shape Model in SSG by Tso and Teng (after (Tso and Teng, 2001))**

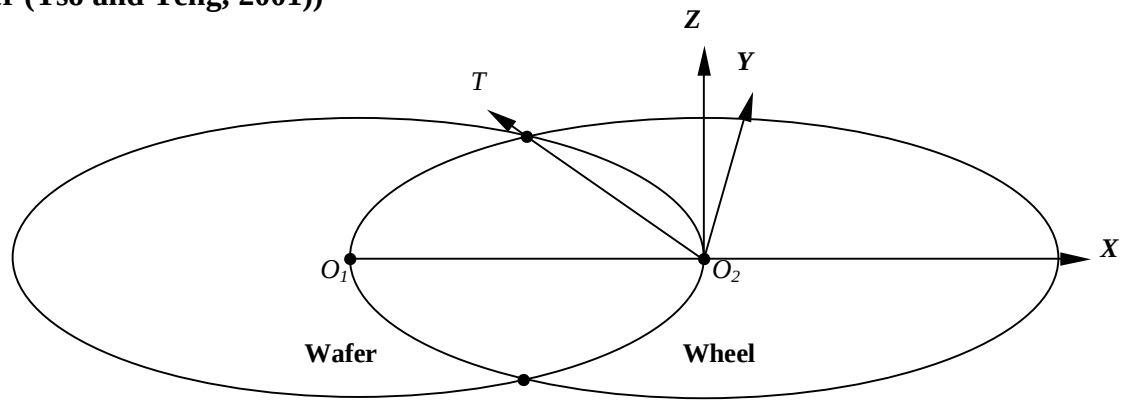


Figure 2.14 illustrates the geometry for developing Tso and Teng' model for the wafer shape in SSG (Tso and Teng, 2001). By tilting the wheel rotation axis around the vector $O_2T$, different profiles of the ground surface (or the wafer shape) could be obtained. They presented several cross-sectional profiles of the wafer (200 mm in diameter) along its diameter for different tilt angles.

### *2.4.4 The Model for the Wafer Shape in Single Side Grinding of Silicon Wafers by Zhou et al. (2003)*

Zhou et al. (2003) presented an equation in matrix forms for the grinding marks in SSG of silicon wafers. Those grinding marks generated in 3-D coordinates could possibly be used to represent the wafer shape. They presented eight basic wafer shapes by means of grinding marks in 3-D coordinates. But, a systematical study of the effects of the process parameters on the wafer shape was not reported.

They also claimed that higher cutting path density always led to removal of more material and resulted in a concave wafer shape. Then the cutting path density at a specific area of the wafer surface was used to investigate the effects of rotation speeds of the wheel and the wafer on the wafer shape. They reported that a more practical solution to offset the effect of the rotation speeds on the wafer shape was to tilt the wafer rotation axis slightly against the wheel rotation axis.

### *2.4.5 The Model for the Wafer Shape in Simultaneous Double Side Grinding of Silicon Wafers by Pitesch and Kerstan (2005)*

**Figure 2.15 Geometry for Developing the Wafer Shapes Model in SDSG by Pietsch and Kerstan (after (Pietsch and Kerstan, 2005))**

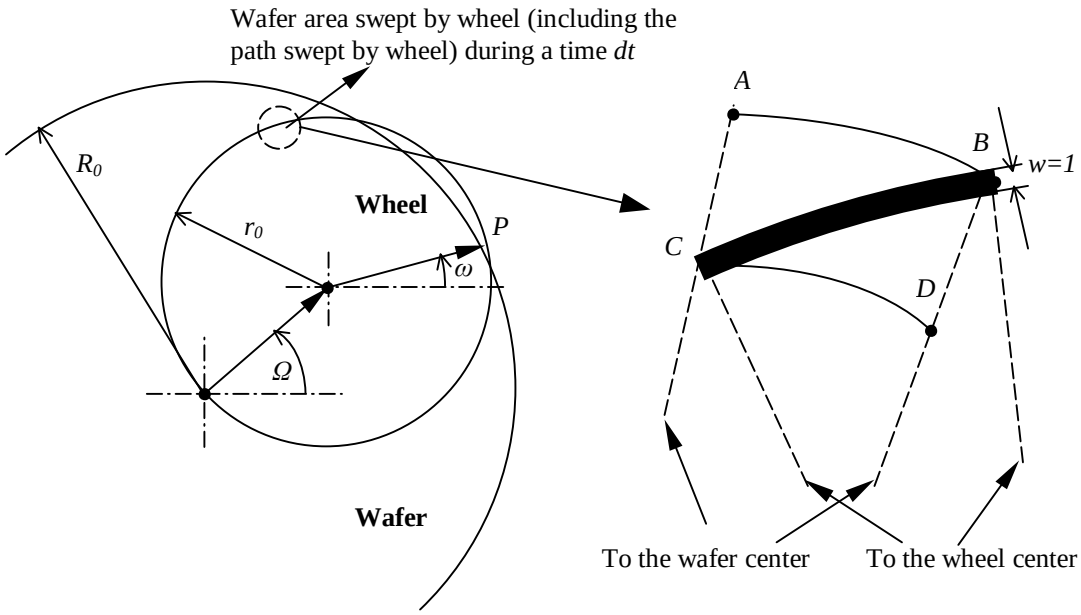

Pietsch and Kerstan (2005) developed a model for the wafer shape in SDSG of silicon wafers. Their assumption was that the wafer shape was determined by the wheel/wafer kinematics (i.e. the wheel rotation speed $\omega$, the wafer rotation speed $\Omega$, the wheel radius $r_0$, and the wafer radius $R_0$). The geometry for developing their model is shown in Figure 2.15. They claimed that the amount of material removed by the wheel at any point along the radial direction on the wafer surface during time $dt$ could be described as:

$$removal = \frac{(path\ swept\ by\ wheel)(wheel\ rim\ width)}{wafer\ area\ swept\ by\ wheel} dt \tag{2.1}$$

As shown in Figure 2.15, the path swept by the wheel was arc $BC$; the rim width $w$ of the wheel was set as unity 1; the wafer area swept by the wheel was the sector $ABCD$.

Their investigation has some conclusions about the wafer shape in SDSG:

1) There was always a dimple at the center of the wafer;
2) The edge of the wafer always tapered off ("roll-off");
3) When the two grinding wheels rotated in different directions, the surface on one side of the wafer was different from the other side. This was a limitation for SDSG if identical wafer surfaces on both sides were required in production. But, the difference could be reduced when the wheels rotated at a high speed making $\omega/\Omega >> 1$.

Their model could predict the wafer shape fairly well for the outer portion. But, there always exist singular solutions around the center of the wafer. It is interesting to note that their predicted wafer shapes were obtained using the stock material removal through Equation (2.1), but in their experiments, the wafer shapes were altered by tilting the wheels. They did not report the effects of the "roll" angle and the "pitch" angle on the wafer shape.

**Table 2.3 Summary of Research Progress in the Wafer Shape**

| Authors (Ref) | Process | Effect of "roll" angle | Effect of "pitch" angle | Effect of wheel diameter | Effect of rotation speed |
|---|---|---|---|---|---|
| Shih and Lee (1999) | Cylindrical surface grinding of metal parts | √ | | | |
| Sun et al. (2004) | SSG of 200 mm silicon wafers | √ | √ | | |
| Tso and Teng (2001) | SSG of 300 mm silicon wafers | √ | √ | | |
| Zhou et al. (2003) | SSG of 300 mm silicon wafers | √ | √ | | √ |
| Pietsch and Kerstan (2005) | SDSG of 300 mm silicon wafers | | | | √ |

Table 2.3 summarizes the aforementioned models for the wafer shape. It indicates that no systematical study has been reported about the effects of important parameters (such as the "roll" angle, "pitch" angle, and wheel diameter) on the wafer shape in SDSG of silicon wafers.

## 2.5 A Brief History of UVAG

**Figure 2.16 Illustration of Ultrasonic Machining (after (Goldman, 1962))**

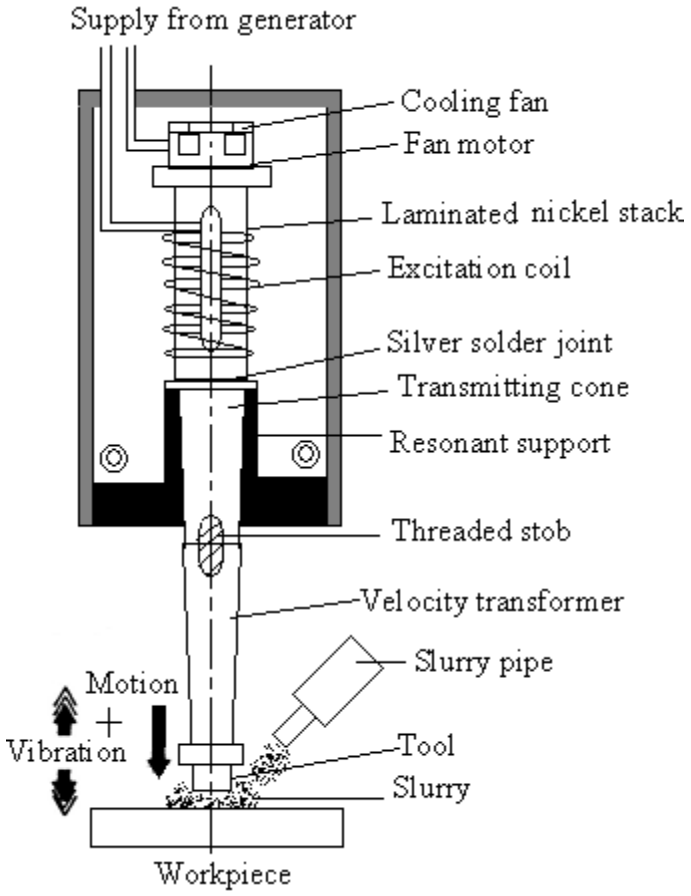


Figure 2.16 is a schematic illustration of ultrasonic machining (USM). The power supply produces an alternating electric current at ultrasonic frequency (18 to 24 kHz) and supplies to the transducer (Goldman, 1962). This causes the core of the transducer to change in length periodically. The amplitude of the vibration of the transducer face is about 0.005 to 0.01mm. This amplitude is increased by using concentrator and tool to a value of 0.03 mm, which is sufficient for practical purposes. The tool is made to vibrate at a high frequency (typically 20 kHz) in a direction perpendicular to the surface to be machined. Abrasive particles like aluminium oxide, boron carbide, etc. are mixed with water and this slurry is allowed to enter the gap between the tool and workpiece. Material is removed in the form of tiny particles by the successive impacting action of the abrasive particles into the workpiece (Jana and Satyanarayana, 1973).

However, in USM, the slurry has to be fed to and removed from the gap between the tool and workpiece. Because of the this fact, there are some disadvantages of the this method: materials removal rate slows down considerably and even stops as penetration depth increases; the slurry may wear the wall of the machined hole as it passes back toward the surface, which limits the accuracy, particularly for small holes; and the action of abrasive slurry also cuts the tool itself, thus causing considerable tool wear, which in turn makes it very difficult to hold close tolerances (Pei, 1995).

**Figure 2.17 Illustration of UVAG (after (Pei, 1995))**

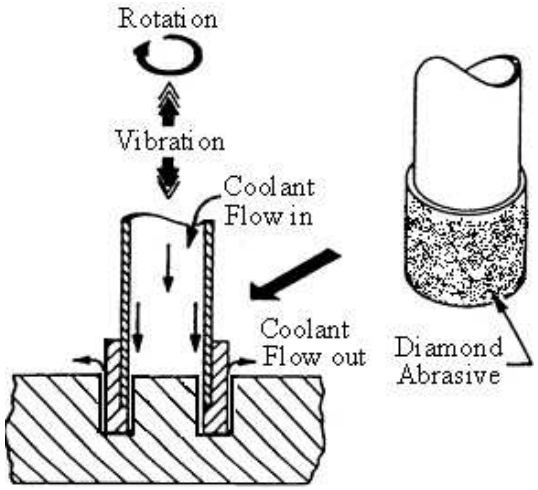


In order to overcome the shortcomings of USM, ultrasonic vibration assisted grinding (UVAG) was invented. UVAG is a hybrid machining process that combines the material removal mechanisms of diamond grinding and USM, resulting in higher material removal rate (MRR) than that obtained by either diamond grinding or USM (Pei, 1995). In UVAG, the slurry is replaced with abrasives bonded to the tool. A rotating core drill with metal-bonded diamond abrasives is ultrasonically vibrated and fed toward to the fixed workpiece at a constant pressure or a constant feedrate. Coolants pumped through the core of the drill wash away the swarf, prevent jamming of the drill, and keep it cool so that the UVAG process could be conducted smoothly. The UVAG process is illustrated in Figure 2.17.

Experimental results (Prabhakar, 1992) have shown that the material removal rate obtained from UVAG is nearly 6-10 times higher than that from a conventional grinding process under similar conditions. In comparison with USM, UVAG is about 10 times faster (Cleave, 1976). Especially, it is much easier to drill deep and small holes with UVAG than with USM. Other advantages of improved hole accuracy and low tool pressure are also reported (Graff, 1975). Now, the UVAG technique has become one of important non-conventional techniques and the UVAG equipments have been utilized in industry to machine various advanced materials.

## 2.6 Edge Chipping in UVAG Process

### *2.6.1 Edge Chipping Phenomenon*

**Figure 2.18 Edge Chipping Induced by UVAG**

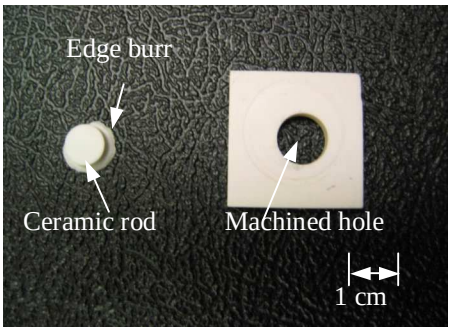


(a) Two parts resulting from UVAG

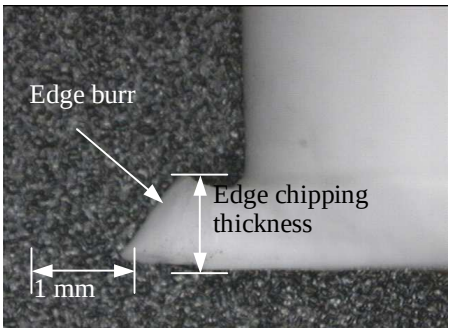


(b) Side view of machined rod

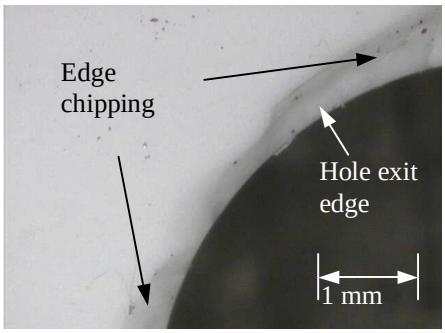


(c) Bottom view of hole exit

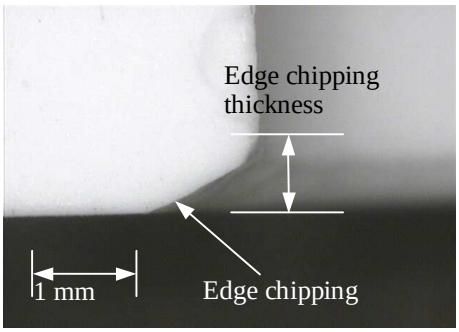


(d) Side view of hole exit

One of the remaining challenges for UVAG is edge chipping (or, chamfer) (Jiao et al., 2005; Li et al., 2004). Figure 2.18 illustrates the edge chipping induced in the UVAG process. Shown in Figure 2.18(a) is a workpiece that has been machined into two pieces by UVAG. One

piece is the machined part with the desired hole, the other is a rod (or slug) removed from the workpiece. Figure 2.18(b) shows the side view of the bottom portion of the machined rod. An edge burr around the bottom of the rod is observable. When the cutting tool nearly drills through the workpiece, the rod breaks off from the workpiece, causing the edge chipping around the hole exit edge as shown in Figure 2.18(c). The edge chipping thickness can be measured either on the rod as sketched in Figure 2.18(b), or on the hole exit as shown in Figure 2.18(d).

The edge chipping in a machined ceramic component not only compromises geometric accuracy, but also causes possible failure of the component during service (Ng et al., 1996). Generally, edge chipping is not acceptable on finished products, and has to be machined off by other processes after the UVAG operation. The larger the edge chipping, the higher the total machining cost. Therefore, research efforts to reduce the edge chipping thickness in UVAG are desirable.

### *2.6.2 Study on Edge Chipping*

Ng et al. (1996) characterized the edge chipping in ceramic milling into three categories: entrance edge chipping, interior edge chipping, and exit edge chipping. They reported that the microstructure and stress distribution were the key factors for the initiation and propagation of the edge chipping. Yoshifumi et al. (1995) studied edge chipping in slot grinding of Mn-Zn ferrite. They concluded that the size of the edge chipping was proportional to the MRR. Based upon Chiu et al.'s work (Chiu et al., 1998) on edge chipping initiation in milling of brittle materials, Cao (2001) studied the factors related to exit edge chipping in milling of dental ceramics using a two-dimensional (2-D) finite element analysis (FEA) model. In his model, a microcrack was used to simulate a critical flaw or pre-existing machining induced damage. His results revealed that the main influencing factors in determining the size of exit edge chipping were the size and length of the microcrack as well as the orientation and location of the applied load.

The aforementioned investigations dealt with the machining induced edge chipping in milling and grinding of brittle materials. Little research on edge chipping in UVAG has been reported. Jiao et al. (2005) studied the edge chipping in UVAG of ceramics using a combined experimental design and finite element method. They used the Withney-Nuismer point stress criterion (more information can be found in the literature about this criterion (Whitney and

Nuismer, 1974; Ritchie et al., 1973)) to predict edge chipping initiation. They reported that the main influencing factor on edge chipping was the cutting force, which, in turn, was determined by the controllable machining variables (such as spindle speed, ultrasonic vibration amplitude, and feedrate). They found that the edge chipping thickness could be reduced by using higher spindle speed and smaller feedrate due to reduced cutting forces. Li et al. (2004) conducted a preliminary study on the initiation of edge chipping in UVAG using a three-dimensional (3-D) FEA model. They used von Mises stress failure criterion to predict edge chipping initiation. They found that the cutting depth and the support length had significant effects on edge chipping initiation. But, they did not report any practical ways to reduce the edge chipping thickness.

The literature review conducted has revealed the lack of a practical solution to reduce the edge chipping in UVAG of ceramics.

## 2.7 Effects of Coolant in UVAG

Coolant is one of the most important factors in UVAG because the coolant pumped through the core of the drill not only washes away the swarf but also prevents jamming of the drill and keeps it cool (Pei et al., 1995[a]). Without coolant, the debris will stick on the tool and work surface, causing the feed speed to slow down, and the tool may be burnt or even completely ruined by high temperatures in the cutting zone (Hu et al., 2002).

**Figure 2.19 Effects of Coolant Pressure on UVAG of Ceramics (Pei et al., 1995[c])**

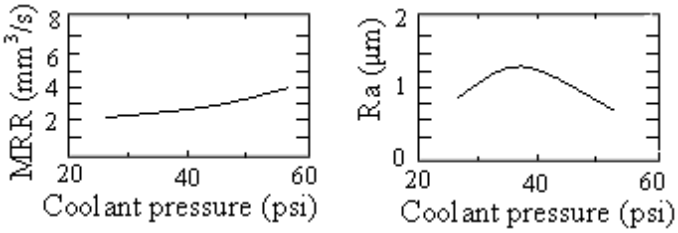


Experimental investigations have been conducted on effects of coolant pressure and coolant type on the performance of UVAG. Coolant pressure does not have a significant effect on MRR but the lowest surface roughness can be achieved at an optimal pressure level (see Figure 2.19). As for coolant type, the synthetic coolant and tap water show better performances in UVAG than the water-based coolant (Hu et al., 2002).

**Figure 2.20 Different Coolant Delivery Modes**

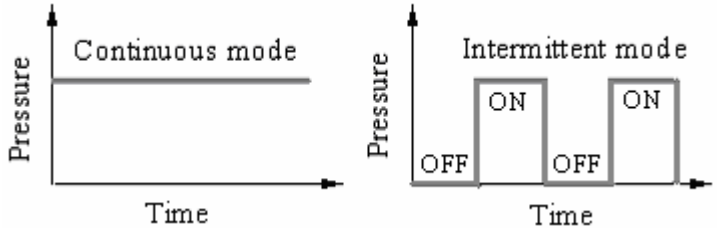


(a) (b)

The latest feedbacks from industry suggest that coolant delivery mode might have a significant effect on the UVAG process. Two delivery modes (continuous and intermittent) are presented. Continuous mode, which delivers the coolant at a constant pressure, as shown in Figure 2.20(a), is currently the dominant coolant delivery mode because it can be realized easily with the regular centrifugal pump. For the intermittent model, in which the coolant pressure will alter between on and off states as shown in Figure 2.20(b), some preliminary experimental results in industry show that the intermittent mode has a positive effect on the UVAG process compared with the continuous mode. But the conclusion is only based on operators' experience and intuition. There is no reported systematic study on the effects of the coolant delivery mode in the UVAG process.

## 2.8 Applications of UVAG in Machining of Various Materials

### *2.8.1 Reported Applications in Machining of Various Materials*

Since its inception in 1960s (Legge, 1964; Legge, 1966), many papers on UVAG have been published. Pei et al. (1995) reported that there exist two material removal modes in UVAG of ceramic materials: brittle fracture mode and ductile model. Models for predicting the material removal rate (MRR) based upon the two material removal modes were developed by Prabhakar et al. (1993) and Pei (1995; 1998). Spur and Holl (1997) investigated tool wear mechanisms in UVAG. Effects of UVAG machining variables (spindle speed; feedrate; ultrasonic vibration amplitude and frequency; diamond type, size and concentration; bond type for the cutting tool; etc.) on the performances (MRR, cutting force, surface roughness, etc.) of UVAG were investigated experimentally (Prabhakar, 1992; Petrukaha et al., 1970; Spur et al., 1997; Kubota et

al., 1997; Zeng et al., 2004; Markov and Ustinov, 1972; Markov and Ustinov, 1977). Extensions of UVAG to face milling (Pei et al., 1995[b]; Pei and Ferreira, 1999), disk grinding (Khanna et al., 1995), and complex contour machining (Uhlmann et al., 1999; Ya et al., 2001) were developed.

**Table 2.4 Summary of Workpiece Materials Machined by UVAG and USM**

| Workpiece materials | Experimental studies | Theoretical studies |
|---|---|---|
| Alumina | Hu et al., 2003; Anantha Ramu et al., 1989; Zeng et al., 2004; Jiao et al., 2005. | Zhang et al., 1995; Jiao et al., 2005. |
| Canasite | Khanna et al., 1995 | |
| Glass | Jana and Satyanarayana, 1973; Treadwell and Pei, 2003; Anonymous, 1966; Anonymous, 1973. | Dam et al., 1995; Lunzer, 1973. |
| Polycrystalline Diamond Compacts | Li et al., 2004. | |
| Silicon Carbide | Dam et al., 1995. | |
| Silicon Nitride | Cleave, 1976; Dam et al., 1995. | |
| Stainless steel | Deng et al., 1993; Dam et al., 1995. | Deng et al., 1993. |
| Titanium Boride | Dam et al., 1995. | |
| Zirconia | Pei et al., 1995b; Anantha Ramu et al., 1989; Prabhakar, 1993; Pei, 1995; Pei et al., 1995[c]. | Pei and Ferreira, 1998; Anantha Ramu et al., 1989; Ya et al., 2002; Zhang et al., 1998; Deng et al., 1993. |

Table 2.4 summarizes reported work on UVAG (or USM) process since it was invented in 1960's. UVAG has been employed to machine many types of materials (Pei and Ferreira, 1998; Kumabe et al., 1989; Pei et al., 1995b; Hu et al., 2003; Zeng et al., 2004; Zhang et al, 2000;

Prabhakar, 1992; Pei, 1995; Pei et al., 1995[c]; Ya et al., 2002; Zhang et al., 1998; Treadwell and Pei, 2002; Khanna and Pei, 1995; Jiao et al., 2005; Prabhakar et al., 1992; Markov and Ustinov, 1973; Markov et al., 1977; Markov, 1966).

### *2.8.2 Potential Applications in Machining of Fiber-reinforced Ceramic Matrix Composites*

Ceramic matrix composites (CMC) combine reinforcing ceramic phases with a ceramic matrix to create materials with superior properties (like high-temperature stability, high thermal-shock resistance, and lightweight), providing unique engineering solutions(Richerson, 1997). The combination of these characteristics makes CMC an attractive alternative to traditional materials such as high alloy steels and refractory metals (Richerson, 1997; Okamura, 1995; Freitag and Richerson, 1998). Benefits of using CMC include increased energy efficiency, increased productivity, and regulatory compliance. CMC have been used in some areas for years, such as cutting tools and wear parts (Anonymous, 2000). Other emerging applications being field-tested or in the development stage include gas turbine seals, hot gas filters and high-pressure heat exchangers (Anonymous, 2000). Currently, a major obstacle to broad applications of CMC is that the CMC materials, especially those with continuous reinforcements, generally require more costly manufacturing processes (Freitag and Richerson, 1998).

Several papers have reported studies on machining of fiber-reinforced CMC. Hamatani et al. conducted experiments on machinability of particulate reinforced CMC ($TiB_2$/SiC) with abrasive water-jet machining (Hamatani and Ramulu, 1990). Hocheng et al. studied ultrasonic machining (USM) of CMC materials reinforced with continuous C/SiC fibers (Hocheng et al., 2000). Ramulu et al. proposed machining of CMC ($TiB_2$/SiC) by electrical discharge machining (EDM) (Ramulu et al., 1990). Tuersley et al. investigated processing of CMC (magnesium alumina silicate matrix, SiC fiber glass reinforcement) with a pulsed Nd-YAG laser (Tuersley et al., 1996; Tuersley et al., 1998). Carroll et al. presented machining of dense SiC/SiC woven composites and green $Si_3N_4$/BN fibrous monolithic composites using a $CO_2$ laser (Carroll et al., 2000). However, water-jet machining often produces delamination, and laser machining produces thermal stress and a heat-affected zone in the workpiece material (Hocheng et al., 2000).

From what overviewed above and Table 2.4, it can be seen that there are no reports published on UVAG of CMC.

### *2.8.3 Potential Applications in Machining of Zirconia/Alumina Composites*

Many potential uses of ceramics, especially those related to structural applications are limited due to their poor mechanical properties (Garcia et al. 2002). This has resulted in the developments of ceramic-ceramic composites. In recent years, zirconia/alumina composites, in which zirconia appears as a secondary dispersed phase, has become a very important material because of its enhanced toughness and strength (Chatterjee et al. 1989). Zirconia/alumina composites combine alumina's high hardness and wear properties with zirconia's toughness and bending strength (Claussen 1976, Lange 1982, Evans 1990). The enhanced strength (especially transverse rupture strength) and toughness have made zirconia/alumina composites more widely applicable and overall more productive than plain ceramics and cermets in machining steels and cast irons (Mondal et al. 1992). Also, zirconia/alumina composites have been introduced into many other engineering applications like pump components, bearings, bushings, valve seats and many other wear components (Sornakumar et al. 2001).

Zirconia/alumina composites are normally fabricated from fine powders through powder processing techniques such as compacting, sintering, and hot isostatic pressing (HIPing). In most cases, the sintered or the HIPed workpieces need to be machined into useful shapes and dimensions to satisfy their engineering applications. Most research work on machining of zirconia/alumina composites has been focused on traditional machining processes like grinding and lapping to attain the required dimensions or the desired level of surface finish (Inasaki et al., 1986). Laser-assisted machining method was ever proposed by some researchers to machine partially stabilized zirconia ceramics (Rebro, P. A. et al., 2002), but laser machining produces thermal stress and some heat-affected zone in the workpiece material. Therefore, to develop more cost-effective machining techniques is still much needed in fabrication of zirconia/alumina composites.

A thorough literature search of UVAG and USM on different high performance materials (refer to Table 2.4) has shown that no reports have been presented on UVAG of zirconia/alumina composites.

# CHAPTER 3 - A Mathematical Study on Grinding Marks in SDSG

## 3.1 Introduction

**Figure 3.1 Silicon Wafer Surface with Grinding Marks after SDSG Operation**

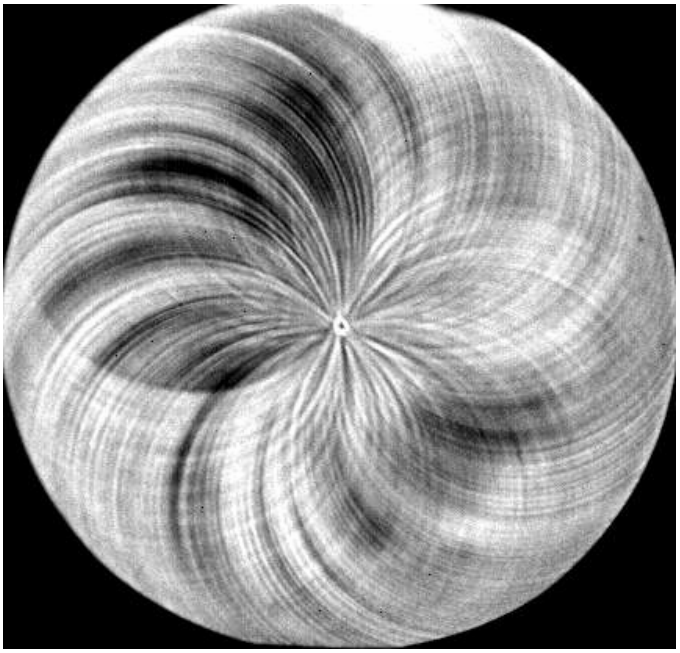

Figure 3.1 shows a wafer surface processed by SDSG. There are many visible grinding marks on the wafer surface. These grinding marks are not acceptable and required to be removed by subsequent processes. One approach to eliminate the grinding marks is to keep polishing until all of them are gone. But, it will lengthen the polishing time and increase manufacturing costs. A better approach is to optimize the SDSG process so that grinding marks can be removed with the minimum polishing amount. The success of the latter approach will, to a certain degree, depend on whether or not the following questions can be answered: How are grinding marks generated? How do process parameters (wheel rotation speed, wafer rotation speed, wheel diameter, and feederate, etc.) affect grinding marks?

Several mathematical models have been reported for grinding marks in cylindrical face grinding of harden steel workpiece (Shih and Lee, 1999) and for grinding marks in SSG of silicon wafers (Chidambaram, 2003; Tso and Teng, 2001; Zhou et al., 2003). These mathematical models can potentially be used to study the grinding marks in SDSG but no such study has ever been published.

This chapter is organized as follows. Following the introduction section, assumptions for a mathematical model for grinding marks in SDSG are presented in section 2. Derivations and computer programs for the mathematical model are developed in section 3 and section 4, respectively. In section 5, this developed model is used to study the effects of the SDSG parameters on the grinding marks. Conclusions are drawn up in section 6.

## 3.2 Assumptions for the Mathematical Model

**Figure 3.2 Geometry of the Mathematical Model to Calculate the Grinding Marks**

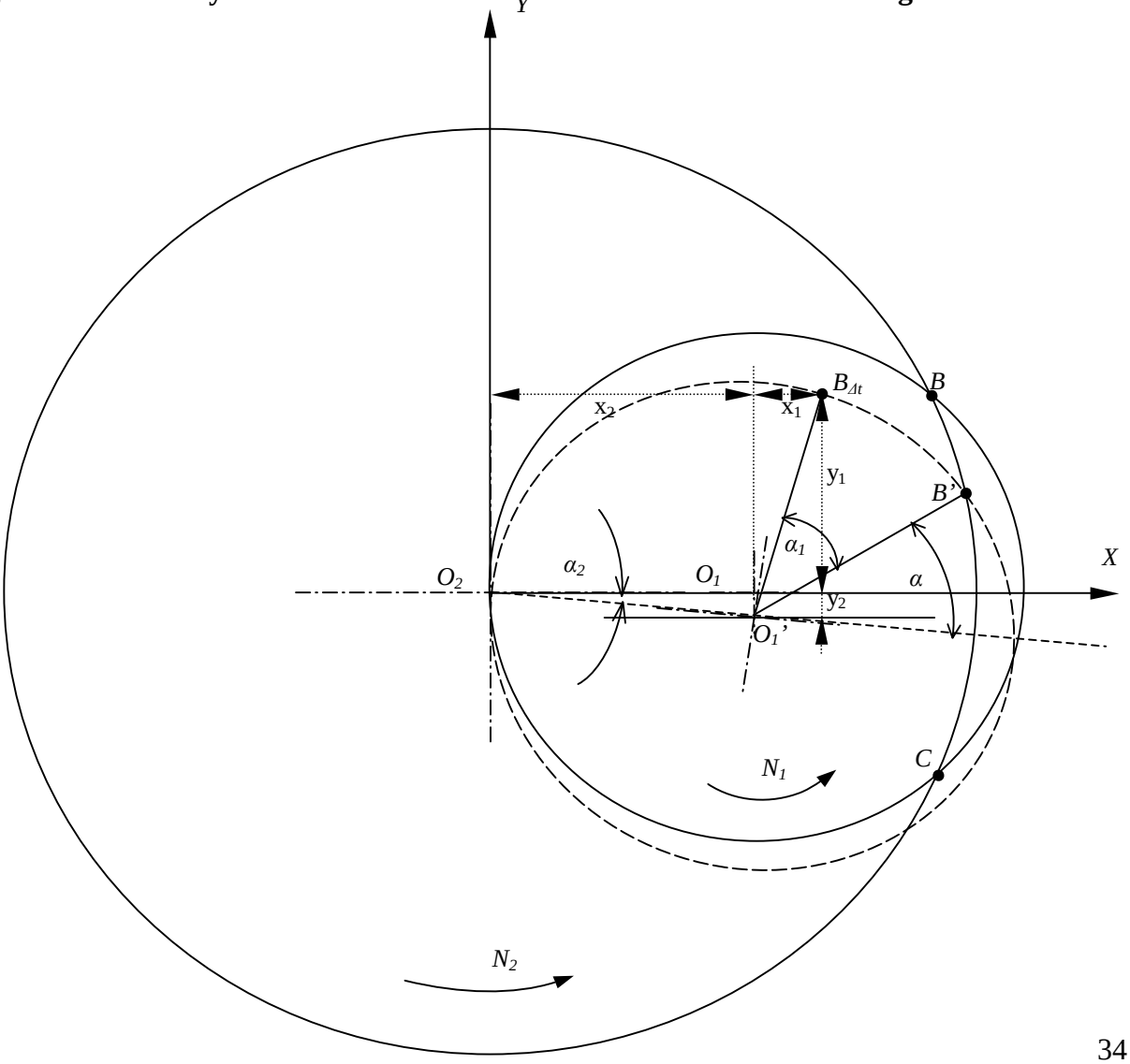

For the model in this chapter, the grinding wheel is assumed to behave like a single-point cutting tool. This assumption has been validated and used by previous research (Shih and Lee, 1999; Chidambaram et al., 2003). For one side of the silicon wafer in SDSG, both the wheel (with a diameter of $D_1$) and the wafer (with as diameter of $D_2$) are assumed to rotate in counter clockwise (C.C.W.) direction. The grinding wheel rotates about it center $O_1$ at a speed of $N_1$ (rpm, or revolution per minute). The wafer rotates about its center $O_2$ at a speed of $N_2$ (rpm).

The grinding wheel removes the material from the wafer rim point ($B$), where the cutting point enters the wafer surface, to the wafer rim point ($C$), where the cutting point exits the wafer surface, along the arc $BO_2C$, as shown in Figure 3.2. A coordinate system $XO_2Y$ is used to define all the points on the wafer and the grinding wheel. The origin of the $XO_2Y$ coordinate system is at the center of the wafer.

As shown in Figure 3.2, at time $t = 0$, it is assumed that the cutting point enters the wafer surface at $B$. After time $t = \Delta t$, the cutting point moves from $B$ to $B_{\Delta t}$. To calculate the position of $B_{\Delta t}$ in $XO_2Y$ coordinate system, the motion from $B$ to $B_{\Delta t}$ of the cutting point is decomposed into two parts. Firstly, the rotation of the wafer in the C.C.W direction is treated by rotating the center of the wheel an angle $\alpha_2$ in clockwise (C.W.) direction. Hence, the cutting point on the rim of the wheel also rotates an angle $\alpha_2$ in C.W. direction from $B$ to $B'$. Secondly (in the mean time), the cutting point on the rim of the wheel has rotated an angle $\alpha_1$ in the C.C.W. direction from $B'$ to $B_{\Delta t}$ during time $\Delta t$.

## 3.3 Derivation of the Mathematical Model

The position of $B_{\Delta t}$ can be described by the following equation in the $XO_2Y$ coordinate system:

$$\begin{cases} x_{\Delta t} = x_1 + x_2 \\ y_{\Delta t} = y_1 = (y_1 + y_2) - y_2 \end{cases} \tag{3.1}$$

where,

$$x_1 = \frac{D_1}{2}\cos(\alpha - \alpha_2 + \alpha_1) \tag{3.2}$$

$$x_2 = \frac{D_1}{2}\cos\alpha_2 \tag{3.3}$$

$$y_1 + y_2 = \frac{D_1}{2}\sin(\alpha - \alpha_2 + \alpha_1) \tag{3.4}$$

$$y_2 = \frac{D_1}{2}\sin\alpha_2 \tag{3.5}$$

$$\alpha = \pi - \angle B'O_1'O_2 = \pi - 2\arcsin\frac{D_2}{2D_1} \text{ (constant)} \tag{3.6}$$

$$\alpha_1 = 2\pi N_1 \Delta t \tag{3.7}$$

$$\alpha_2 = -2\pi N_2 \Delta t \tag{3.8}$$

Then the position of $B_{\Delta t}$ can be described as the following equation by substituting Equations (3.2)-(3.8) into Equation (3.1):

$$\begin{cases} x_{\Delta t} = \dfrac{D_1}{2}\cos(-2\pi N_2 \Delta t) + \dfrac{D_1}{2}\cos\left(\pi - 2\arcsin\left(\dfrac{D_2}{2D_1}\right) + 2\pi N_1 \Delta t - 2\pi N_2 \Delta t\right) \\ y_{\Delta t} = \dfrac{D_1}{2}\sin(-2\pi N_2 \Delta t) + \dfrac{D_1}{2}\sin\left(\pi - 2\arcsin\left(\dfrac{D_2}{2D_1}\right) + 2\pi N_1 \Delta t - 2\pi N_2 \Delta t\right) \end{cases} \tag{3.9}$$

By increasing the time *t*, the grinding mark of the cutting point on the wafer surface (within one wheel rotation) can be obtained by the following equation:

$$\begin{cases} x(t) = \dfrac{D_1}{2}\cos(-2\pi N_2 t) + \dfrac{D_1}{2}\cos\left(\pi - 2\arcsin\left(\dfrac{D_2}{2D_1}\right) + 2\pi N_1 t - 2\pi N_2 t\right) \\ y(t) = \dfrac{D_1}{2}\sin(-2\pi N_2 t) + \dfrac{D_1}{2}\sin\left(\pi - 2\arcsin\left(\dfrac{D_2}{2D_1}\right) + 2\pi N_1 t - 2\pi N_2 t\right) \end{cases} \tag{3.10}$$

$$0 \le t \le \frac{1}{2\pi N_1}\left(4\arcsin\left(\frac{D_2}{2D_1}\right)\right)$$

Please note that more grinding marks can be generated as the time further increases in the following ranges:

$$\frac{k}{N_1} \le t \le \frac{1}{2\pi N_1}\left(4\arcsin\left(\frac{D_2}{2D_1}\right)\right) + \frac{k}{N_1} \qquad k = 0,1,2,3,4\ldots.$$

The same procedure can be applied to develop the mathematical model if the wafer and the wheel rotate in different directions.

## 3.4 Computer Programs for the Mathematical Model

The model developed above is used to develop programs with a commercial software package Matlab (The MathWorks, Inc., 3 Apple Hill Drive, Natick, MA 01760, USA). All programs accept SDSG parameters (i.e. wheel rotation speed $N_1$, wafer rotation speed $N_2$, wheel diameter $D_1$, and wafer diameter $D_2$) as input variables and plot the grinding marks as output.

**Figure 3.3 Illustration of Rotation Directions of the Wafer and the Wheels**

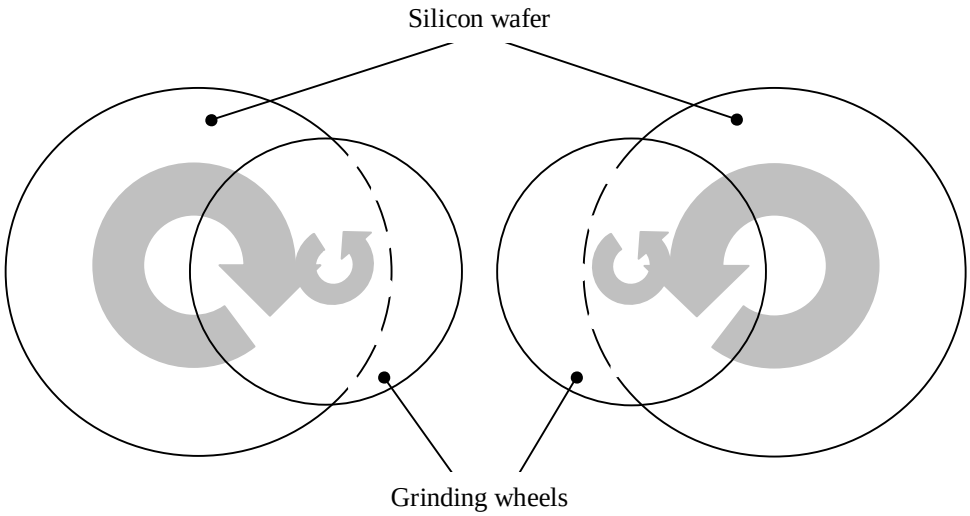


(a) Wafer front side (b) Wafer back side

The rotation directions of the two wheels and the wafer in SDSG operation are illustrated in Figure 3.3. For wafer front side, the wheel rotates in counter clockwise (C.C.W.) direction while the wafer rotates in clockwise (C.W.) direction. For wafer back side, the wheel rotates in C.C.W. direction while the wafer rotates in C.C.W. direction. In the rest of this chapter, unless specified otherwise, the wafer has a diameter of 300 mm while the wheel has a diameter of 160 mm.

Simulation results are used to study the effects of SDSG parameters on the distance between adjacent grinding marks and the curvature of the grinding marks. The distance between two adjacent grinding marks is obtained through dividing the wafer circumference by the number of total grinding marks around the wafer center.

## 3.5 The Effects of Process Parameters on Grinding Marks

### *3.5.1 Effects on the Distance between Adjacent Grinding Marks*

**Figure 3.4 Effects of Speed Ratio and Wheel Diameter on the Distance between Grinding Marks on Wafer Front Side**

| | | Speed ratio $N_1/N_2$ | | |
|---|---|---|---|---|
| | | 5 | 10 | 20 |
| Wheel diameter $D_1$ (mm) | 150 | 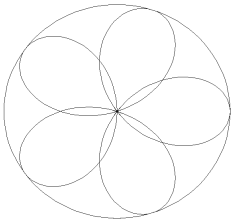 | 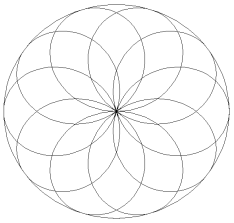 | 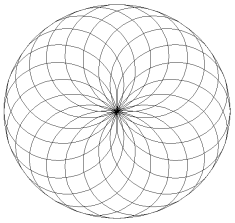 |
| | 200 | 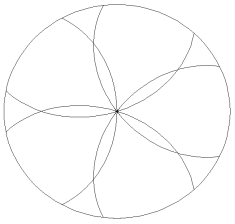 | 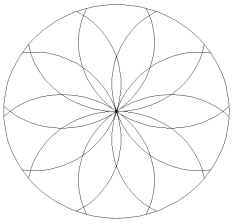 | 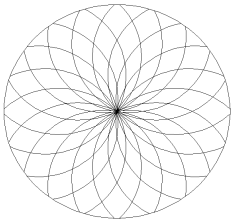 |
| | 250 | 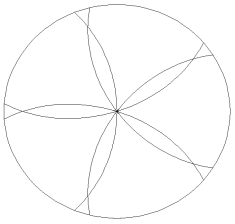 | 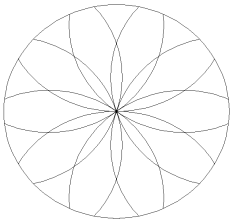 | 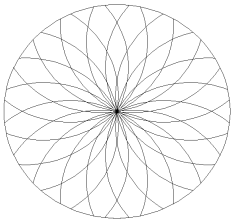 |

**Figure 3.5 Effects of Speed Ratio and Wheel Diameter on the Distance between Grinding Marks on Wafer Back Side**

| | | Speed ratio $N_1/N_2$ | | |
|---|---|---|---|---|
| | | 5 | 10 | 20 |
| Wheel diameter $D_1$ (mm) | 150 | 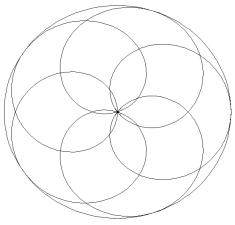 | 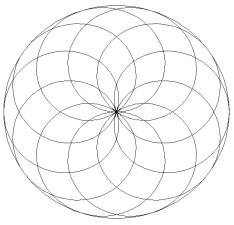 | 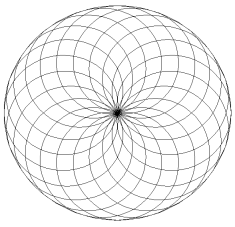 |
| | 200 | 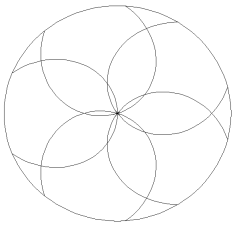 | 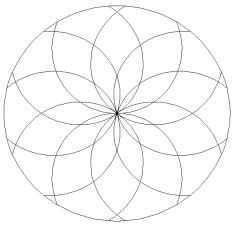 | 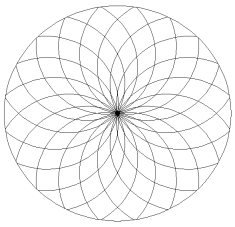 |
| | 250 | 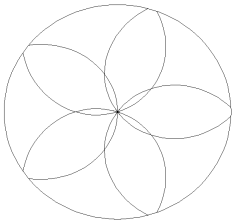 | 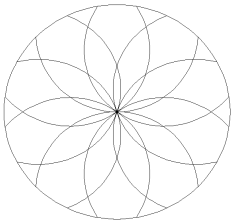 | 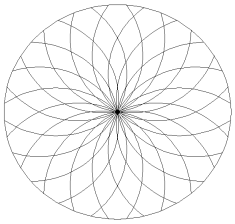 |

Figs. 3.4 and 3.5 show the effects of process parameters ($N_1/N_2$: ratio of the wheel rotation speed versus the wafer rotation speed; $D_1$: wheel diameter) on the distance between adjacent grinding marks on the front and back sides of the wafer, respectively. The distance between adjacent grinding marks on the front side is the same as that on the back side. As the speed ratio increases, the distance between adjacent grinding lines decreases. As the wheel diameter increases, the line distance does not change.

### *3.5.2 Effects on the Curvature of Grinding Marks*

**Figure 3.6 Effects of Speed Ratio and Wheel Diameter on the Curvature of Grinding Marks on Wafer Front Side**

| | | Speed ratio $N_1/N_2$ | | |
|---|---|---|---|---|
| | | 5 | 10 | 20 |
| Wheel diameter $D_1$ (mm) | 150 | 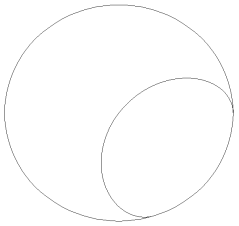 | 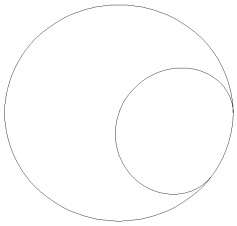 | 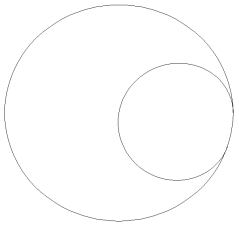 |
| | 200 | 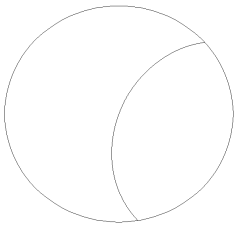 | 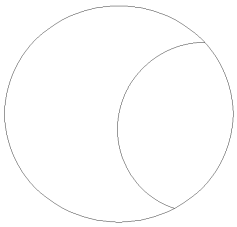 | 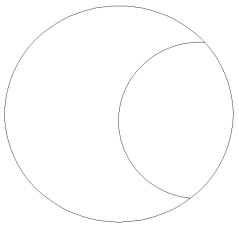 |
| | 250 | 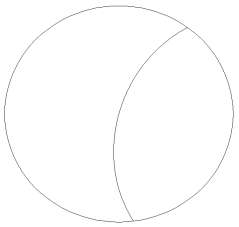 | 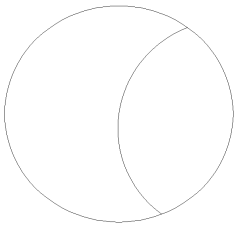 | 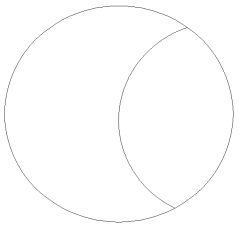 |

**Figure 3.7 Effects of Speed Ratio and Wheel Radius on the Curvature of Grinding Marks on Wafer Back Side**

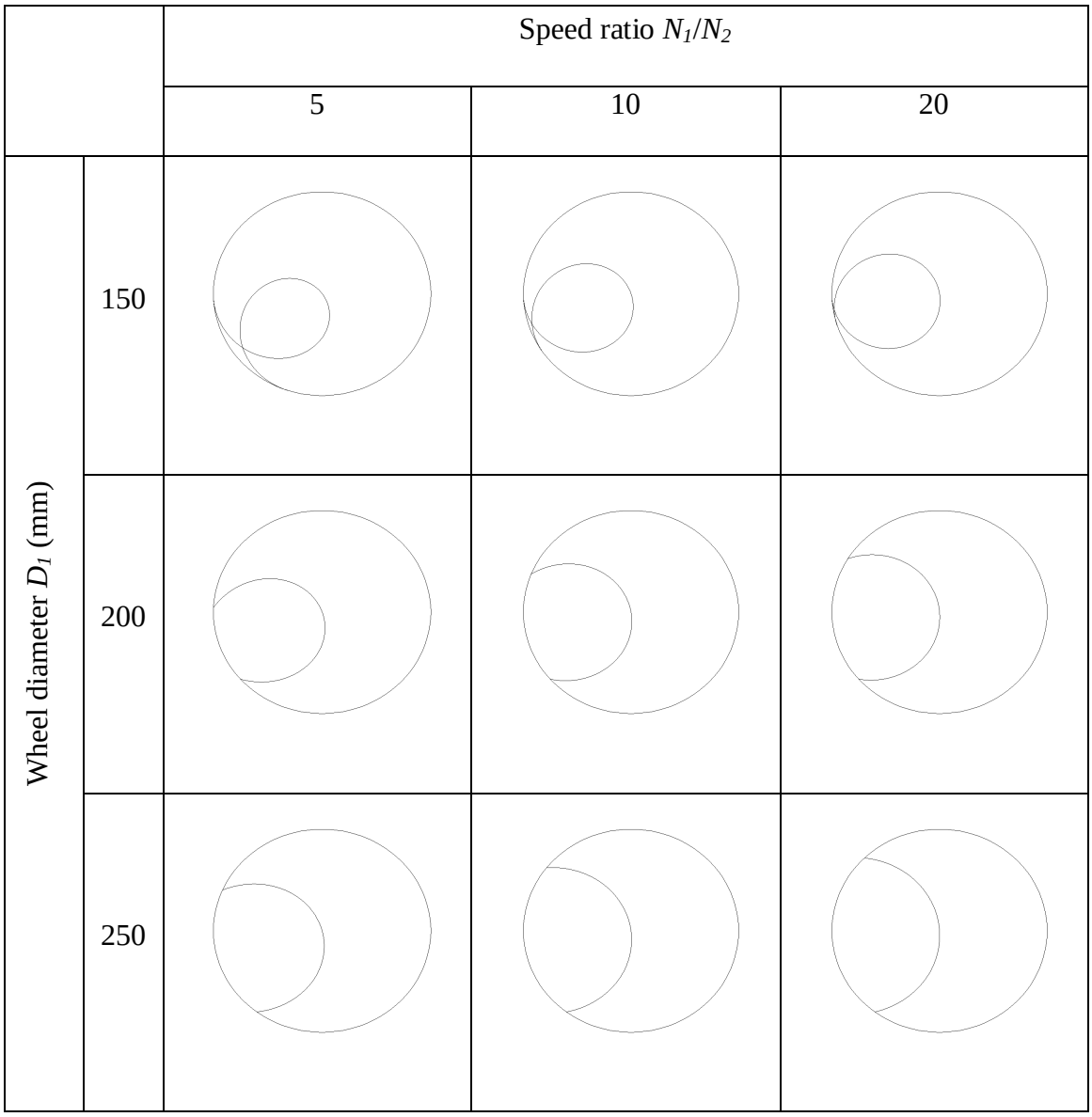


Figs. 3.6 and 3.7 show the variation of the grinding mark curvature on both wafer sides as the speed ratio (the wheel rotation speed versus the wafer rotation speed) and the wheel diameter change. It can be seen that the grinding mark curvature on one side of the wafer is different from that on the other side due to different rotation directions of the two grinding wheels. For both wafer sides, as the speed ratio increases, the grinding marks tend to be less curved. Furthermore, as the wheel diameter increases, the grinding marks also become less curved.

## 3.6 Conclusions

In this chapter, a mathematical model is developed for the grinding marks in SDSG of silicon wafers. The following conclusions can be drawn from this study:

1) The grinding mark curvature on the front side of the wafer is different from that on the back side due to different rotation directions of the two grinding wheels.
2) The distance between the adjacent grinding lines on both sides of the wafer is determined by the ratio of the wheel rotation speed versus the wafer rotation speed. As the ratio of the wheel rotation speed versus the wafer rotation speed increases, the line distance increases. The wheel diameter does not affect the line distance.
3) The curvature of the grinding marks is determined by the wheel diameter and the ratio of the wheel rotation speed versus the wafer rotation speed. As the wheel diameter increases, the grinding lines tend to become less curved. As the speed ratio increases, the grinding lines tend to become less curved.

# CHAPTER 4 - A Mathematical Study on Wafer Shape in SDSG

## 4.1 Introduction

The wafer shape in this paper is the shape of the wafer surface (Sun et al., 2004; Piestch and Kerstan, 2005). The wafer shape has significant effects on the wafer flatness. It is important to understand and control the wafer shape generated by the SDSG process.

Mathematical models have been reported for the part surface profile in cylindrical face grinding of steel parts (Shih and Lee, 1999) and for the wafer shape in SSG of silicon wafers (Sun et al., 2004; Tso and Teng, 2001; Zhou et al., 2003). These models can potentially be used to study the wafer shape in SDSG but no such study has ever been published. Pietsch and Kerstan (2005) presented a mathematical model for the wafer shape in SDSG, but did not report any systematical study on the effects of SDSG parameters on the wafer shape.

In this chapter, following the introduction section, assumptions for a mathematical model for the wafer shape in SDSG are presented in section 2. Derivations and computer programs for the mathematical model are developed in section 3 and section 4, respectively. In section 5, this developed model is used to systematically study the effects of SDSG parameters on the wafer shape. Conclusions are drawn up in Section 6.

## 4.2 Assumptions for the Mathematical Model

**Figure 4.1 Illustration of the "Roll" Angle (α) and "Pitch" Angle (β)**

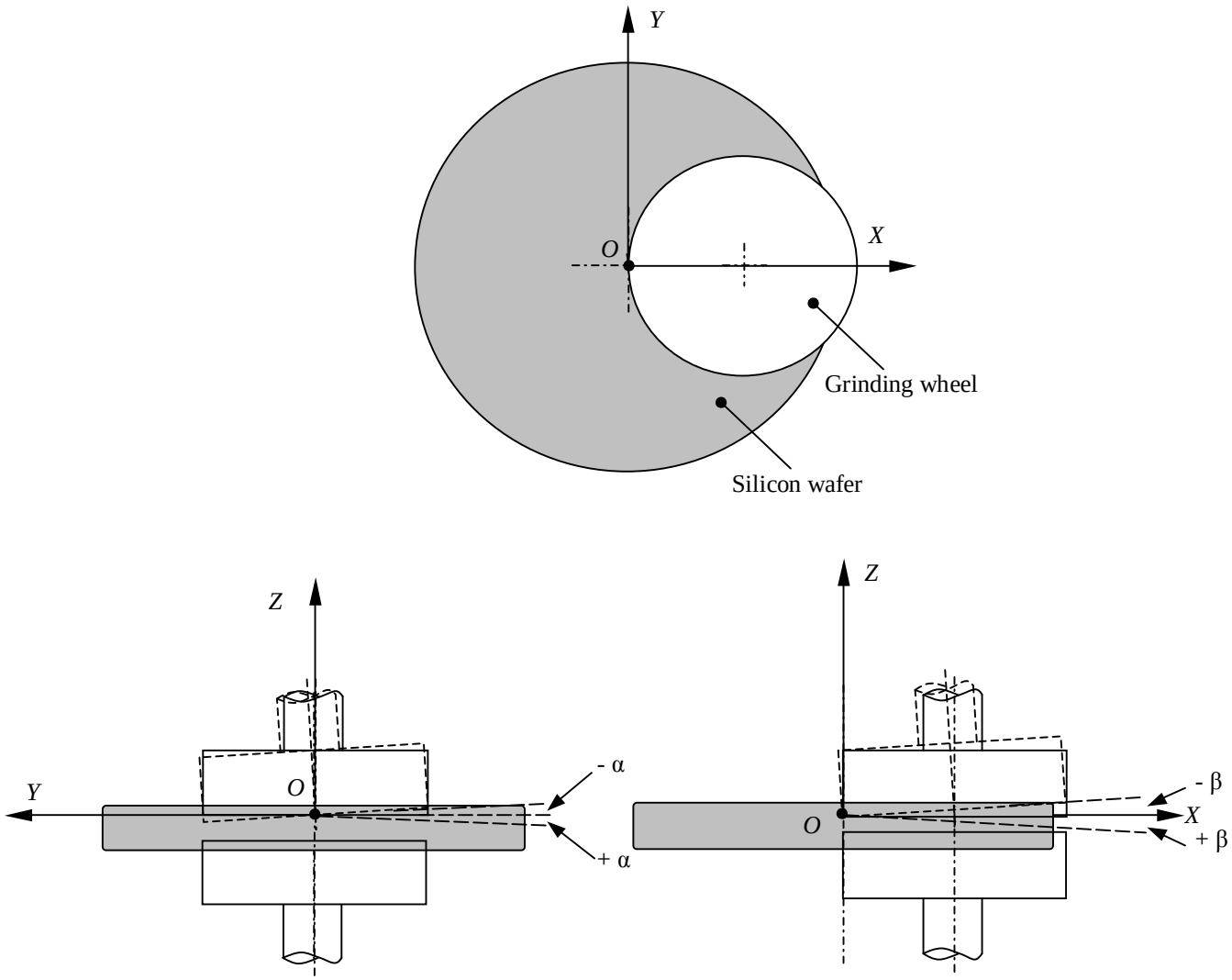


For the model in this chapter, each grinding wheel in the SDSG process is assumed as a ring of rotating abrasives and the ring of rotating abrasives always passes through the wafer center. As shown in Figure 4.1, the "roll" angle α is defined as the tilt angle of the grinding wheel around the *OX* axis. The "pitch" angle is defined as the tilt angle of the grinding wheel around the *OY* axis. In this paper, the wafer shape studied is the shape of one surface of the wafer. It is determined by the "roll" and "pitch" angles of the grinding wheel that grinds this side of the wafer. The shape of the other surface of the wafer can be studied in the same manner.

**Figure 4.2 Geometry for Developing the Wafer Shape Model**

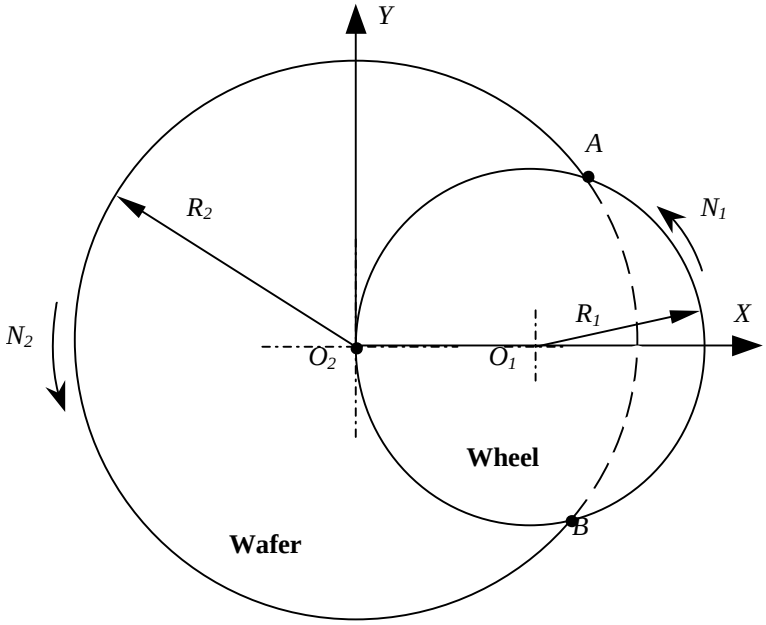


As illustrated in Figure 4.2, the ring of rotating abrasives enters the wafer surface at point *A* along arc $AO_2B$, and exits the wafer surface at point *B*. A coordinate system $XO_2Y$ is used to define all the points on the wafer and the grinding wheel. The origin of the $XO_2Y$ coordinate system is at the center of the wafer. Mathematically, the envelope swept by arc $AO_2B$ when it is rotated around the *Z*-axis forms the wafer shape.

## 4.3 Derivations of the Mathematical Model

When the wheel surface is parallel to the $XO_2Y$ plane ($\alpha = 0$ and $\beta = 0$), arc $AO_2B$ can be described by the following equations:

$$\begin{cases} X(t) = R_1 \cos(2\pi N_1 t) + R_1 \\ Y(t) = R_1 \sin(2\pi N_1 t) \\ Z(t) = 0 \end{cases}, \quad \frac{\pi - 2\arcsin\left(\frac{R_2}{2R_1}\right)}{2\pi N_1} \le t \le \frac{\pi + 2\arcsin\left(\frac{R_2}{2R_1}\right)}{2\pi N_1} \tag{4.1}$$

where *X(t)*, *Y(t)*, and *Z(t)* are the coordinate components of every point on arc $AO_2B$; $R_1$ and $R_2$ the wheel diameter and wafer diameter, respectively; $N_1$ the wheel rotation speed; *t* the time.

When the wheel is tilted around the *X*-axis by an angle of α and around the *Y*-axis by an angle of β, arc $AO_2B$ will be represented as:

$$\begin{bmatrix} X'(t) \\ Y'(t) \\ Z'(t) \end{bmatrix} = \begin{bmatrix} 1 & 0 & 0 \\ 0 & \cos\alpha & -\sin\alpha \\ 0 & \sin\alpha & \cos\alpha \end{bmatrix} \cdot \begin{bmatrix} \cos\beta & 0 & \sin\beta \\ 0 & 1 & 0 \\ -\sin\beta & 0 & \cos\beta \end{bmatrix} \cdot \begin{bmatrix} R_1\cos(2\pi N_1 t) + R_1 \\ R_1\sin(2\pi N_1 t) \\ 0 \end{bmatrix} \tag{4.2}$$

$$\text{or: } \begin{cases} X'(t) = \cos\beta[R_1\cos(2\pi N_1 t) + R_1] \\ Y'(t) = \sin\alpha\sin\beta[R_1\cos(2\pi N_1 t) + R_1] + \cos\alpha[R_1\sin(2\pi N_1 t)] \\ Z'(t) = -\cos\alpha\sin\beta[R_1\cos(2\pi N_1 t) + R_1] + \sin\alpha[R_1\sin(2\pi N_1 t)] \end{cases} \tag{4.3}$$

The relation between the length in wafer radial direction and the height of the wafer surface can be obtained from the above equation. This relation will produce a line profile to describe the wafer shape (2-D). The 3-D wafer shape can be obtained by rotating the line profile around the *Z*-axis.

## 4.4 Computer Programs for the Mathematical Model

The model developed above is used to write programs with a commercial software package Matlab (The MathWorks, Inc., 3 Apple Hill Drive, Natick, MA 01760, USA). All programs accept SDSG parameters (i.e. the "roll" angle α in micro-radian (μrad), the "pitch" angle β in μrad, the wheel radius $R_1$, and the wafer radius $R_2$) as input variables and plot the wafer shapes (2-D or 3-D) as output. In the rest of this paper, unless specified otherwise, the wafer has a diameter of 300 mm while the wheel has a diameter of 160 mm.

## 4.5 Simulation Results and Discussion

### *4.5.1 Basic Wafer Shapes*

Figure 4.3 shows the wafer shapes (3-D) for different combinations of the "roll" angle and "pitch" angle. It can be seen that there are eight basic wafer shapes generated by changing the "roll" angle and the "pitch" angle. Note that the wafer shape is not affected by the tilt direction of the "roll" angle, hence the wafer shapes shown in Figure 4.3(a,d,g) are the same as those in Figure 4.3(c,f,i), respectively.

**Figure 4.3 3-D Wafer Shapes for Different Combinations of "Roll" and "Pitch" Angles**

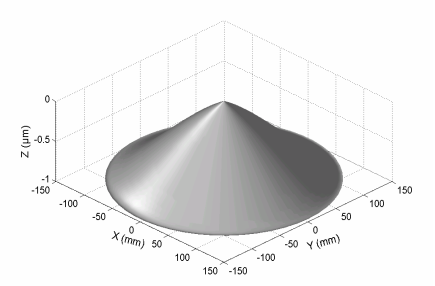


(a) α = +5 µrad, β = +5 µrad

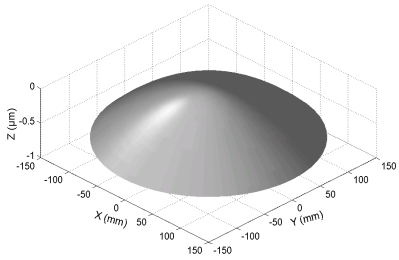


(b) α = 0 µrad, β = +5 µrad

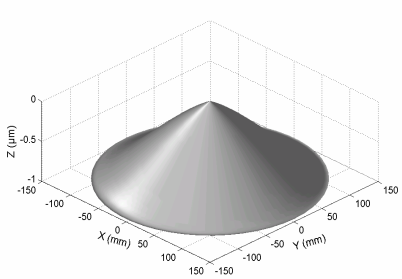


(c) α = -5 µrad, β = +5 µrad

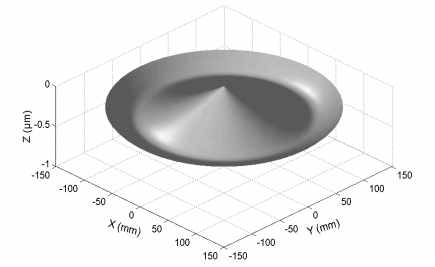


(d) α = +5 µrad, β = 0 µrad

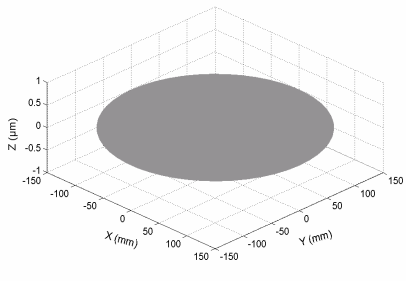


(e) α = 0 µrad, β = 0 µrad

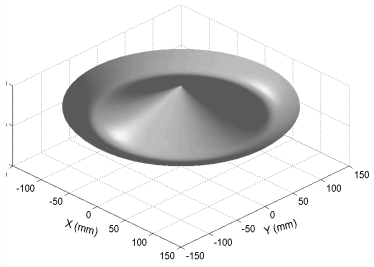


(f) α = -5 µrad, β = 0 µrad

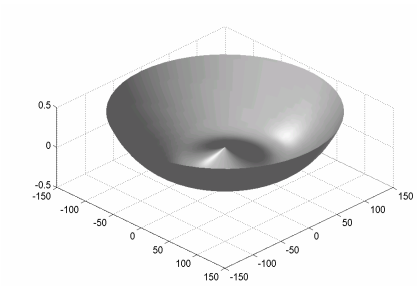


(g) α = +5 µrad, β = -5 µrad

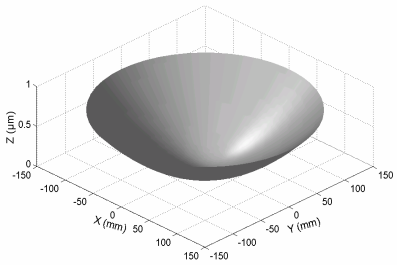


(h) α = 0 µrad, β = -5 µrad

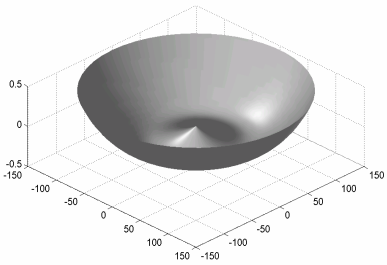


(i) α = -5 µrad, β = -5 µrad

**Figure 4.4 Two Components of the Wafer Shape (Sun et al., 2005)**

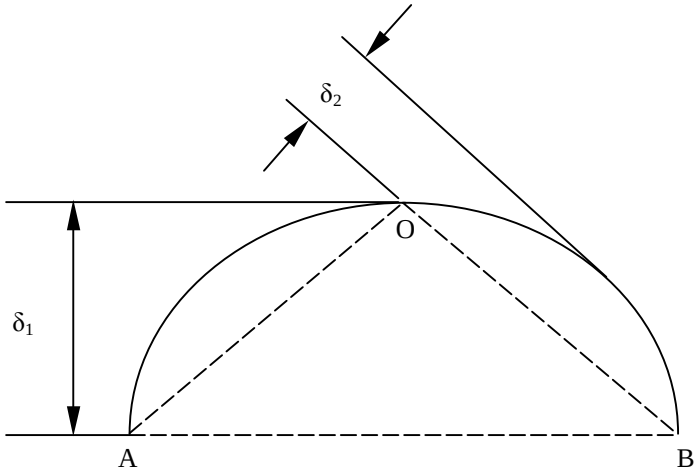


For further discussion, the wafer shape is resolved into two components, the virtual component and the elliptical component as shown in Figure 4.4 (Sun et al., 2005). The virtual component characterizes the wafer shape along the wafer diameter, and is measured by $\delta_1$, the distance from the wafer center (point O) to the line (line AB) connecting two ends (on the diameter of the wafer surface) of the wafer surface. The elliptical component characterizes the wafer shape along the wafer radius, and is measured by $\delta_2$, the maximum distance from any points on the wafer surface to the line (line OA) connecting the wafer center and the edge of the wafer surface. $\delta_1$ and $\delta_2$ are assigned with the "+" or "–" sign by the following rule: when a component (either the virtual component or the elliptical component) is convex, the corresponding distance (either $\delta_1$ or $\delta_2$) will bear a positive sign; when a component is concave, the distance will have a negative sign.

### *4.5.2 Effects of the "Roll" Angle on the Wafer Shape*

**Figure 4.5 Wafer Shape Variation with Different "Roll" Angles (when "Pitch" Angle β = 0 μrad)**

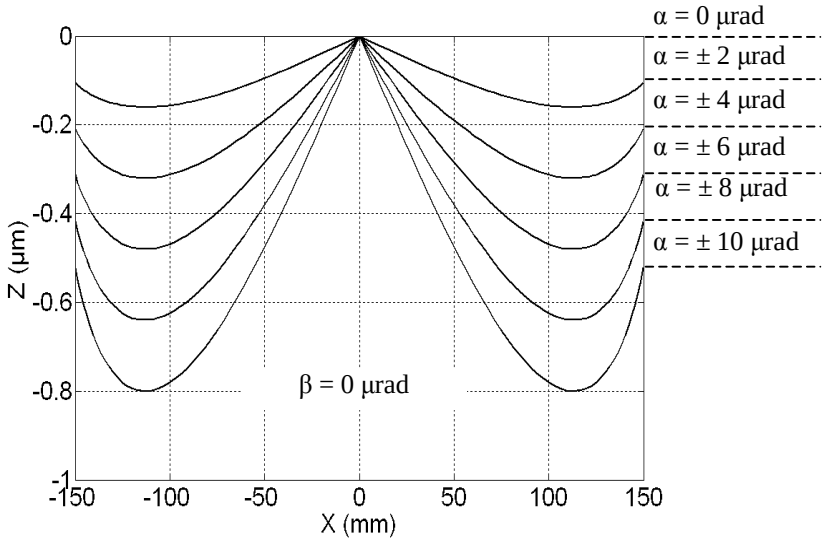


**Figure 4.6 Wafer Shape Variation with Different "Roll" Angles (when "Pitch" Angle β = +2 μrad)**

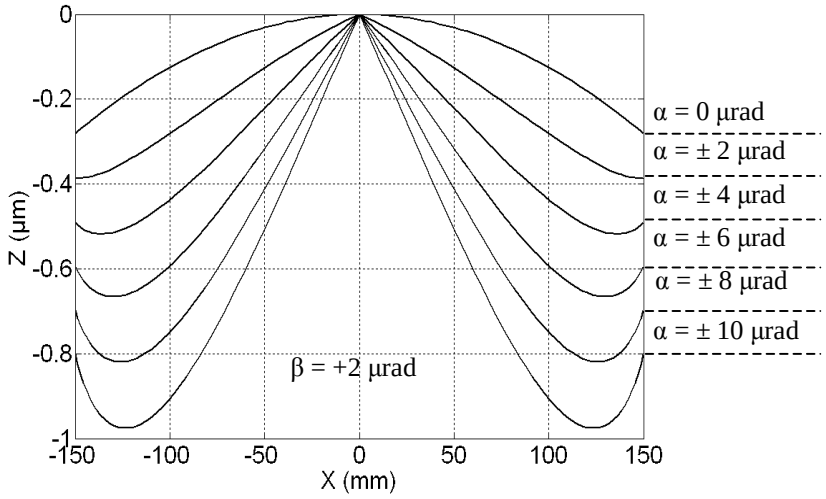

**Figure 4.7 Wafer Shape Variation with Different "Roll" Angles (when "Pitch" Angle β = -2 μrad)**

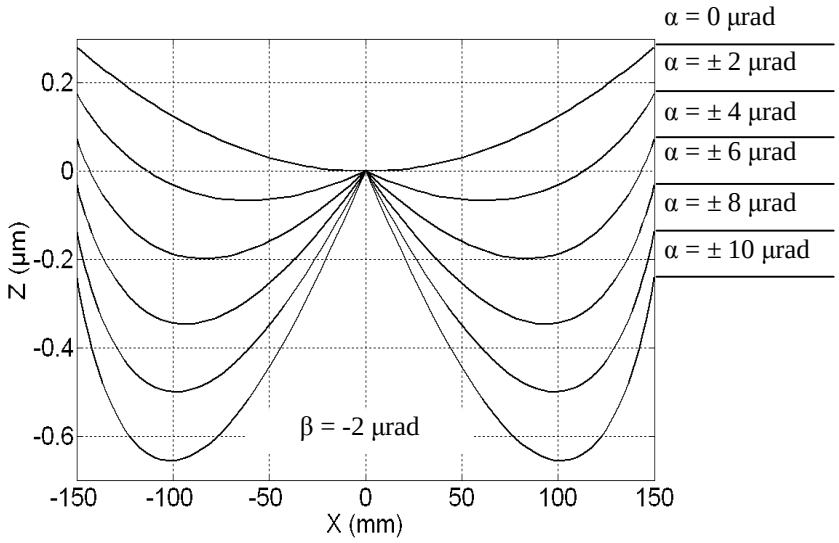


Figure 4.5 shows various wafer shapes for different "roll" angles when the "pitch" angle β = 0 μrad. As the absolute value of the "roll" angle increases, $\delta_1$ increases positively but $\delta_2$ decreases negatively. Figure 4.6 shows various wafer shapes for different "roll" angles when the "pitch" angle β = +2 μrad. As the absolute value of the "roll" angle increases, $\delta_1$ increases positively but $\delta_2$ decreases from positive to negative. Figure 4.7 shows various wafer shapes for different "roll" angles when the "pitch" angle β = -2 μrad. As the absolute value of the "roll" angle increases, $\delta_1$ increases from negative to positive and $\delta_2$ decreases negatively.

### *4.5.3 Effects of the "Pitch" Angle on the Wafer Shape*

**Figure 4.8 Wafer Shape Variation with Different "Pitch" Angles (when "Roll" Angle α= 0 μrad)**

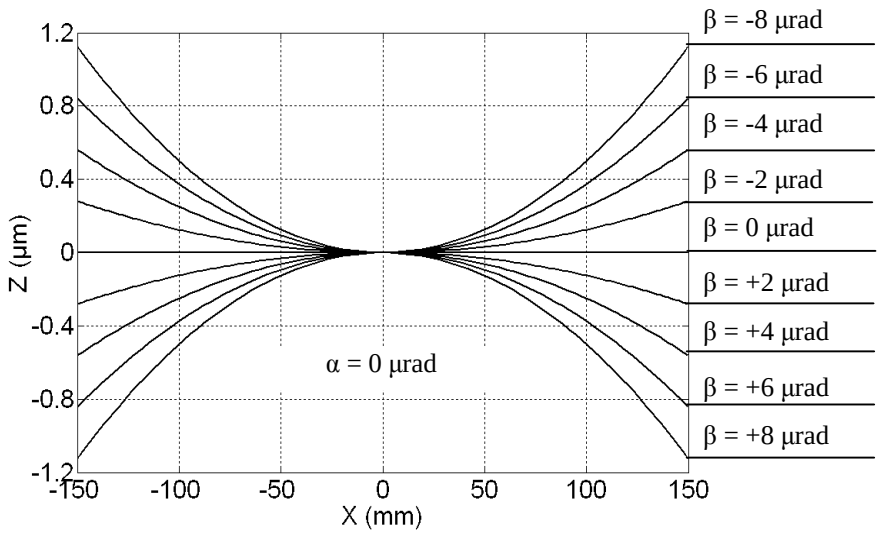

**Figure 4.9 Wafer Shape Variation with Different "Pitch" Angles (when "Roll" Angle α= ±2 μrad)**

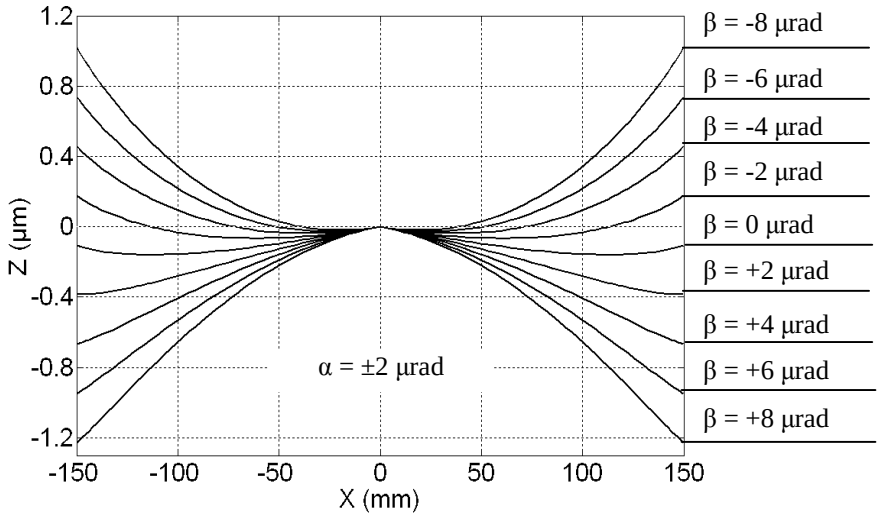


Figs. 4.8 and 4.9 show various wafer shapes for different "pitch" angles when the "roll" angle α = 0 μrad and α = ±2 μrad, respectively. Wafer shapes are not only related to the absolute value but also to the sign of the "pitch" angle. As the "pitch" angle increases from -8 μrad to +8 μrad, both $\delta_1$ and $\delta_2$ increases from negative to positive.

### *4.5.4 Effects of the Wheel Diameter on the Wafer Shape*

**Figure 4.10 Wafer Shape Variation with Different Wheel Radii (α= 0 μrad, β = +5 μrad)**

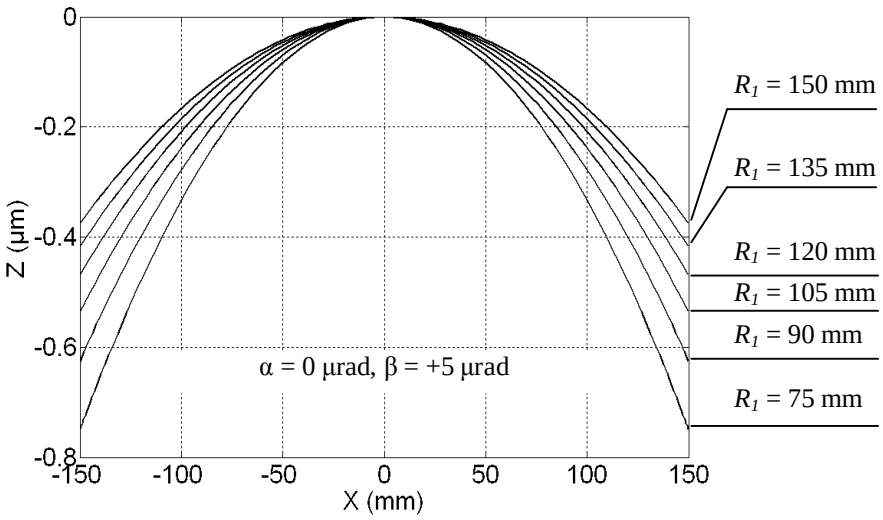

**Figure 4.11 Wafer Shape Variation with Different Wheel Radii (α= 0 μrad, β = -5 μrad)**

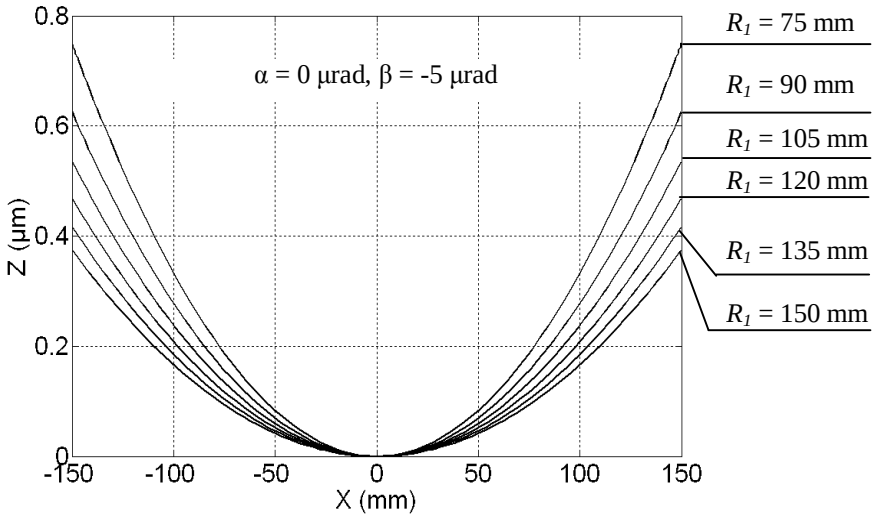


**Figure 4.12 Wafer Shape Variation with Different Wheel Radii (α= ±5 μrad, β = 0 μrad)**

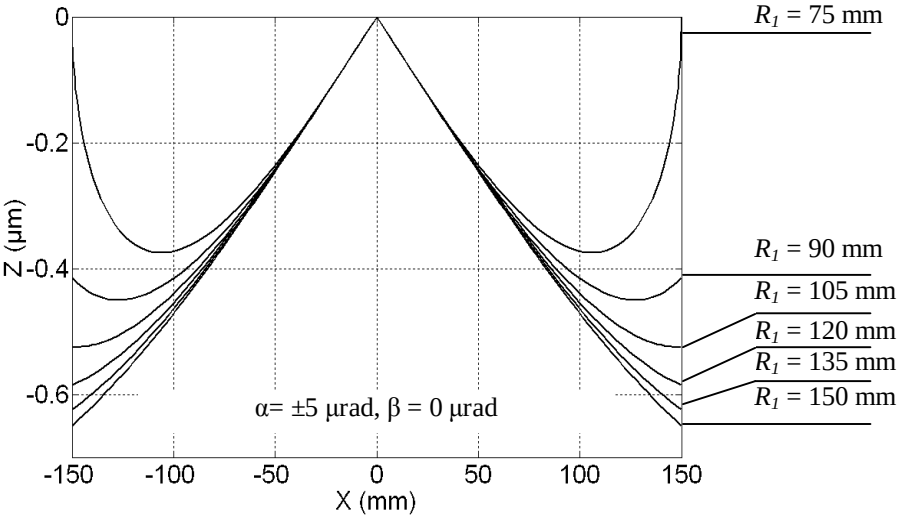


Figure 4.10 shows various wafer shapes as the wheel radius increases from 75 to 150 mm when α = 0 μrad and β = +5 μrad. As the wheel radius increases, both $\delta_1$ and $\delta_2$ decreases positively. Figure 4.11 shows various wafer shapes as the wheel radius increases from 75 to 150 mm when α = 0 μrad and β = -5 μrad. As the wheel radius increases, both $\delta_1$ and $\delta_2$ increases negatively. Figure 4.12 shows various wafer shapes as the wheel radius increases from 75 to 150 mm when α = ±5 μrad and β = 0 μrad. As the wheel radius increases, $\delta_1$ increases positively and $\delta_2$ increases negatively.

## 4.6 Conclusions

In this chapter, a mathematical model is developed for the wafer shape in SDSG of silicon wafers. The following conclusions can be drawn from this study:

1) The wafer shape is related only to the absolute value of the “roll” angle. With the increase of the absolute value of the “roll” angle, $\delta_1$ increases but $\delta_2$ decreases.
2) The wafer shape is not only related with the value of the “pitch” angle but also the tilt direction. As the “pitch” angle increases from negative to positive, both $\delta_1$ and $\delta_2$ increases.
3) The wafer shape is also related with the wheel radius. When it only comes to the “pitch” angle, both $\delta_1$ and $\delta_2$ decreases with the increase of the wheel radius. When only the “roll” angle is involved or both the “roll” angle and the “pitch” angle are involved, both $\delta_1$ and $\delta_2$ increases with the increase of the wheel radius.

# CHAPTER 5 – Finite Element Analysis of Edge Chipping in UVAG

## 5.1 Introduction

In this chapter, a 3-D FEA model for UVAG is developed to investigate the effects of three parameters (cutting depth, support length, and pretightening load) on the maximum stresses (the maximum normal stress and von Mises stress) in the region where the edge chipping initiates. The FEA model is then used to study the relation between the edge chipping thickness and the support length. A possible solution to reduce the edge chipping thickness through increasing the support length is proposed and verified by experiments.

## 5.2 Development of the Finite Element Analysis Model

### *5.2.1 Assumptions for Edge Chipping Initiation*

**Figure 5.1 Illustration of UVAG Process and FEA Parameters**

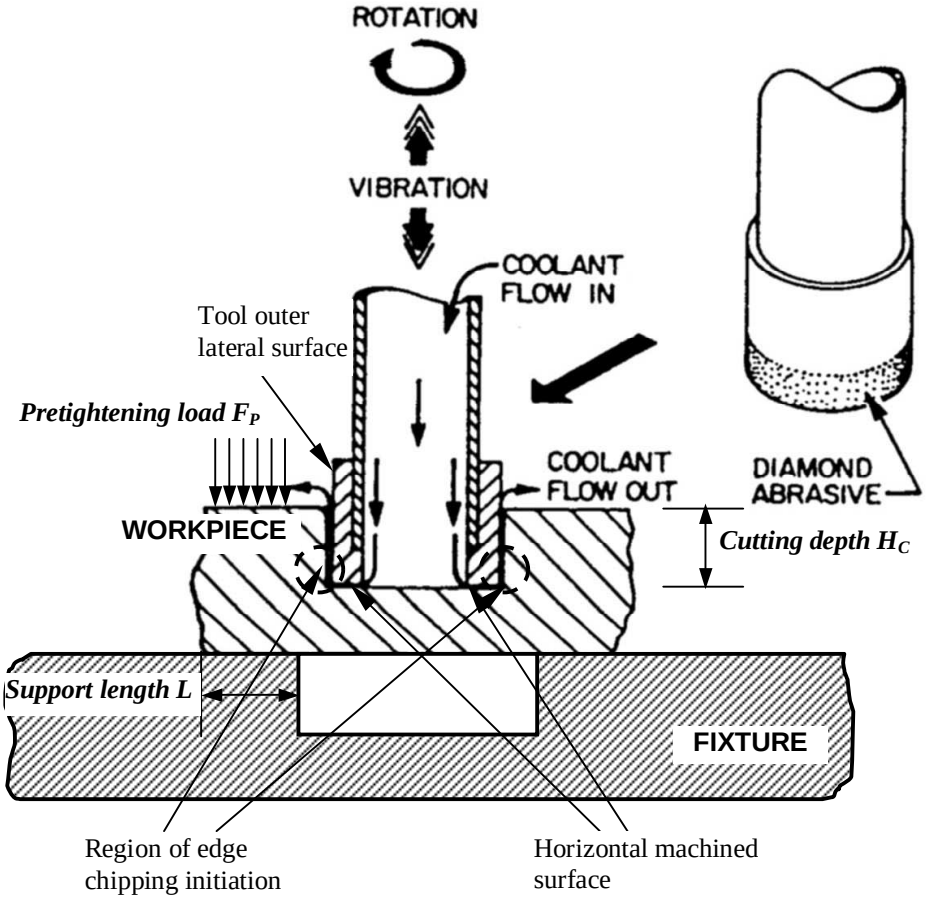

The FEA model in this study only concerns the static stress distribution in the region when edge chipping initiates. The dynamic component of the material removal process is not taken into account. As shown in Figure 5.1, it is assumed that the edge chipping will initiate in a brittle fracture mode when the maximum stress satisfies the failure criterion. The edge chipping thickness predicted by the FEA model is the vertical distance between the location where the edge chipping initiates and the workpiece bottom surface. The two stress failure criteria used are the maximum normal stress criterion and von Mises stress criterion, two commonly used criteria applicable to isotropic materials (Walter, 1997).

**Table 5.1 Workpiece Material Properties**

| Property | Unit | Value |
|---|---|---|
| Young's modulus | MPa | 190 |
| Poisson ratio | | 0.25 |
| Density | $g/cm^3$ | 3.50 |
| Tensile strength | MPa | 130 |
| Compressive strength | MPa | 1750 |
| Vicker's hardness | $kg/mm^2$ | 1190 |

Based on the maximum normal stress criterion, edge chipping is assumed to initiate if $\sigma \geq \sigma_{ut}$ where $\sigma$ is the maximum principle stress obtained from the FEA simulation and $\sigma_{ut}$ is the tensile strength of the workpiece material (listed in Table 5.1).

With the von Mises stress criterion, edge chipping is assumed to initiate when the von Mises equivalent stress reaches the tensile strength of the workpiece material. The von Mises equivalent stress is defined as:

$$\sigma_{eq} = \sqrt{\frac{(\sigma_1 - \sigma_2)^2 + (\sigma_2 - \sigma_3)^2 + (\sigma_1 - \sigma_3)^2}{2}} \tag{5.1}$$

where $\sigma_1$, $\sigma_2$, and $\sigma_3$ are stresses in the principle directions.

### *5.2.2 Geometry and Mesh Design for the FEA Model*

**Figure 5.2 Mesh Design for the FEA Model**

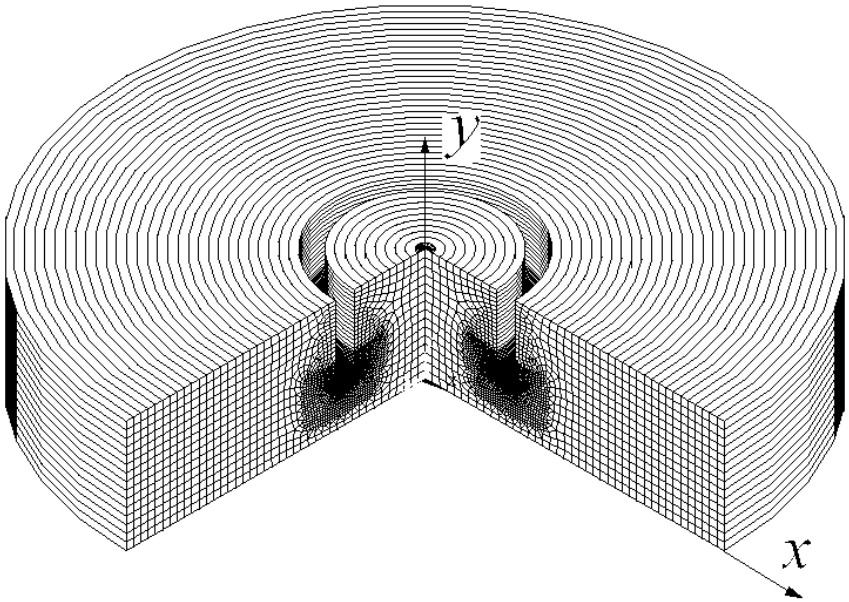


(a) Overview in 3-D coordinates

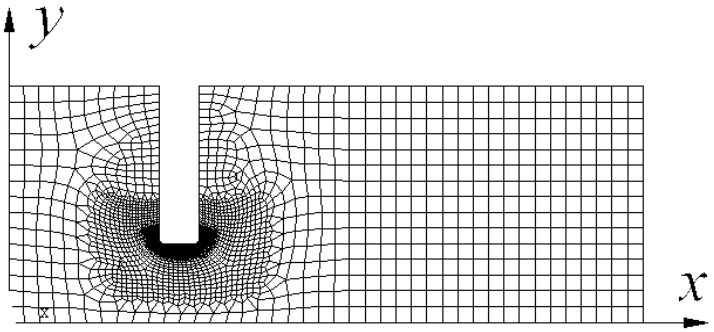


(b) Overview in 2-D coordinates

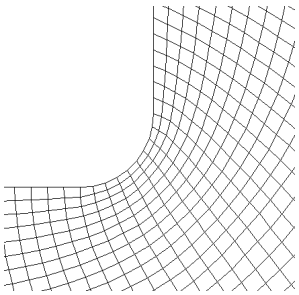

(c) Around the edge chipping initiation region

Three parameters to be studied are defined as follows (refer to Figure 5.2). The cutting depth ($H_C$) is the distance between the top surface of the workpiece and the horizontal machined surface, ranging from 0 to 6.30 mm. The support length ($L$) is the radial length of the contact area between the workpiece and the fixture, ranging from 3 to 11 mm. The pretightening load ($F_P$) is the pressure applied on the top surface of the workpiece to tighten the workpiece, ranging from 3 to 15 MPa.

A commercial software (ANSYS7.0) was used to develop the FEA model. The 3-D FEA model of the workpiece is constructed using axisymmetric eight-node quadrilateral elements. The mesh is shown in Figure 5.3. The elements are refined progressively near the region where the edge chipping initiates. The workpiece is assumed to have a cylinder shape with a radius of 16 mm and thickness of 6.30 mm.

### *5.2.3 Boundary Conditions*

**Figure 5.3 Boundary Conditions and Applied Loads for the FEA Model**

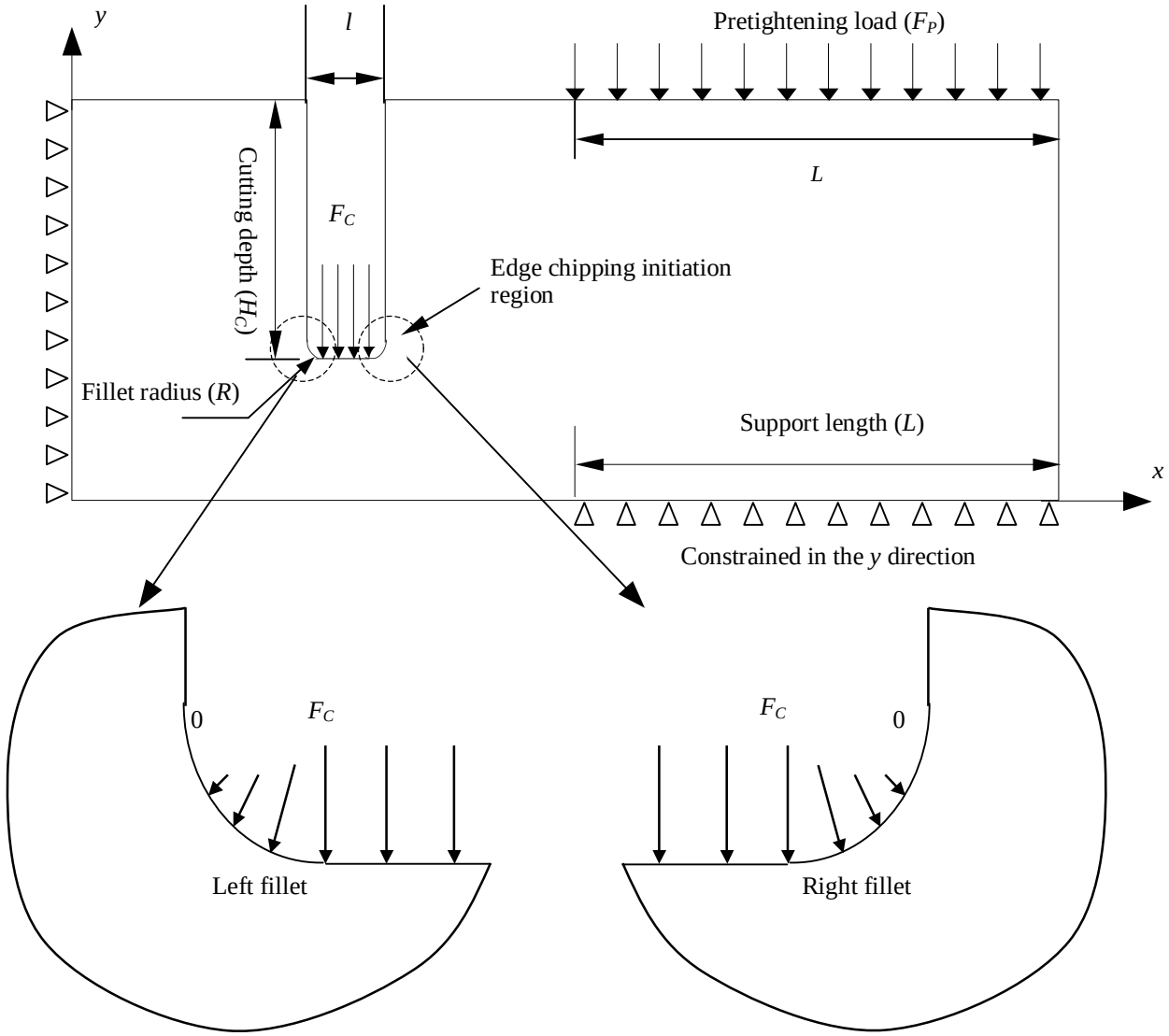

Due to the symmetry of the workpiece and fixture, one half of the workpiece is modeled in the axisymmetric plane, as shown in Figure 5.3. The workpiece is modeled as a rectangle with a rectangular recess. The workpiece is constrained in the *y*-direction on the bottom surface over the support length *L*. The axisymmetric line of the workpiece is constrained in the *x*-direction. A uniformly distributed pressure ($F_P$) is applied on the top surface of the workpiece over a length equal to the support length *L*.

The contact area (with a length of *l*) between the tool end surface and the horizontal machined surface in the workpiece consists of a left fillet contact region, a middle horizontal contact region, and a right fillet contact region. Both of the two fillet contact regions are modeled with a fillet radius of 0.1 mm (approximately equal to the "nose radius" of the end face of the cutting tool). A uniformly distributed pressure ($F_C$ = 15 MPa, a typical value of the grinding force in the tool axial direction when rotary ultrasonic machining of the workpiece material used for this study) is applied to the middle horizontal contact region. A linearly varying pressure, whose value ranges from zero at the vertical edge to $F_C$ at the horizontal edge, is applied on both fillet contact regions, as shown in Figure 5.3.

## 5.3 Results of FEA Simulations

### *5.3.1 Stress Distributions*

**Figure 5.4. Contour Plots of Stress Distributions ($H_C$ = 5 mm; $L$ = 8 mm; $F_P$ = 3.7 MPa)**

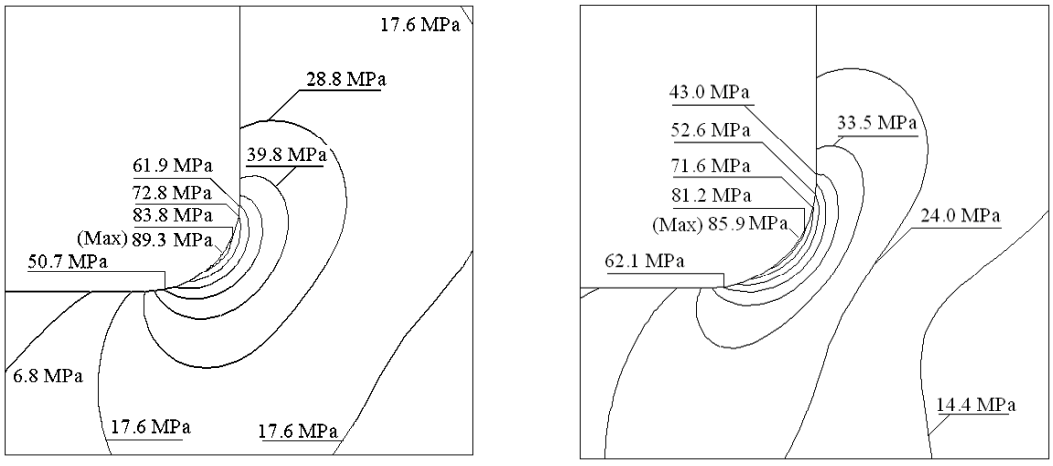


(a) Maximum normal stress (b) von Mises stress

Figure 5.4 shows the distributions of the maximum normal stress and the von Mises stress in the region of edge chipping initiation when $H_C$ = 5 mm, $L$ = 8 mm, and $F_P$ = 3.7 MPa. It can be seen that both of the maximum normal stress and the von Mises stress increase significantly as the distance to the fillet decreases. The maximum values of the two stresses occur on the fillet.

### *5.3.2 Effects of the Three Parameters on the Maximum Stresses*

**Figure 5.5 Effects of Cutting Depth on the Maximum Stress Values**

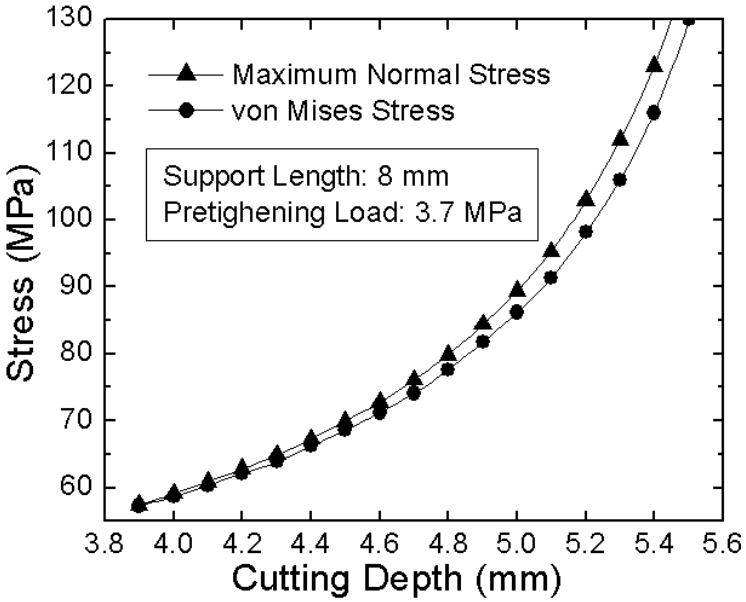


**Figure 5.6 Effects of Pretightening Load on the Maximum Stress Values**

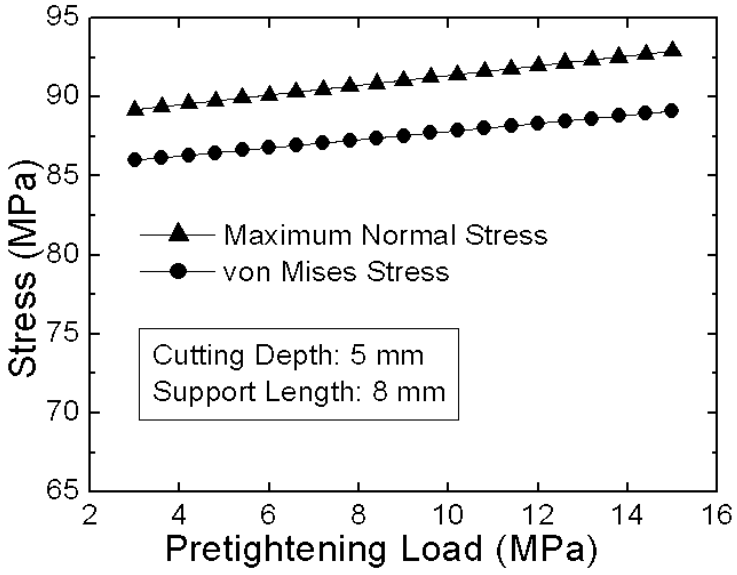

**Figure 5.7 Effects of Support Length on the Maximum Stress Values**

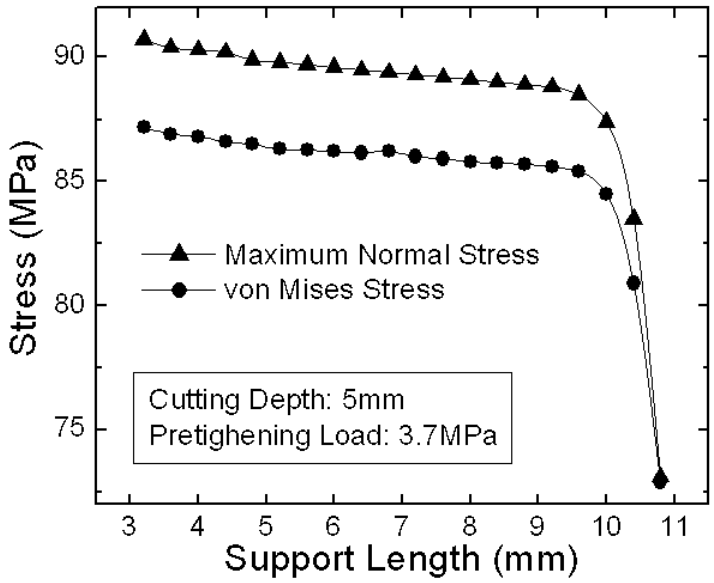


Figs. 5.5-7 show the effects of the three parameters (cutting depth $H_C$, pretightening load $F_P$, and support length $L$) on the maximum values of the maximum normal stress and the von Mises stress. Figure 5.5 shows that the maximum values of the maximum normal stress and the von Mises stress nonlinearly increase as the cutting depth increases. Figure 5.6 shows the effects of the pretightening load. It can be seen that, as the pretightening load increases, the maximum values of the two stresses increase slightly. From Figure 5.7, it can be seen that the maximum values of the two stresses decrease slightly as the support length increases from 3 to 10 mm. When the support length exceeds 10 mm, sharp decreases in the maximum values of the two stresses can be observed. This indicates that increasing the support length can reduce the maximum values of the two stresses. In this way, the edge chipping initiation can be postponed so that the edge chipping thickness can be reduced.

### *5.3.3 Relation between Edge Chipping Thickness and Support Length*

The procedure to estimate the edge chipping thickness using the maximum normal stress criterion is as follows. With the increase of the cutting depth, the maximum values of the maximum normal stress are plotted against support lengths. Based on the maximum normal stress criterion, the critical cutting depth where the edge chipping initiates ($\sigma \geq \sigma_{ut}$) can be found. For the workpiece with the thickness of 6.30 mm, the edge chipping thickness can be

calculated by subtracting the critical cutting depth from the workpiece thickness. For example, when $L$ = 10.5 mm, the critical cutting depth will be 5.47 mm. Hence, the edge chipping thickness = 6.30 – 5.47 = 0.83 mm. A similar procedure was used to estimate the edge chipping thickness based upon the von Mises stress criterion.

**Figure 5.8 Predicted and Experimental Results for the Effects of Support Length on Edge Chipping Thickness ($F_P$ = 3.7 MPa; $F_C$ = 15 MPa for FEA)**

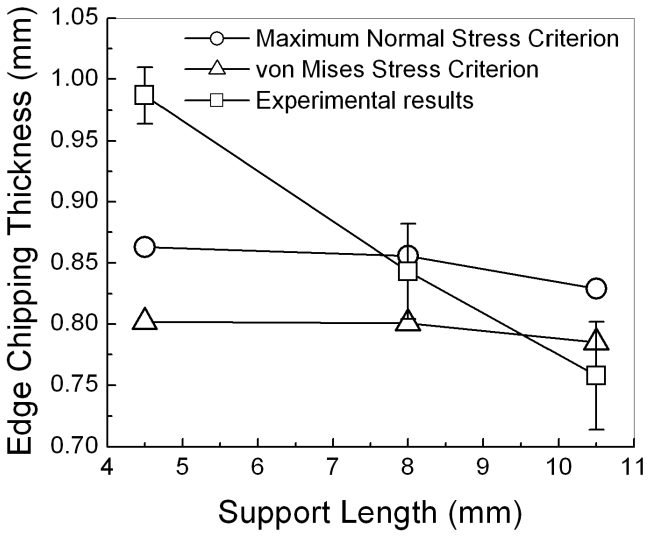


Figure 5.8 shows the predicted relation between the support length and the edge chipping thickness from FEA simulations. With the increase of support length from 4.5 to 10.5 mm, the predicted edge chipping thickness decreases from 0.86 to 0.83 mm when the maximum normal stress criterion is used; the predicted edge chipping thickness decreases from 0.80 to 0.79 mm when the von Mises stress criterion is used.

## 5.4 Pilot Experimental Verification

### *5.4.1 Experimental Setup and Conditions*

**Table 5.2 Experimental Conditions.**

| Machining variable | Unit | Value |
|---|---|---|
| Spindle speed | $rev \cdot s^{-1}$ | 50 |
| Feedrate | $mm \cdot s^{-1}$ | 0.09 |
| Ultrasonic vibration power supply* | | 35% |
| Ultrasonic vibration frequency | kHz | 20 |
| Coolant pressure | MPa | 0.21 |

* Power supply percentage controls the amplitude of ultrasonic vibration.

A series of UVAG tests have been conducted to verify the predicted relation between the support length and edge chipping thickness. In UVAG operation, a blind hole is usually drilled in the fixture under the workpiece to receive the rod, as shown in Figure 5.1. The support length is determined by the diameter of the blind hole. To verify the effects of support length, three blind holes with diameters of 23, 16, and 11 mm, respectively, are drilled in the fixture. Accordingly, three different support lengths of 4.5, 8, and 10.5 mm can be achieved. For each support length, UVAG test is repeated three times.

UVAG tests are performed on an ultrasonic machine of Sonic Mill Series 10 (Sonic-mill®, Albuquerque, NM, USA). For the metal-bonded diamond core drill (N.B.R. Diamond Tool Corp., LaGrangeville, NY, USA), the outer and inner diameters are 9.64 and 7.72 mm, respectively. The mesh size is from 80 to 100. The dimension of the workpieces (92% $Al_2O_3$ sintered) (Ferro-ceramic Grinding, Inc., Wakefield, MA, USA) is 32 mm × 32 mm × 6.30 mm. Properties of the workpiece material are listed in Table 5.1. Mobilemet® S122 water-soluble cutting oil (MSC Industrial Supply Co., Melville, NY, USA) is used as coolant (diluted with water by 1 to 20 ratio). Other UVAG conditions are listed in Table 5.2.

### *5.4.2 Measurement of Edge Chipping Thickness*

A digital video microscope (Olympus DVM-1, Olympus America, Inc., Melville, NY, USA) is utilized to inspect the chipping at the hole exit edge. Using a vernier caliper, the edge chipping thickness is measured on the rod as sketched in Figure 2(b).

### *5.4.3 Experimental Results and Discussion*

**Table 5.3 Experimental Results**

| Support length (mm) | Chipping thickness (mm) | | |
|---|---|---|---|
| | Run 1 | Run 2 | Run 3 |
| 4.5 | 1.01 | 0.99 | 0.96 |
| 8 | 0.89 | 0.83 | 0.81 |
| 10.5 | 0.76 | 0.72 | 0.80 |

The values of the edge chipping thicknesses are listed in Table 5.3. It can be seen that the edge chipping thickness decreases as the support length increases. Figure 5.9 also plots the experimental relation between the support length and the edge chipping thickness. With the increase of support length, the edge chipping thickness decreases. This trend agrees well with that predicted from the FEA simulations.

However, there are differences between the FEA simulations and experimental results. One difference is in the absolute values of the chipping thickness, the other is in the slopes of the curves (or, the degrees of the effects of support length of the chipping thickness). Possible reasons for such differences include that some assumptions of the FEA model may not be accurate.

## 5.5 Conclusions

This chapter presents an investigation into the edge chipping during UVAG of ceramics with the help of FEA simulations. A possible solution to reduce the edge chipping thickness is firstly proposed and validated by experiments. The main conclusions are:

1. As the cutting depth increases, the maximum values of the maximum normal stress and the von Mises stress increase.
2. The effects of pretightening load on the maximum values of the maximum normal stress and the von Mises stress are not significant.
3. There exists a critical support length. As the support length increases before reaching the critical length, the maximum values of the maximum normal stress and the von Mises stress decrease slightly. When the support length exceeds the critical length, there are sharp decreases in the maximum values of the maximum normal stress and the von Mises stress.
4. The edge chipping thickness can be reduced by increasing the support length.

The results of this study have indicated a practical way to reduce or eliminate the edge chipping in ultrasonic vibration assisted grinding of ceramics. The diameter of the blind hole in the fixture underneath the workpiece should be as small as possible (as long as it can still receive the machined rod).

# CHAPTER 6 - Coolant System for UVAG

## 6.1 Introduction

**Figure 6.1 Coolant Delivery Mode by Using AODDP**

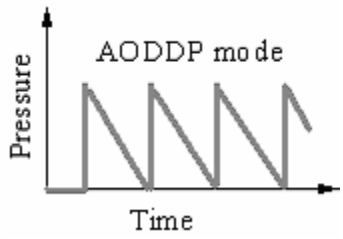


In this chapter, in order to investigate the coolant effects in UVAG process systematically, the air-operated double diaphragm pump (AODDP) is introduced into the UVAG coolant system for the first time. The intermittent coolant delivery mode is realized approximately with the AODDP for its characteristic of intermittent pumping. Figure 6.1 shows the actual coolant delivery mode when using AODDP. Then the vertical cutting force, material removal rate (MRR) and machined surface roughness in different modes and in different coolant pressures when using AODDP are compared and analyzed.

## 6.2 Experimental Setup and Procedure

### *6.2.1 AODDP, UVAG, and Improved Coolant System*

The air-operated diaphragm pump has been developed for handling corrosive liquids and those containing suspensions of abrasive solids. There are two sections separated by a diaphragm of rubber, leather or plastic material. In one section a piston or plunger operates in a cylinder in which a non-corrosive fluid is displaced. The movement of the fluid is transmitted by means of flexible diaphragm to the liquid to be pumped. Under the action of the air distribution system in the AODDP, the reciprocating motion of the diaphragm is realised by the compressed air so that the coolant can be pumped out intermittently. Compared with regular centrifugal pumps, AODDPs are more available in many industrial applications for their inherent features including

ease of maintenance, variable speed, variable pressure, ability of self-prime and run dry, dead-bead capability to pass solids, and the absence of leak prone dynamic seals (Bowan, 1997; Butcher, 1990; Rupp, 1977). Furthermore, more different coolant types (even slurry) and more flexible coolant pressure can be realized for the UVAG process with the AODDP.

**Figure 6.2 Schematic Illustration of Experimental Setup**

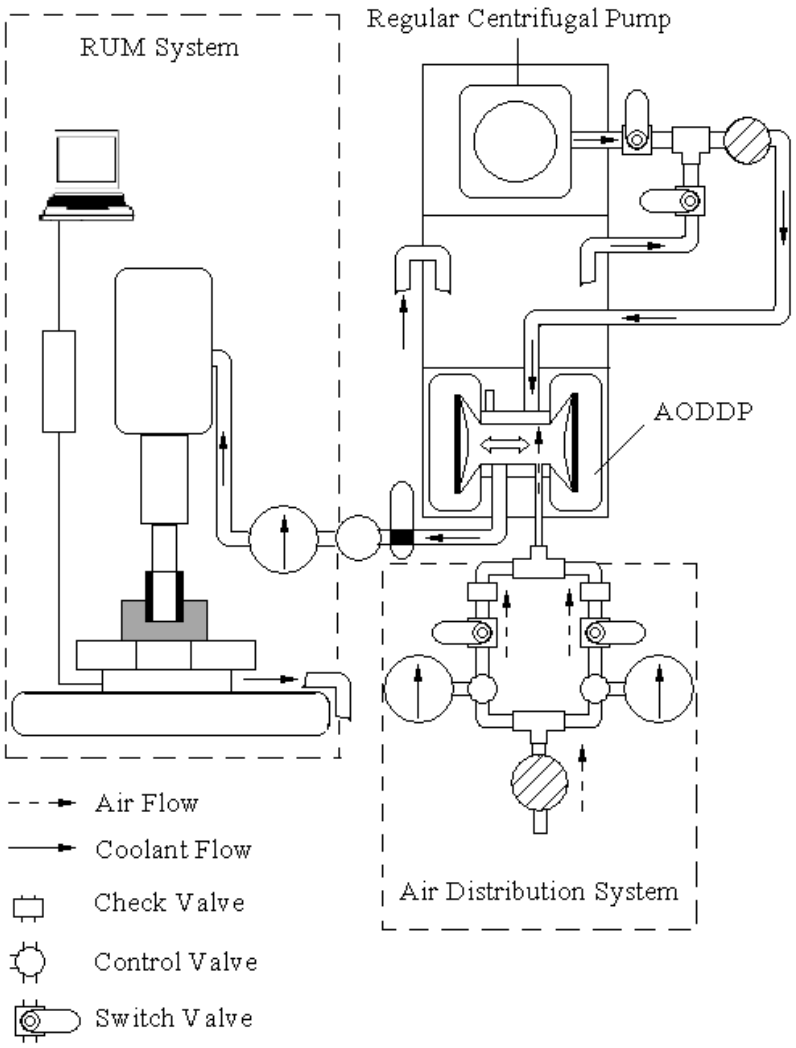


The experimental set-up is illustrated in Figure 6.2. It consists of

- A UVAG system
- A coolant system including a regular centrifugal pump and an AODDP
- An air distribution system for AODDP.

The UVAG system comprises an ultrasonic spindle, a power supply and a motor speed controller. By changing the setting of output control of power supply, the amplitude of ultrasonic vibration can be adjusted. Different rotational speed levels can be obtained by adjusting the motor speed controller. The coolant is pumped by two different pumps (one is the AODDP, the other is the regular centrifugal pump) so that both the stable coolant pressure (continuous mode) and fluctuating coolant pressure (intermittent mode) can be obtained in one system. The air pressure distribution system is employed to achieve different pressure levels for the AODDP.

### *6.2.2 Experimental Conditions*

**Table 6.1 Machining Conditions**

| Condition | Details |
|---|---|
| UVAG machine | Sonic Mill SERIES 10 |
| Diamond core drill | Outer diameter ~3/8", inner diameter ~3/11", grit Mesh Size #140~170, and metal bond |
| Coolant | Mobile met S 122, Mobil Oil Corp, 20:1 dilution of water-soluble cutting oil |
| Centrifugal pump | MSPR7, Graymills |
| AODDP | Ingersoll-Rand Company M 6661A3-344-C |

**Table 6.2 UVAG Parameters**

| Parameter | Value |
|---|---|
| Spindle speed | 3000 (rpm) |
| Feedrate | 0.05 (mm/s) |
| Ultrasonic vibration | Power supply: 30%; Frequency:20 KHz |

The characteristic features of test material (92% Alumina) are the same as those in Table 5.1. The machining conditions are dilated in Table 6.1. The UVAG parameters are listed in Table 6.2.

The cutting force was measured using a KISTLER 9257 dynamometer. The vertical drilling force that is perpendicular to the horizontal plane is measured. A standard unit of 1 kilogram is used to calibrate the dynamometer before test.

The material removal rate (MRR) was determined by the relationship below:

$$MRR = \frac{\pi \cdot \left[ (D_{outer}/2)^2 - (D_{inner}/2)^2 \right] \cdot d}{T} \tag{6.1}$$

where, *Douter* is the diameter of the drilled hole, *Dinner* is the diameter of the drilled rod, *d* is the workpiece thickness, and *T* the time it takes to drill the hole.

The surface roughness is measured on the cylindrical surfaces of machined rods and machined holes along feed direction. The machined hole and machined rod, which are used for measurement of surface roughness after machining, are illustrated in Figure 6 too. The instrument used is Mitutoyo Surftest-402 (Mitutoyo Corp, Japan). The tested range is set as 0.25 mm. Parameter $R_a$ is chosen to represent surface roughness.

## 6.3 Results and Discussion

### *6.3.1 Coolant Output Pressure*

**Figure 6.3 Comparison of Output Coolant Pressure for Different Coolant Delivery Modes**

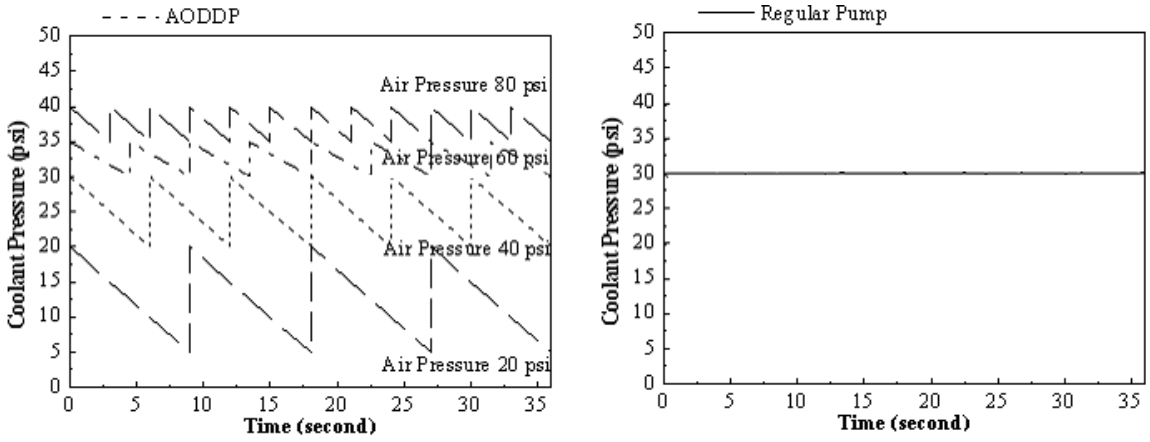


Figure 6.3(a) shows the effect of air pressure on coolant output pressure when using AODDP. Four dotted lines in Figure 6.3(a) reflect four different step-change coolant output pressures (intermittent modes) from AODDP. The solid line in Figure 6.3(b) represents a stable

coolant output pressure (continuous mode) of 30 psi from regular centrifugal pump. It is obvious that the frequency and variation amplitude of the coolant output pressure when using AODDP are dependent on the air pressure applied. The higher the air pressure is, the higher the frequency and the lower the variation amplitude.

The continuous mode of coolant delivery is realized with the regular centrifugal pump while the intermittent mode is realized approximately with the AODDP. The output coolant pressure of the regular centrifugal pump is fixed as 30 psi. As for the AODDP, the output coolant pressure effect on UVAG is investigated by applying different air pressures. Experimental results by using different pumps are put together in the subsequent figures to compare the effect of different pumps (i.e. different coolant delivery modes) on UVAG process.

### *6.3.2 Cutting Force*

**Figure 6.4 Comparison of Cutting Force in Different Coolant Delivery Modes.**

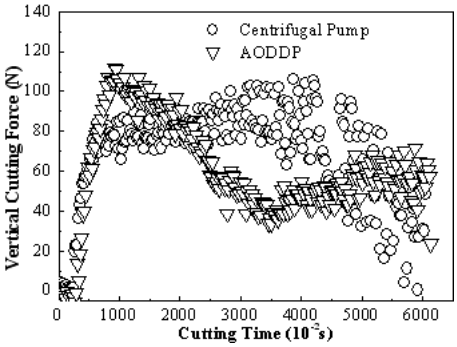


**Figure 6.5 Effect of Coolant Delivery Modes on Cutting Force**

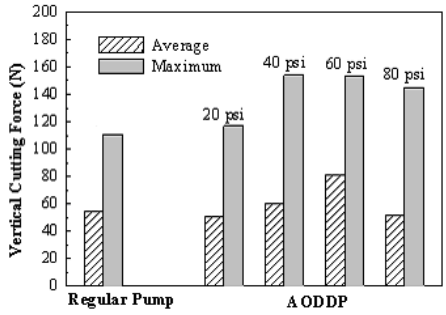


In Figure 6.4 and Figure 6.5, the results of comparison cutting force when machining with different pumps (centrifugal pump and AODDP) show that the pump type (coolant delivery mode) affects the cutting force slightly. The air pressure for the AODDP is about 20 psi (the coolant output pressure can be referred to Figure 6.3) in Figure 6.4. It can be seen that $F_z$ when

machining with regular centrifugal pump is nearly the same as that by using AODDP. The maximum value and average value of the vertical cutting forces when machining with different pumps are compared in Figure 6.5. From Figure 6.5, the vertical force when machining with AODDP will slightly increase with the increase of the air pressure.

### *6.3.3 Material Removal Rate*

**Figure 6.6 Effect of Coolant Delivery Modes on MRR**

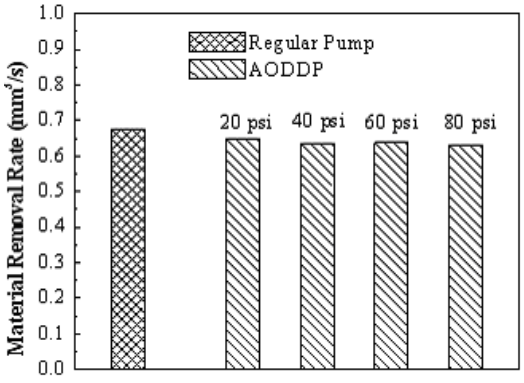


Figure 6.6 shows that the pump type (coolant delivery mode) has no significant effect on MRR. At the same time, under the same machining parameters (spindle speed, feed rate and vibration amplitude) when machining with the AODDP, the MRR will keep at a stable level with the increase of the air pressure. The results are consisting with previous report that the coolant pressure only affects the MRR slightly (Hu et al., 2002).

### *6.3.4 Surface Roughness*

**Figure 6.7 Effect of Coolant Delivery Modes on Cutting Force**

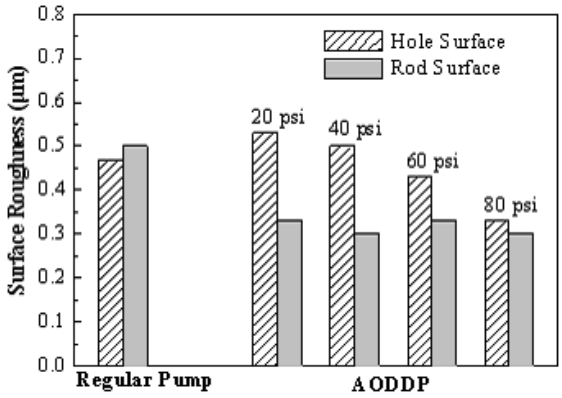

It is interesting to note that the surface roughness after machining decrease obviously, especially for the machined rod surface by using AODDP as shown in Figure 6.7.

From Figure 6.7, compared with the regular centrifugal pump (the surface roughness for the machined hole and machined rod are 0.51 μm and 0.47 μm, respectively), AODDP has no significant effect on the machining hole surface roughness in low air pressure but the hole surface roughness will slightly decrease from 0.55 μm to 0.35 μm with the increase of the air pressure for AODDP. The machined rod surface roughness can be improved obviously by using AODDP when machining and with the increase of the air pressure for AODDP the machined rod surface will keep at a stable level with $R_a$ of 0.31 μm.

In UVAG process, because of the drill vibration, the air gap between the drill bit and the workpiece can be realized so that the coolant can flow in and flow out smoothly when machining. Previous report presented that the machined holes surface roughness will decrease with the increase of the coolant pressure by using regular centrifugal pump (Hu et al., 2002). For AODDP in this report, the average coolant output pressure will increase with the increase of the air pressure, so the same results for machined holes surface roughness can be observed by using AODDP in UVAG as shown as Figure 6.7. The reason can be described as follows: the higher coolant output pressure surely leads to the higher coolant flow rate inside and outside of the core drill, so that more micro swarfs which might have a considerable worse effect on the surface roughness will be washed away from the contact area between drill and workpiece.

## 6.4 Conclusions

A new coolant system with two different pumps (regular centrifugal pump and air-operated double diaphragm pump) has been designed and realized for to study the UVAG processes in two different coolant delivery modes. The coolant output parameters for the intermittent mode such as average value, frequency and variation amplitude when machining by using AODDP under different air pressures have been measured. Experimental investigations have been conducted on effect of coolant pumped by different pumps on the performance of UVAG. Output variables studied include cutting force, MRR, and surface roughness. Major conclusions are:

1) Compared with the regular centrifugal pump, the AODDP has no significant effect on the vertical cutting force and MRR in the UVAG process but obviously affect the machined surface roughness. When using AODDP, the machined holes surface roughness decrease from 0.55 μm to 0.31 μm with the increase of the air pressure from 20 psi to 80 psi.
2) The reason for the improvement of the machined holes surface quality is that the higher coolant output pressure will lead to more micro swarfs, which has a considerable worse effect on the machined surface roughness, be washed away from the contact area between tool and workpiece.

As for the machined rod surface, it can be observed that the machined rod surface roughness decrease significantly by using AODDP in UVAG process.

# CHAPTER 7 - UVAG of Fiber-reinforced Ceramic Matrix Composites

## 7.1 Introduction

In this chapter, the viability of UVAG on two types of fiber-reinforced CMC materials is investigated. Cutting forces and material removal rate are compared for machining of CMC with and without ultrasonic vibration and for two types of CMC materials and one type of ceramic material (92% alumina). Chippings at the hole exit induced by UVAG process are discussed. The main and interaction effects of UVAG process parameters (spindle speed, feedrate, and ultrasonic power) on CMC machining are also studied using a set of designed experiments.

## 7.2 Experimental Conditions and Procedure

### *7.2.1 Setup and Conditions*

**Figure 7.1 Illustration of Experimental Setup**

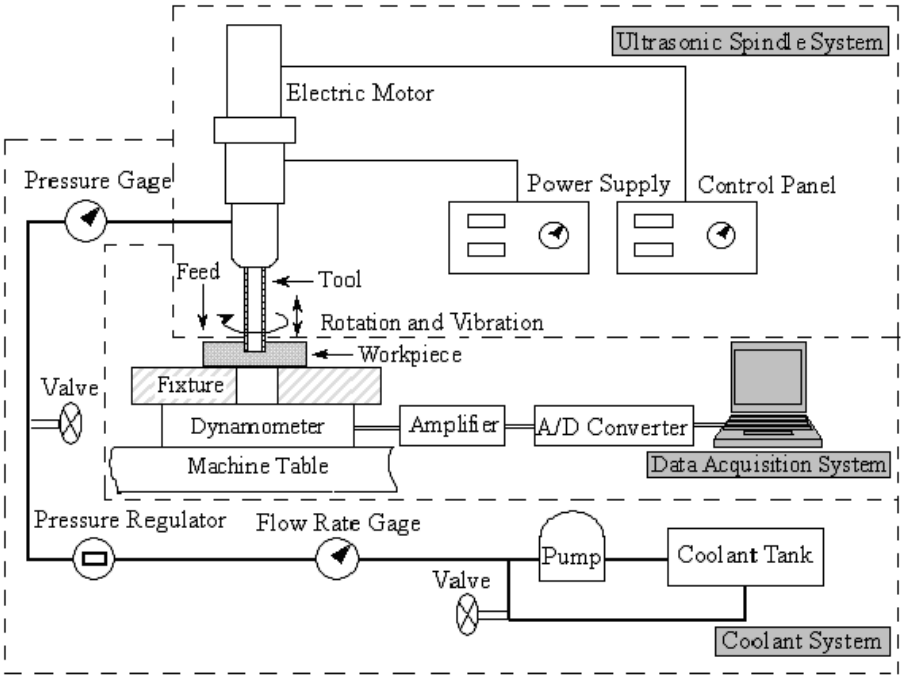

The experimental setup is schematically illustrated in Figure 7.1. It mainly consists of an ultrasonic spindle system, a data acquisition system, and a coolant system. UVAG tests are performed on an ultrasonic machine of Sonic Mill Series 10 (Sonic-mill®, Albuquerque, NM, USA). Diamond core drills (N.B.R. Diamond Tool Corp., LaGrangeville, NY, USA) for UVAG are used to drill CMC and alumina workpieces. The drills with outer and inner diameters of 9.54 mm and 7.82 mm respectively, consist of metal-bonded diamond grains of mesh size from 140 to 170. Mobilemet® S122 water-soluble cutting oil (MSC Industrial Supply Co., Melville, NY, USA) is used as UVAG coolant and diluted with 1 to 20 parts water.

**Table 7.1 Properties of Workpiece Materials**

| Sample | Density ($g/cm^3$) | Specific heat ($J/g\cdot {}^oK$) | Tensile strength (MPa) | Compressive strength (MPa) | Hardness (Vicker's) |
|---|---|---|---|---|---|
| Alumina | 3.5 | 0.71 | 129.4 | 1751 | 1190 |
| CMC #1 | 2.6 | 0.75 | 308.6 | - | ** |
| CMC #2 | * | - | 279.1 | - | ** |

*Determined by water immersion.
**Related to reinforcement fibers.

Two types of CMC panels (Aircraft Wheel & Brakes Goodrich Corp., Santa Fe Springs, CA, USA) are used in this study. CMC #1 panel (110 mm × 120 mm × 3 mm) is fabricated from Nicalon brand (Nippon Carbon Co., Tokyo, Japan) silicon carbide fiber, with converted phenolic resin char, densified by carbon chemical vapor infiltration (CVI) processing. The carbon matrix contains boron carbide filler, which acts as an oxidation inhibiter for this application. The porosity of this panel is 8-10%. CMC #2 panel (110 mm × 120 mm × 3.6 mm) is fabricated from Tyranno brand (Ube Industries Ltd., Ube, Japan) silicon carbide fiber, with a silicon carbide partial matrix, which was further densified by the melt-infiltration process with silicon metal to 1-3% porosity. Alumina workpieces (92% $Al_2O_3$ sintered), supplied by Ferro-ceramic Grinding, Inc., Wakefield, MA, USA, have dimension of 32 mm × 32 mm × 6.35 mm. Properties of these three types of workpieces are listed in Table 7.1.

**Table 7.2 Machining Conditions for the Feasibility Experiments**

| Parameter | Value |
|---|---|
| Spindle speed | 50 ($rev \cdot s^{-1}$) |
| Feedrate | 0.09 ($mm \cdot s^{-1}$) |
| Ultrasonic vibration | Power supply*: 35%; Frequency: 20 (KHz) |
| Coolant pressure | 0.207 (MPa) |

* Power supply percentage controls the amplitude of ultrasonic vibration.

Other machining conditions for the feasibility experiments are presented in Table 7.2.

### *3.2.2 Design of Experiments*

A $2^3$ (three variables, two levels, 8-tests) full factorial design is used for the experiments with 2 replications. Detailed description of factorial design can be found in many textbooks such as the one by DeVor et al. (DeVor et al., 1992). Three UVAG process parameters investigated are:

1) Spindle speed: rotational speed of the diamond core drill;
2) Feedrate: feedrate of the drill in the direction normal to the workpiece surface; and
3) Ultrasonic power: percentage of the high-frequency electrical power, which controls the amplitude of ultrasonic vibration.

**Table 7.3 Variable Levels**

| Variable | Unit | Low level (−) | High level (+) |
|---|---|---|---|
| Spindle speed | $rev \cdot s^{-1}$ | 17 | 50 |
| Feedrate | $mm \cdot s^{-1}$ | 0.09 | 0.15 |
| Ultrasonic power* | | 35% | 50% |

* To control ultrasonic vibration amplitude.

**Table 7.4 Matrix for the Parametric Experiments**

| Test number | Spindle speed | Feedrate | Ultrasonic power |
|---|---|---|---|
| Test 1 & Test 7 | − | − | − |
| Test 2 & Test 5 | + | − | + |
| Test 3 & Test 6 | − | − | + |
| Test 4 & Test 10 | − | + | − |
| Test 8 & Test 9 | − | + | + |
| Test 11 & Test 13 | + | + | + |
| Test 12 & Test 16 | + | + | − |
| Test 14 & Test 15 | + | − | − |

The parameter levels are listed in Table 7.3 and the matrix of the experiments is shown in Table 7.4. These tests are conducted in a random order.

### *3.2.3 Measurement of Output Variables*

**Figure 7.2 Measurement of Cutting Force**

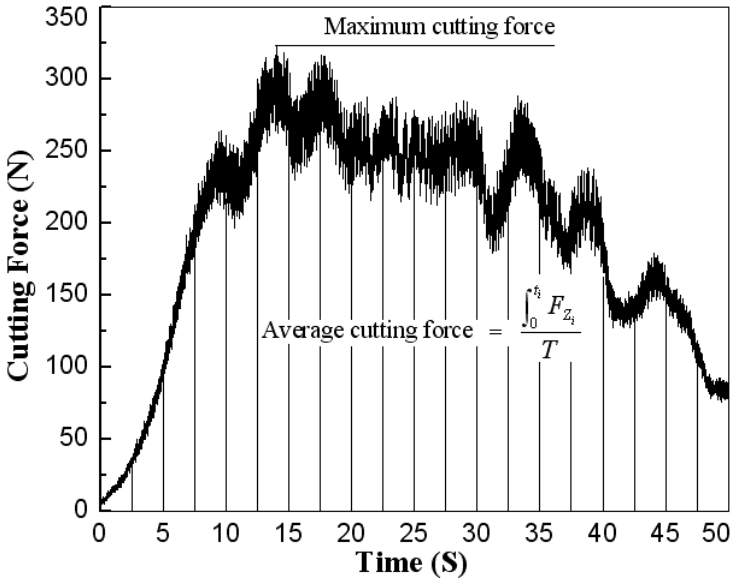

Three output variables are measured: cutting force, material removal rate (MRR), and hole quality. The cutting force along the feedrate direction is measured by a KISTLER 9257 dynamometer (Kistler Instrument Corp, Amherst, NY, US). The dynamometer is mounted atop the machine table and beneath the workpiece to measure the cutting force, as shown in Figure 7.1. The electrical signals from the dynamometer are transformed into numerical signals by an A/D converter. Then the numerical signals to measure the cutting force are displayed and saved on the computer with the help of National Instruments LabVIEW$^{TM}$ (Version 5.1). Sampling frequency to obtain the cutting force signals is 100 Hz. During UVAG tests, both of the maximum and average cutting forces are recorded. The maximum cutting force is the maximum value on the cutting force curve while the average cutting force is the mean value of the entire cutting force curve, as shown in Figure 7.2.

**Figure 7.3 Illustration of CMC Chipping Size and Chipping Thickness**

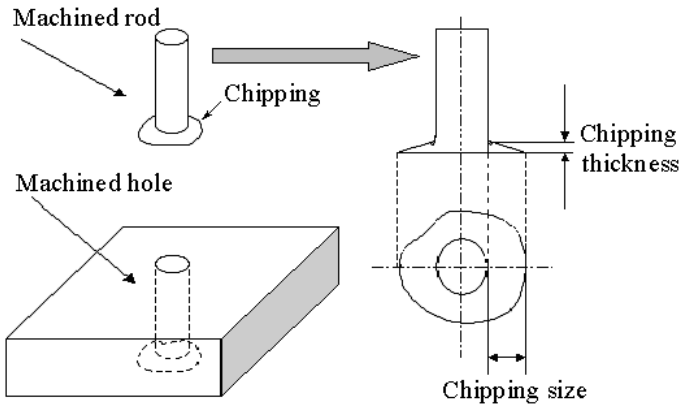


Using equation (6.1), material removal rate (MRR) in the experiments is calculated from measured hole and rod dimensions (as shown in Figure 7.3) and machining time.

A digital video microscope of Olympus DVM-1 (Olympus America Inc., Melville, NY, US) is utilized to inspect the chippings at the exit side of the machined hole. The hole quality is quantified by the thickness and size of the edge chipping formed on the machined CMC rod, as shown in Figure 7.3.

## 7.3 Results of Feasibility Experiments

### *7.3.1 Comparison of Cutting Force*

**Figure 7.4 Comparison of Cutting Forces when Drilling CMC #2 Panel**

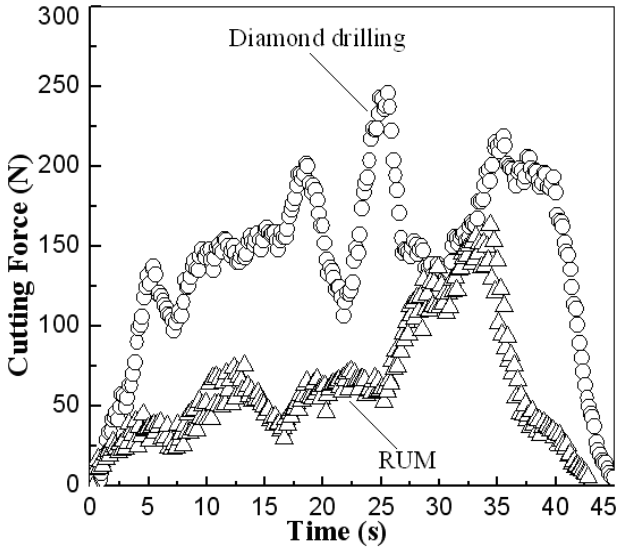


**Figure 7.5 Comparison of Cutting Forces for UVAG and Diamond Drilling**

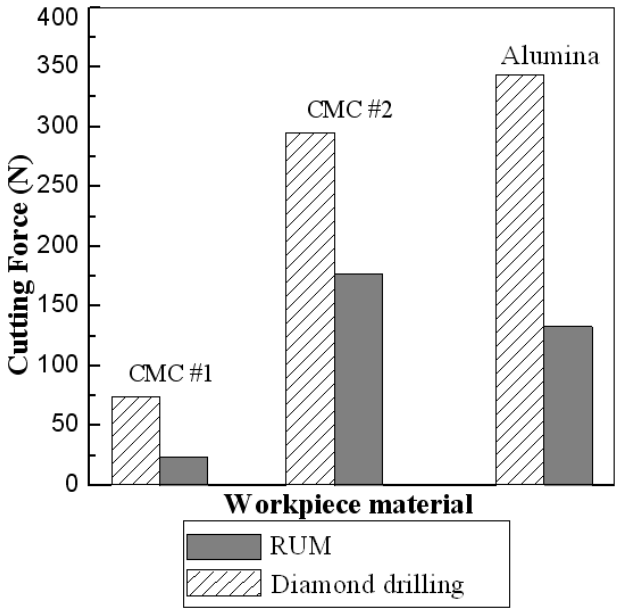

Cutting force curves when UVAG and diamond drilling of CMC #2 panel are displayed in Figure 7.4. It can be seen that cutting forces were significantly reduced with UVAG. Compared with the diamond drilling process, the maximum cutting forces when using UVAG to drill CMC#1, CMC#2, and alumina are about 60%, 40%, and 60% lower respectively, as shown in Figure 7.5. The cutting force results on alumina are consistent with those published earlier, where the maximum value and mean value of the cutting force during UVAG of alumina were about 66% and 65% lower respectively than during diamond drilling (Zeng et al., 2004). The cutting force curves for UVAG of CMC materials exhibit much larger fluctuations, as can be seen in Figure 7.4. This is possibly caused by that the CMC materials have hard inclusions in the ceramic matrix.

### *7.3.2 Comparison of Material Removal Rate*

**Figure 7.6 Comparison of MRR for UVAG and Diamond Drilling**

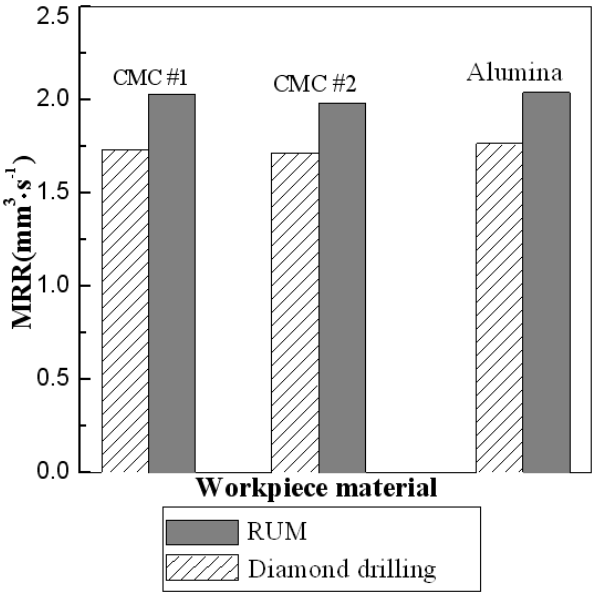


Figure 7.6 compares the MRR in UVAG and diamond drilling. It can be seen that MRR is 10% higher with UVAG than with diamond drilling for both CMC and alumina. A lot of research work has been conducted on comparison between UVAG and USM (Graff, 1975; Petrukha et al., 1970; Markov and Ustinov, 1973; Markov et al., 1977; Markov, 1966). As for comparison of UVAG and diamond drilling, it was believed that the ultrasonic vibration of the tool in UVAG

would not only result in a large dynamic force on the workpiece but also lead to more effective flushing away of debris. Therefore, MRR will increase with the assistance of tool vibration (Zhang et al., 2000).

### *7.3.3 Observation of Chippings*

**Figure 7.7 Chippings of Alumina and CMC #2 after UVAG Process**

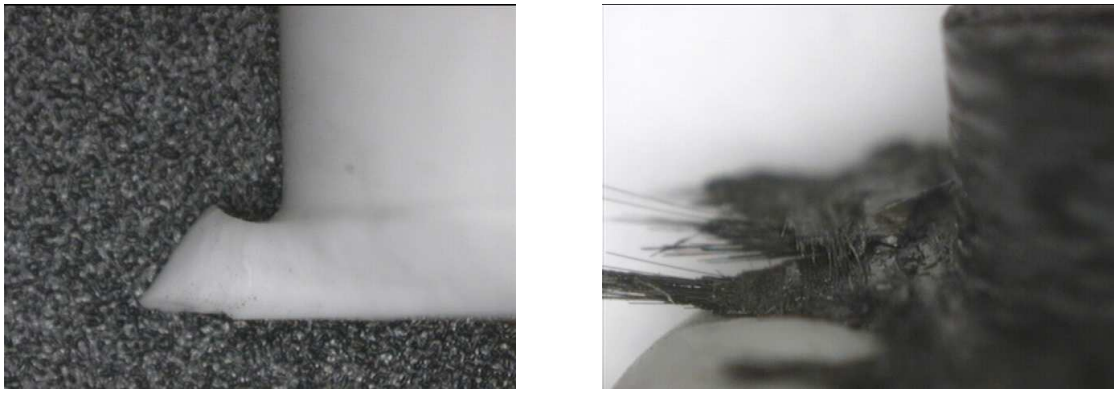

(a) Alumina chippings (b) CMC #2 chippings

The quality of the holes on CMC #1 panel drilled by UVAG is good, however, it becomes unstable when drilling holes on CMC #2 panel with UVAG. The chippings on CMC #2 panel and alumina workpiece after UVAG drilling are shown in Figure 7.7. From Figure 7.7 (a), it can be observed that the cracks in the alumina workpiece occur and propagate along a direction that is about 45° from the workpiece surface and consequently lead to chipping in a brittle fracture mode. As for the CMC #2 panel, chipping originates along the fibers in the panel in a ductile delamination mode, as shown in Figure 7.7 (b).

**Figure 7.8 Observation of the Machined Holes on CMC #2 Panel**

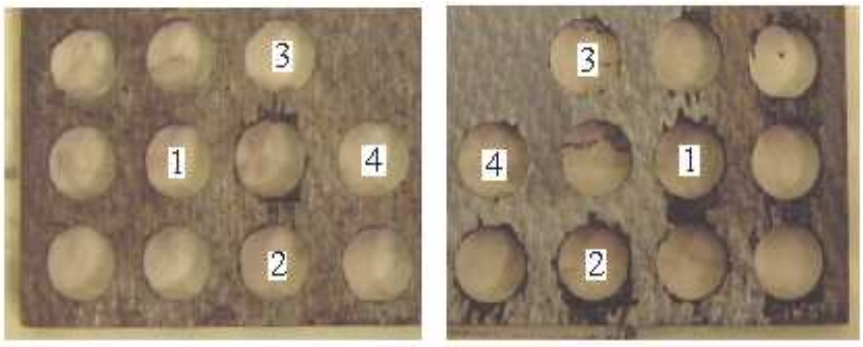


(a) Entrance (b) Exit

This observation of chippings in CMC and alumina workpieces suggests that the mode of CMC chippings in UVAG is ductile interlayer peel-off while the alumina chippings occur as brittle intergranular fracture. The mode of ductile interlayer peel-off makes it possible that the chippings of CMC panel might be reduced or even prevented by adjusting machining parameters or using sharp tools. Actually, some experimental results show that high-quality holes on CMC #2 panel can be obtained with UVAG, as shown in Figure 7.8. The edge quality at the hole entrance is nearly free of fiber pull-out and unaffected by machining conditions, as shown in Figure 7.8 (a). Figure 7.8 (b) shows the edge quality at the hole exits. From Figure 7.8 (b), there are nearly no chippings for hole #3 and hole #4. But hole #1 and hole #2 have severe chippings.

## 7.4 Results of Designed Experiments

In this section, the results of the designed experiments for UVAG on CMC panel #2 are presented. The Software called DESIGN EXPERT (Version 5, Stat-Ease Corporation, Minneapolis, MN, USA) is used to process the data. To identify the significant effects, the analysis of variance (ANOVA) is performed for each output variable. Detailed statistical analysis will not be explained here. Geometric representations of the significant effects at the significance level of $\alpha = 0.05$ (or $\alpha = 0.1$) are presented with discussions.

### *7.4.1 Cutting Force*

As shown in Figure 7.4, the cutting force curves when machining CMC have much significant undulation. This is due to the fiber lamellar structure and some hard inclusions in the CMC materials. These two characteristics of CMC make it difficult to estimate main and interaction effects for the maximum cutting forces. Therefore, the average cutting forces instead of the maximum cutting forces are used in this section.

**Table 7.5 Average Cutting Force Data**

| Spindle speed | Feedrate | Ultrasonic power | Average cutting force (N) | |
|---|---|---|---|---|
| | | | Replication1 | Replication2 |
| − | − | − | 378 | 398 |
| + | − | + | 471 | 476 |
| − | − | + | 407 | 332 |
| − | + | − | 463 | 352 |
| − | + | + | 329 | 397 |
| + | + | + | 443 | 465 |
| + | + | − | 490 | 394 |
| + | − | − | 459 | 472 |

**Figure 7.9 Effects on Average Cutting Force**

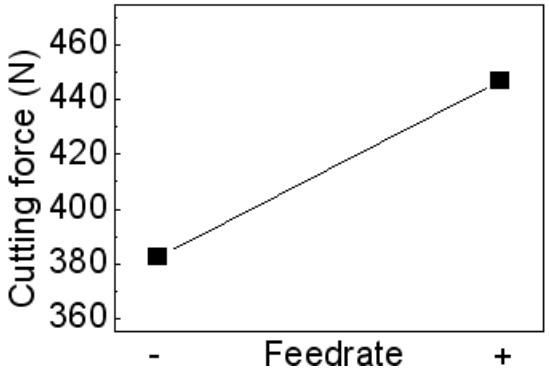


The results on the average cutting forces are shown in Table 7.5. ANOVA results show that only the effect of feedrate is significant at the significance level $\alpha = 0.05$. The main effect of feedrate is shown in Figure 7.9. The average cutting force will increase with the increase of feedrate. There are no significant interactions between the process parameters. This trend is consistent with that when UVAG of alumina (Jiao et al., 2005). However, the earlier study (Jiao et al., 2005) also shows that, for UVAG of alumina, the cutting force will decrease with the

increase of spindle speed and ultrasonic power. Also, there exist significant interactions between the process parameters.

### *7.4.2 Material Removal Rate*

**Table 7.6 Material Removal Rate Data**

| Spindle speed | Feedrate | Ultrasonic power | MRR ($mm^3 \cdot s^{-1}$) | |
|---|---|---|---|---|
| | | | Replication 1 | Replication 2 |
| − | − | − | 1.38 | 1.33 |
| + | − | + | 1.81 | 2.05 |
| − | − | + | 1.55 | 1.45 |
| − | + | − | 1.49 | 1.63 |
| − | + | + | 1.81 | 1.69 |
| + | + | + | 2.14 | 2.24 |
| + | + | − | 1.97 | 1.98 |
| + | − | − | 1.66 | 1.55 |

**Figure 7.10 Effects on Material Removal Rate**

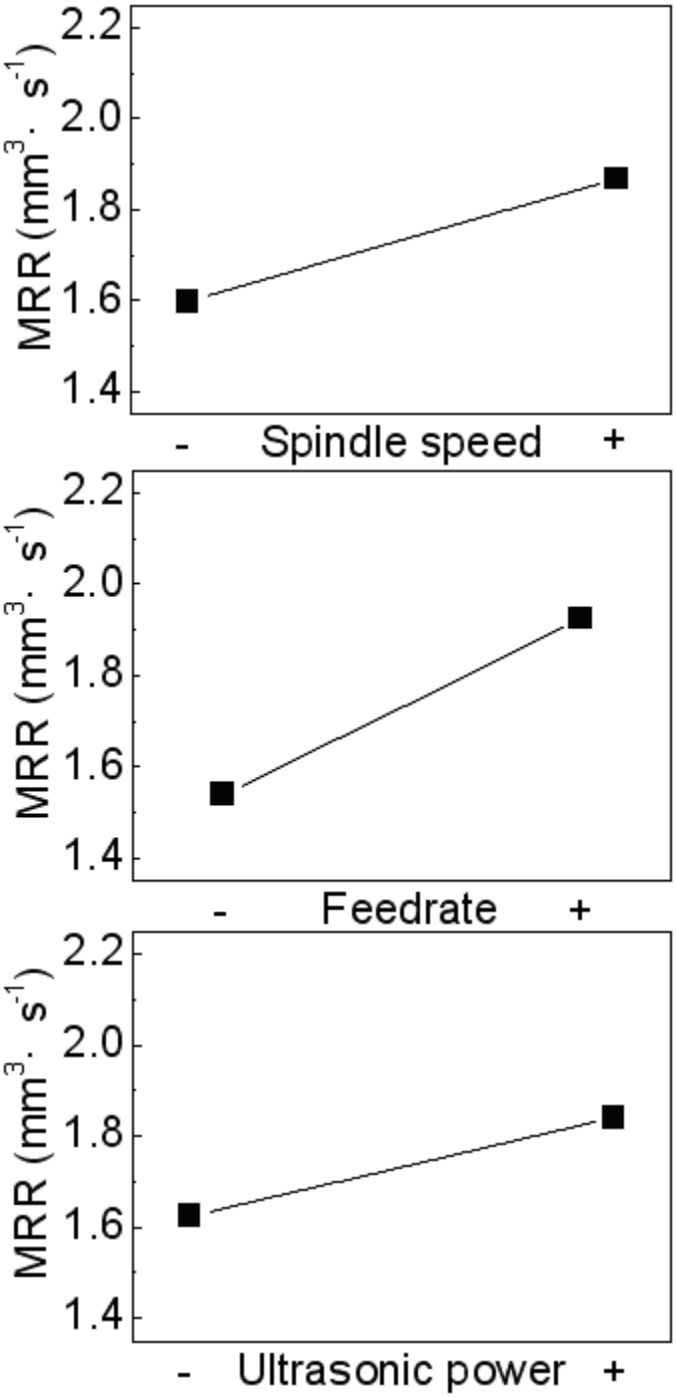


Table 7.6 shows the results on MRR. The main effects of process parameters on MRR are shown in Figure 7.10. ANOVA results show that the effects of spindle speed, feedrate, and ultrasonic power on MRR are significant at the significance level of $\alpha = 0.01$, $\alpha = 0.002$, and

$\alpha = 0.03$ respectively. MRR increases as spindle speed, feedrate, and ultrasonic power increase. There are no significant interaction effects on MRR between the process parameters.

As for spindle speed, current results are consistent with the experimental data on brittle materials reported by Markov and Ustinov that MRR increases as the peripheral speed of the drill is increased (Markov and Ustinov, 1973; Markov, 1977; Markov, 1966). From the theoretical model to predict MRR in UVAG of ceramics (Pei et al., 1995[c]), spindle speed will cause a change in the length of contact which is the distance moved by an indentation abrasive when in contact with the workpiece. As the spindle speed increases, the indentation volume changes proportionally and the MRR will increase.

When it comes to ultrasonic power, which controls the vibration amplitude, current experimental results agree with previous studies on MRR in UVAG of ceramics: MRR will increase with the increase of vibration amplitude (Zhang et al., 2000; Pei et al., 1995[c]; Pei and Ferreira, 1998; Prabhakar et al., 1992). As vibration amplitude increases, the cutting depth of each diamond abrasive bonded on the core drill will increase so that MRR for each diamond abrasive will also increase. The increase of MRR for each diamond abrasive will lead to the increase of MRR for the entire UVAG process.

### *7.4.3 Hole Quality*

**Table 7.7 Hole Quality Data**

| Spindle speed | Feedrate | Ultrasonic power | Chipping thickness (mm) | | Chipping size (mm) | |
|---|---|---|---|---|---|---|
| | | | Replication 1 | Replication 2 | Replication 1 | Replication 2 |
| − | − | − | 0.49 | 0.35 | 4.03 | 3.24 |
| + | − | + | 0.82 | 0.71 | 4.83 | 5.53 |
| − | − | + | 0.52 | 0.37 | 3.53 | 2.01 |
| − | + | − | 0.43 | 0.36 | 3.23 | 1.89 |
| − | + | + | 0.36 | 0.42 | 1.04 | 1.93 |
| + | + | + | 0.54 | 0.49 | 2.88 | 1.45 |
| + | + | − | 0.40 | 0.40 | 1.00 | 2.13 |
| + | − | − | 0.61 | 0.78 | 4.68 | 3.27 |

**Figure 7.11 Relationship between Chipping Thickness and Chipping Size**

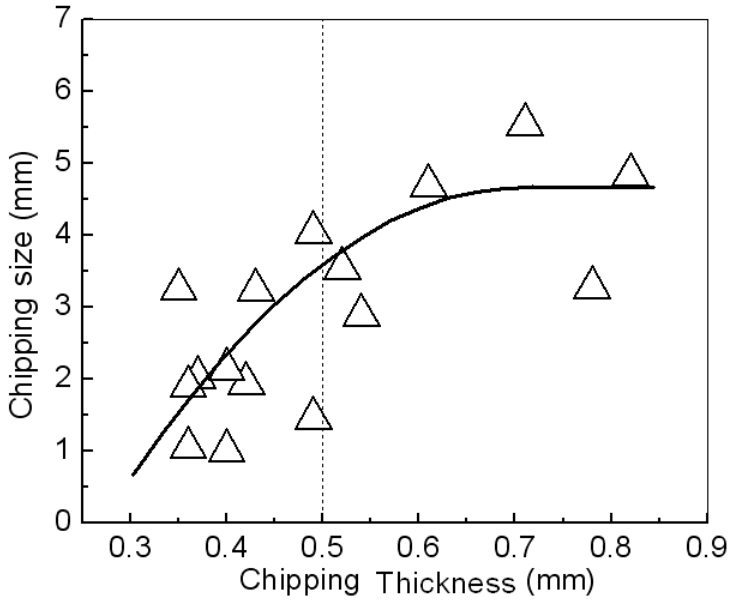


Drilled holes on CMC panels are very different from those on metal workpieces. Chippings are the key barrier of drilling high-quality holes on CMC panels. Conventional criteria like hole roundness, parallelism, and roughness are not enough to characterize the CMC hole quality. Chipping size and chipping thickness as shown in Figure 7.3 are proposed as two additional criteria to evaluate the hole quality on CMC panels. In general, the lower the values of chipping size and chipping thickness are, the better the hole quality will be. By quantifying the chipping size and chipping thickness, the hole quality on CMC panels can be evaluated.

Figure 7.11 depicts a rough relationship between the chipping thickness and chipping size. The best hole shows 0.35 mm chipping thickness and less than 1 mm chippings size. When the chipping thickness exceeds 0.5 mm, the chippings size will fluctuate at the level of 4.5 mm.

**Figure 7.12 Effects on Chipping Thickness**

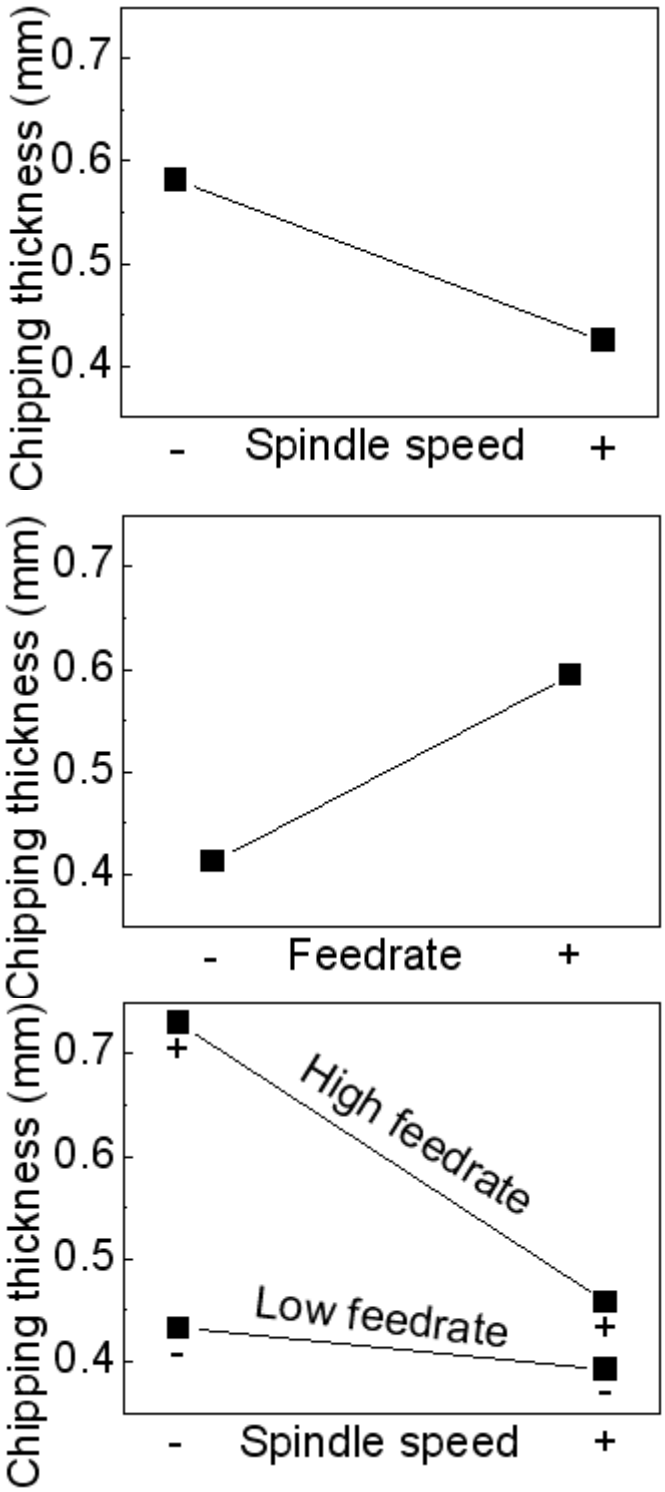


Results on chipping size and chipping thickness are presented in Table 7.7. Figure 7.12 shows the main and interaction effects on chipping thickness. The spindle speed has a significant

effect on chipping thickness at the significance level of $\alpha = 0.004$. From Figure 7.12, it can be seen that the chipping thickness decreases with an increase of spindle speed. That is to say, higher spindle speed will be effective to reduce the chipping thickness. The chipping thickness will increase as feedrate increases and the effect of feedrate on the chipping thickness is significant at the significance level $\alpha = 0.002$. For the chipping thickness, there exists an obvious interaction effect between spindle speed and feedrate at the significance level $\alpha = 0.02$. The effect of spindle speed is much stronger at the higher level of the feedrate.

**Figure 7.13 Effects on Chipping Size**

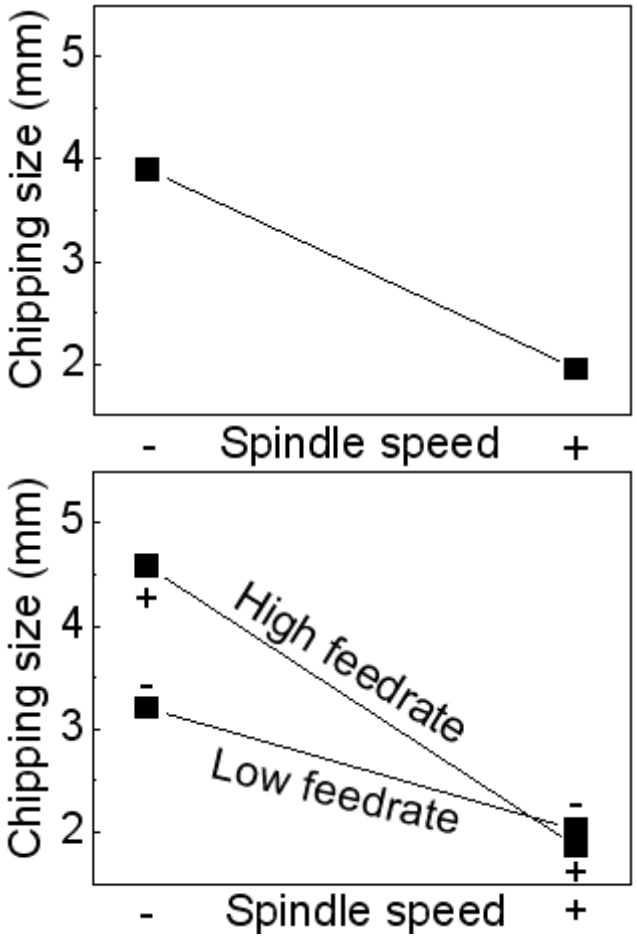

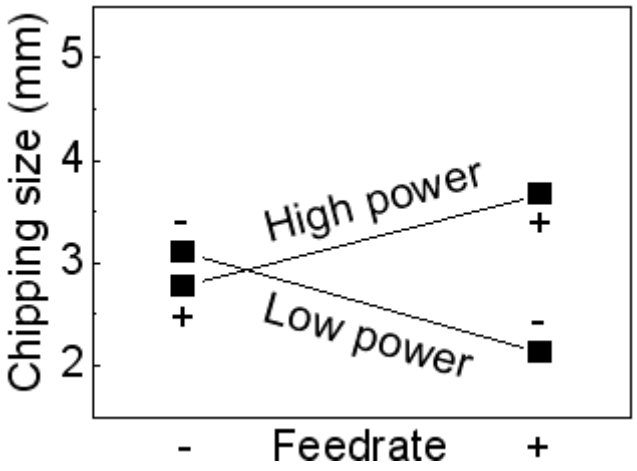


Figure 7.13 shows the main and interaction effects on chipping size. From Figure 7.13, it can be observed that the chipping size decreases with an increase of spindle speed. The spindle speed has a significant effect on chipping size at the significance level of $\alpha = 0.002$. It indicates that higher spindle speed will be effective to prevent larger chippings. The two-factor interactions between spindle speed and feedrate is significant at the significance level $\alpha = 0.1$. The effect of spindle speed is stronger at the higher level of the feedrate. The interaction between feedrate and ultrasonic power is significant at the significance of level $\alpha = 0.05$. With the increase of feedrate, the chipping size will increase at the higher level of ultrasonic power while decrease at the lower level of ultrasonic power.

## 7.5 Conclusions

In this chapter, ultrasonic vibration assisted grinding (UVAG) is introduced into drilling CMC materials. The feasibility of drilling holes with UVAG on two types of CMC panels was studied. A full factorial design was used to conduct a set of parametric experiments of UVAG on CMC. The main effects and two-factor interactions of process parameters (spindle speed, feedrate, and ultrasonic power) on output variables (cutting force, MRR, chipping thickness and chipping size) are obtained. The following conclusions can be drawn from the study:

1) Compared with diamond drilling process, the cutting force can be reduced significantly (about 50%) and MRR can be improved (about 10%) with UVAG.
2) High-quality holes on CMC panels can be achieved by UVAG with proper machining parameters.
3) For main effects, feedrate has the most significant effects on cutting force.

4) All three process parameters (spindle speed, feedrate, and ultrasonic power) have significant effects on MRR.
5) Spindle speed and feedrate, as well as their interaction, have significant effects on hole quality.

# CHAPTER 8 – UVAG of Zirconia/Alumina Composites

## 8.1 Introduction

In this chapter, the viability of UVAG on five types of zirconia/alumina composites with different mixture ratios is investigated for the first time. Cutting forces are measured. Some advantages of UVAG over diamond drilling are presented by comparing the cutting force.

## 8.2 Experimental Detail

### *8.2.1 Preparation of Samples*

**Table 8.1. Description of Samples**

| | Thickness (mm) | Diameter (mm) | Characteristic description |
|---|---|---|---|
| #1 | 6.43 | 11.83 | 100% alumina (APK-50) |
| #2 | 6.43 | 11.83 | 75% alumina (APK-50)<br>+ 25% zirconia (Cerac) |
| #3 | 6.43 | 11.83 | 50% zlumina (TMDAR)<br>+ 50% zirconia (Cerac) |
| #4 | 6.43 | 11.83 | 25% alumina (TMDAR)<br>+ 75 % zirconia (45% TZ3YS + 55% Cerac) |
| #5 | 6.43 | 11.83 | 100% zirconia (Cerac) |

Zirconia/alumina composites with five different mixture ratios are prepared at Michigan State University for UVAG drilling tests. These five samples contain 0%, 25%, 50%, 75%, and 100% of alumina respectively while the remainders are partially stabilized zirconia. These samples are prepared by ball-milling various powders for 24 hours. Then the mixtures are pressed uniaxially in a cylindrical steel die at approximately 23 MPa. The green compacts are then sintered at 1475°C in air for 4 hours with a heating and cooling rate of 10°C/min. The

alumina powders used in this work are AKP-50 (Sumitomo Chemical, Japan) and TMDAR (Tamei Chemical Corporation, Japan) and the partially stabilized zirconia powders are Cerac powder (Milwaukee, WI) and TZ3YS (Tosoh Corp., Tokyo, Japan). Table 8.1 shows size of the samples prepared and the powders used to make each sample.

### *8.2.2 Setup and Conditions*

**Tabile 8.2. Machining Conditions**

| Condition | Specification |
|---|---|
| Diamond drills | Drill #1: Outer diameter 3/8", Grit Mesh Size #80~100, Metal Bond.<br>Drill #2: Outer diameter 1/8", Grit Mesh Size #80~100, Metal Bond.<br>Drill #3: Outer diameter 1/8", Grit Mesh Size #80~100, Metal Bond. |
| Coolant | 20:1 water-soluble cutting oil Mobile met S 122, Mobil Oil Co |
| Spindle speed | 3000 (rpm) |
| Feedrate | 0.068 (mm/s) |
| Ultrasonic vibration | Power supply: 35%*<br>Frequency: 20 (KHz) |
| Coolant pressure | 30 (psi) |

*It controls amplitude of ultrasonic vibration.

The experimental setup for UVAG drilling mainly consists of an ultrasonic spindle system, a data acquisition system, and a coolant system. A KISTLER 9257 dynamometer is mounted atop the machine table to measure cutting force. The zirconia/alumina composite samples are mounted on a fixture that is on the dynamometer. UVAG tests are performed on an ultrasonic machine produced by Sonic Mill (Sonic Mill Series 10). Other machining conditions for the experiments are presented in Table 8.2.

## 8.3 Results and Discussion

### *8.3.1 Effects of Different Sample Materials on Cutting Force*

**Figure 8.1 Cutting Forces in UVAG of Five Different Samples**

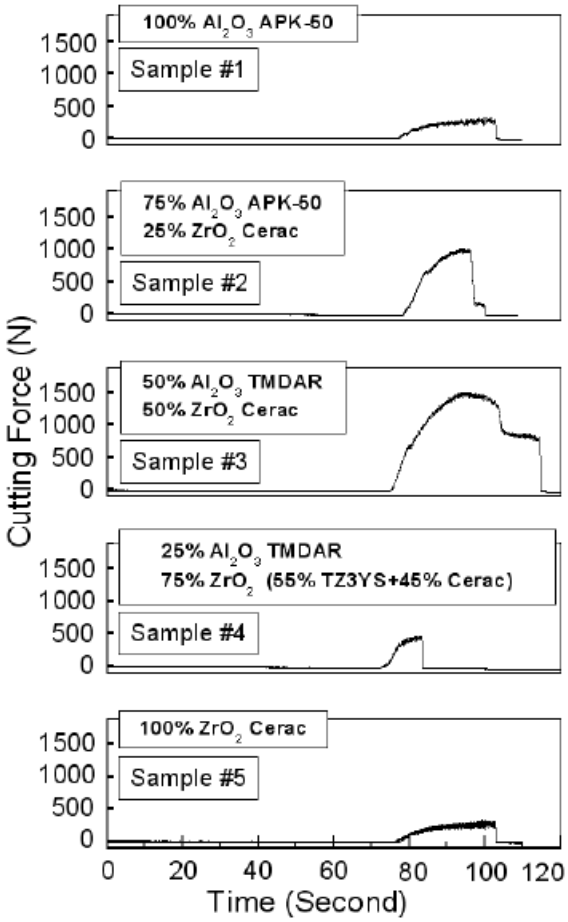


In this section, the cutting force when Ultrasonic vibration assisted grinding of 5 different zirconia/alumina composite samples are evaluated. Experiments are conducted by using drill #1. Figure 8.1 shows cutting force curves when machining these 5 different samples. It can be seen that sample #1 (100% alumina), sample #4 (25% alumina + 75% zirconia) and sample #5 (100% zirconia) can be machined easily by UVAG with cutting forces of less than 500 N.

As for sample #2 (75% alumina + 25% zirconia), it also could be drilled using UVAG with about 1000 N cutting force. But, the entire machining process is not very stable compared with sample #1, sample #4, and sample #5.

**Figure 8.2 Comparison of the Maximum Cutting Forces in UVAG of Five Different Samples**

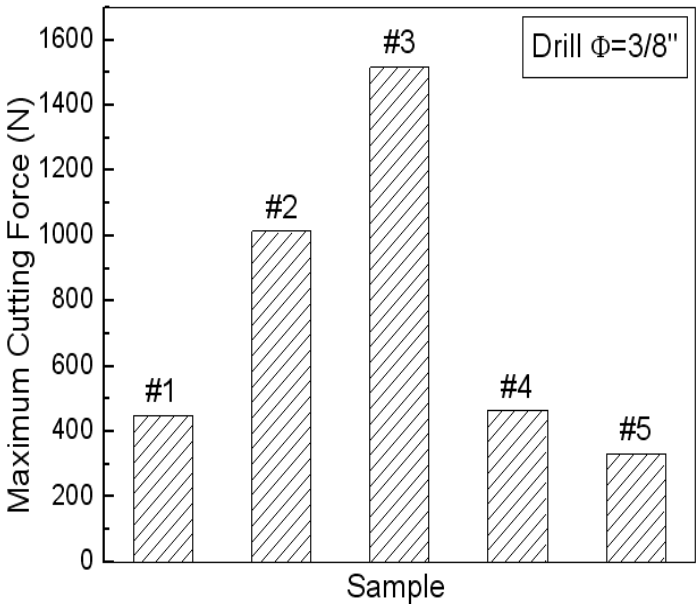


When it comes to sample #3 (50% alumina + 50% zirconia), the severe increase of the cutting force (at least 1500 N) was observed, as shown in Figure 8.1. The drilling process was stopped before a through hole was completely drilled because of the severe increase in the cutting force. Machining tests have to be stopped when the cutting forces exceed 1500 N to protect the diamond core drill and UVAG spindle.

Figure 8.2 shows the comparison of the maximum cutting forces during UVAG process of 5 different zirconia/alumina composite samples. The maximum cutting force when machining sample #3 (50% alumina + 50% zirconia) is 1516 N, which is about four times of those when machining sample #1, sample #4, and sample #5. In this case, the diamond core drill will tend to be damaged. The maximum cutting force when machining sample #2 is 1014 N. The maximum cutting forces when machining sample #1 (100% alumina), sample #4 (25% alumina + 75% zirconia), and sample #5 (100% zirconia) are 448 N, 466 N, and 331 N respectively. The result

for sample #1 is nearly consistent with the published data in which the maximum cutting force when using UVAG to machine alumina is 403 N (Hu et al. 2002).

From Figure 8.1 and Figure 8.2, it can be seen that UVAG is a promising process to machine samples #1, #4, and #5. As for sample #2 and sample #3, more UVAG experiments are needed for further investigation.

**Figure 8.3 Comparison between Published Mechanical Properties of Zirconia/Alumina Composites and the Maximum Cutting Force in UVAG (Yu et al. 2003)**

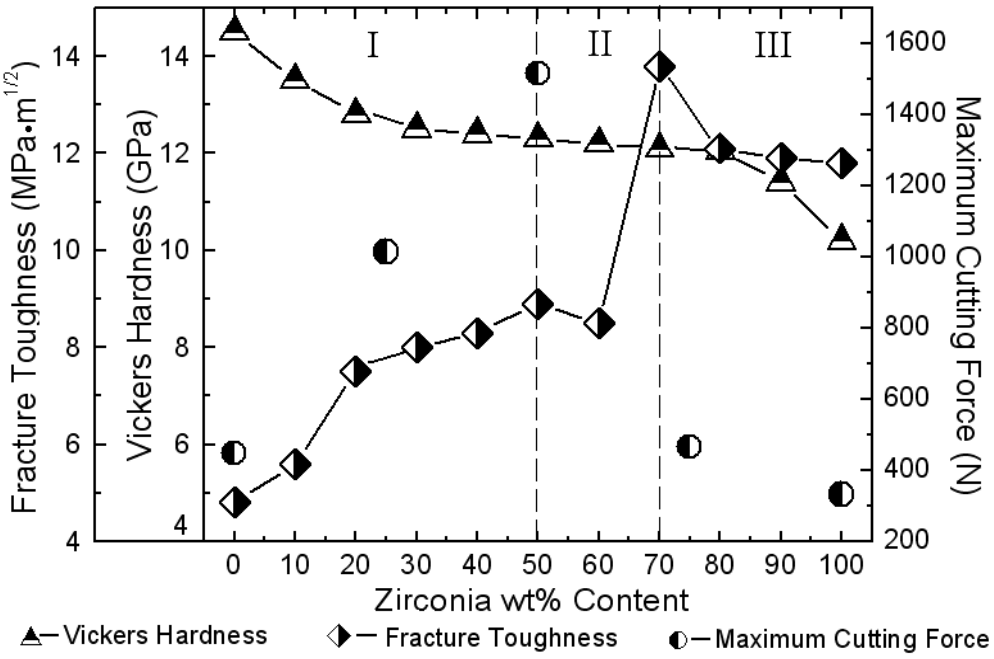


Mechanical properties (hardness and fracture toughness) of zirconia/alumina composites with the change of composition are cited and shown in Figure 8.3 (Yu et al. 2003). From Figure 8.3, it can be seen that with the variety of zirconia content, the change of fracture toughness exhibit a saddle shape which could be divided into three zones. They were zirconia toughened alumina (ZTA) zone (area I, the content of zirconia is 0-50 wt%), transition zone (area II, the content of zirconia is 50-70 wt%) and alumina dispersed zirconia (ADZ) zone (area III, the content of zirconia is 70-100 wt%). The hardness of the composites continues to decrease as the zirconia content increases. It could be concluded that sample #1 (100% alumina), sample #2 (75% alumina + 25% zirconia), and sample #3 (50% alumina + 50% zirconia) in this study

should be in the ZTA zone where the increase of zirconia will lead to the increase of fracture toughness and decrease of hardness; sample #4 (25% alumina +75% zirconia) and sample #5 (100% zirconia) should be in the ADZ zone where the increase of zirconia will lead to the decrease of fracture toughness and hardness.

To study the effect of mechanical properties on the cutting force in UVAG process, the maximum cutting force is also shown in Figure 8.3. In the ZTA zone (sample #1, #2, and #3), it can be observed that the maximum cutting force will increase with a significant increase of fracture toughness and a slight decrease of hardness. In the ADZ zone (sample #4 and #5), the maximum cutting force will decrease as both fracture toughness and hardness decrease.

Also, from Figure 8.3, it can be seen that the ADZ samples (#4 and #5) show much higher fracture toughness and much lower hardness than the ZTA samples (#1, #2, and #3). Experimental results of the maximum cutting force show that the ADZ samples are much easier to machine by UVAG than the ZTA samples. It shows that both mechanical properties and microstructures have to be considered when analyzing the machinability of ZTA composites in UVAG process.

### *8.3.2 Effects of Ultrasonic Vibration on Cutting Force*

**Figure 8.4 Comparison of Cutting Force between UVAG and Diamond Drilling on Samples #1 (100% Alumina)**

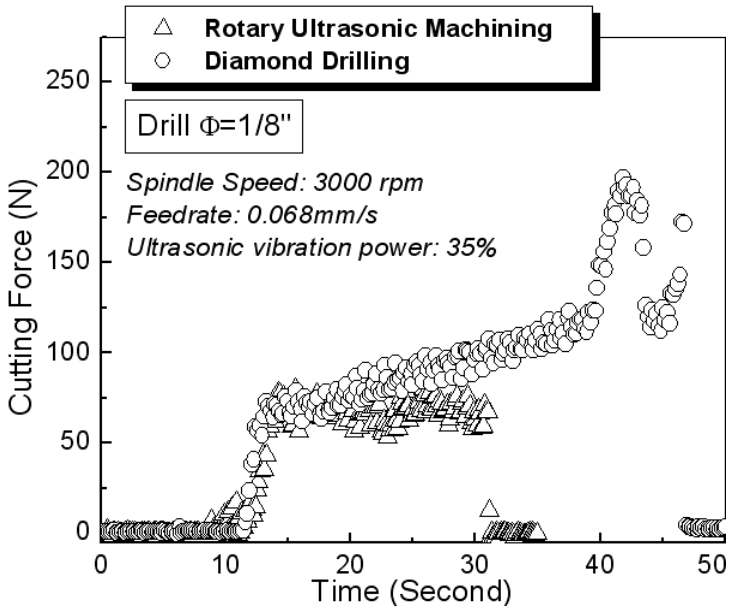

**Figure 8.5 Comparison of Cutting Force between UVAG and Diamond Drilling on Sample #2 (75% Alumina +25% Zirconia)**

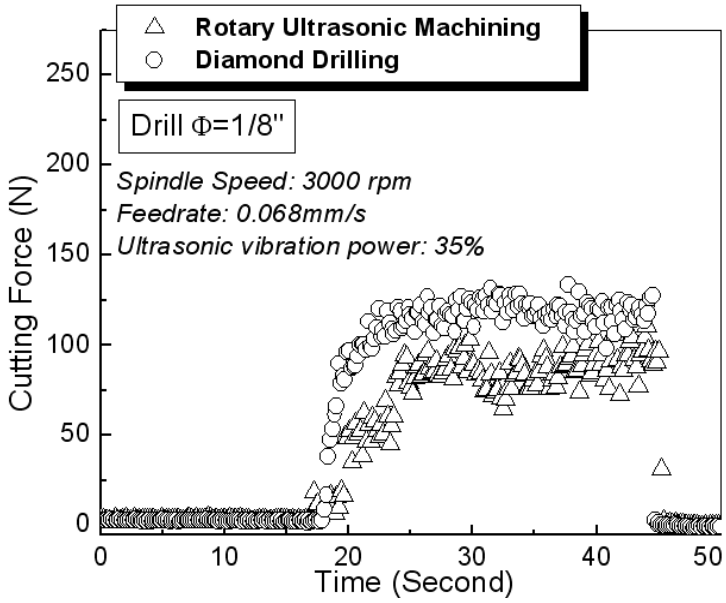


**Figure 8.6 Comparison of Cutting Force between UVAG and Diamond Drilling on Sample #3 (50% Alumina+50% Zirconia)**

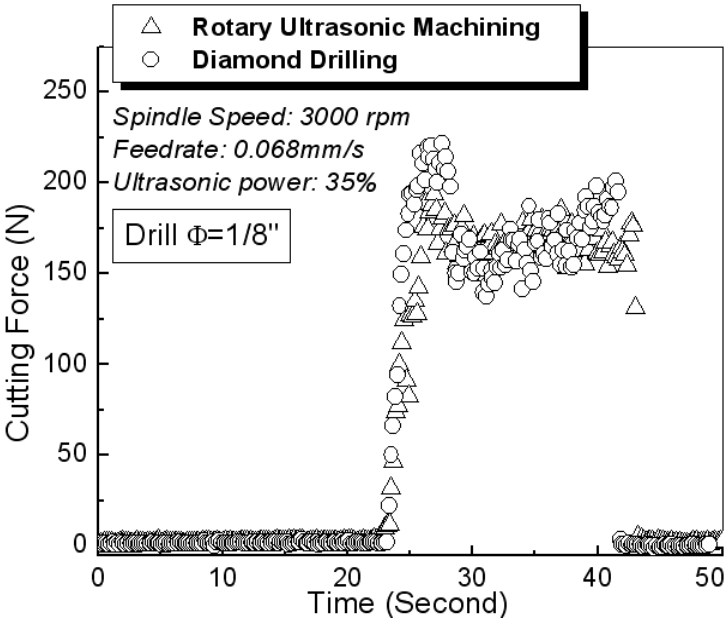

**Figure 8.7 Comparison of Cutting Force between UVAG and Diamond Drilling on Sample #5 (100% Zirconia)**

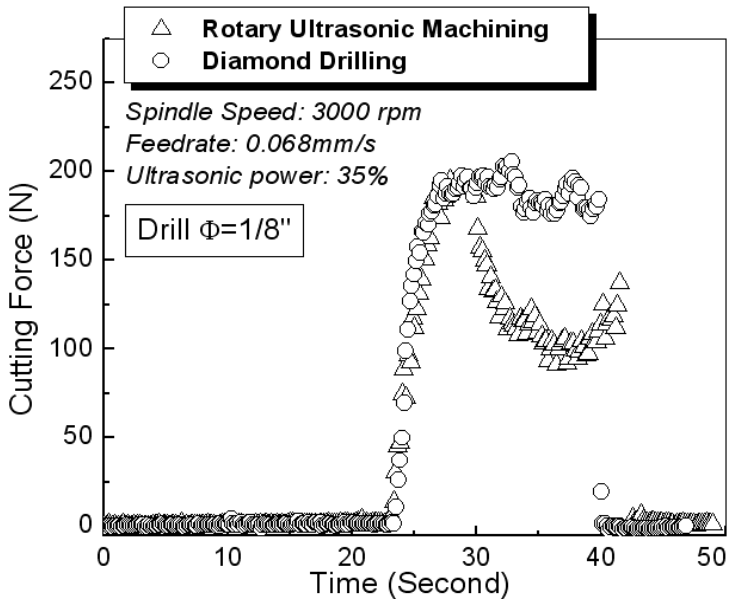


Cutting forces with and without ultrasonic vibration assistance are compared in Figs 8.4-7. Sample #4 (25% alumina + 75% zirconia) is broken in a previous UVAG test, so only sample #1, sample #2, sample #3, and sample #5 are used in the following experiments to compare the cutting forces between UVAG and diamond drilling. Limited by the size of samples, drills #2 and #3 with a smaller diameter are used to drill samples in these tests. One is used for UVAG process; the other is applied for diamond drilling process without ultrasonic vibration assistance. It needs to point out that the tool diameter has a significant effect on the cutting force. Generally, the smaller the diameter is, the lower the cutting force will be. So, from Figs 8.4-7, it can be seen that the cutting forces when using tools #2 and #3 (outer diameter = 1/8 inch) are much lower than those when using tool #1 (outer diameter = 3/8 inch).

From Figure 8.4, Figure 8.5, and Figure 8.7, it can be observed that the cutting forces when machining sample #1 (100% alumina), sample #2 (75% alumina + 25% zirconia), and sample #5 (100% zirconia) can be reduced significantly with the assistance of ultrasonic vibration. Especially, for sample #1(100% alumina) and sample #5 (100% zirconia), the cutting forces in UVAG process are much lower than those in diamond drilling process. The cutting force also can be reduced by about 20% with the assistance of ultrasonic vibration when machining sample #2 (75% alumina + 25% zirconia).

Based on past research work, it has been presented that there exist three mechanisms involved in material removal in UVAG process (Ya et al. 2002): 1) Impacting: the abrasive particles in the tool end face impact the machined surface. 2) Abrasion: the abrasive particles scratch out micro-grooves on the machined surface. 3) Ultrasonic cavitation: when the amount of ultrasonic energy applied to a fluid exceeds the attractive forces holding together the molecules, which make up the material, a phenomenon called cavitation occurs. Also, in UVAG, coolant pumped through the core of the drill washes away the swarf, prevents jamming of the drill, and keeps it cool. Compared with diamond drilling process, two more material removal processes (impacting and ultrasonic cavitation) and coolant flow-in-and-out during machining are involved in UVAG. The decrease of the cutting forces when apply UVAG to drill samples #1, #2, and #5 might be resulted from the ultrasonic impacting, ultrasonic cavitation, coolant flow-in-and-out, or some combined effects.

When it comes to sample #3 (50% alumina + 50% zirconia), the difference in cutting force between UVAG process and diamond drilling process is quite small. The ultrasonic vibration assistance has no noticeable effect on the cutting force.

## 8.4 Conclusions

Preliminary experiments are conducted to test the feasibility of machining 5 different zirconia/alumina samples using UVAG process by measuring cutting force. The following conclusions can be drawn from the study:

1) Ultrasonic vibration assisted grinding can be feasible technique for machining of zirconia/alumina composites for applications requiring drilling of holes.
2) From the comparison of the cutting forces when using UVAG to machine the 5 different zirconia/alumina composite samples, the cutting forces can be compared as following: #5 < #1 < #4 <#2 <#3.
3) UVAG is promising process to machine sample #1 (100% alumina), and sample #5 (100% zirconia) with cutting forces less than 500 N.
4) As for sample #4 (25% alumina + 75% zirconia), UVAG could be applied to machine it with cutting force less than 500N. But, further comparison between diamond drilling and UVAG need to be investigated.

5) For Sample #2 (75% alumina + 25% zirconia) and sample #3 (50% alumina + 50% zirconia), more UVAG experiments are needed for further investigation.

# CHAPTER 9 - Summaries

## 9.1 Summaries of This Research

Firstly, a mathematical model is developed for the grinding marks in SDSG of silicon wafers. The following conclusions can be drawn from the study of grinding marks:

1) The grinding mark curvature on the front side of the wafer is different from that on the back side due to different rotation directions of the two grinding wheels.
2) The distance between the adjacent grinding lines on both sides of the wafer is determined by the ratio of the wheel rotation speed versus the wafer rotation speed. As the ratio of the wheel rotation speed versus the wafer rotation speed increases, the line distance increases. The wheel diameter does not affect the line distance.
3) The curvature of the grinding marks is determined by the wheel diameter and the ratio of the wheel rotation speed versus the wafer rotation speed. As the wheel diameter increases, the grinding lines tend to become less curved. As the speed ratio increases, the grinding lines tend to become less curved.

Secondly, a mathematical model is developed for the wafer shape in SDSG of silicon wafers. The following conclusions can be drawn from the study of wafer shape:

1) The wafer shape is related only to the absolute value of the "roll" angle. With the increase of the absolute value of the "roll" angle, $\delta_1$ increases but $\delta_2$ decreases.
2) The wafer shape is not only related with the value of the "pitch" angle but also the tilt direction. As the "pitch" angle increases from negative to positive, both $\delta_1$ and $\delta_2$ increases.
3) The wafer shape is also related with the wheel radius. When it only comes to the "pitch" angle, both $\delta_1$ and $\delta_2$ decreases with the increase of the wheel radius. When only the "roll" angle is involved or both the "roll" angle and the "pitch" angle are involved, both $\delta_1$ and $\delta_2$ increases with the increase of the wheel radius.

Thirdly, A 3-D FEA model has been developed to analyze the edge chipping in UVAG. A solution to reduce the edge chipping is proposed and verified by pilot experiments. The conclusions can be summarized as following:

1) As the cutting depth increases, the maximum values of the maximum normal stress and the von Mises stress in the edge chipping initiation region will increase.
2) The effects of pretightening load on the maximum values of the maximum normal stress and the von Mises stress are not significant.
3) There exists a critical support length. As the support length increases before reaching the critical length, the maximum values of the maximum normal stress and the von Mises stress decrease slightly. When the support length exceeds the critical length, there are sharp decreases in the maximum values of the maximum normal stress and the von Mises stress.
4) The edge chipping thickness can be reduced by increasing the support length.

Fourthly, experimental investigations have conducted to study two different coolant delivery modes in UVAG. Major conclusions are:

1) Compared with the regular centrifugal pump, the AODDP has no significant effect on the vertical cutting force and MRR in the UVAG process but obviously affect the machined surface roughness. When using AODDP, the machined holes surface roughness decrease from 0.55 μm to 0.31 μm with the increase of the air pressure from 20 psi to 80 psi.
2) The reason for the improvement of the machined holes surface quality is that the higher coolant output pressure will lead to more micro swarfs, which has a considerable worse effect on the machined surface roughness, be washed away from the contact area between tool and workpiece.
3) As for the machined rod surface, it can be observed that the machined rod surface roughness decrease significantly by using AODDP in UVAG process.

Fifthly, UVAG experiments have been conducted on CMC materials for the first time. The following conclusions can be drawn from the study:

1) Compared with diamond drilling process, the cutting force can be reduced significantly (about 50%) and MRR can be improved (about 10%) with UVAG.

2) High-quality holes on CMC panels can be achieved by UVAG with proper machining parameters.
3) For main effects, feedrate has the most significant effects on cutting force.
4) All three process parameters (spindle speed, feedrate, and ultrasonic power) have significant effects on MMR.
5) Spindle speed and feedrate, as well as their interaction, have significant effects on hole quality.

Finally, some preliminary experiments are conducted to test the feasibility of machining 5 different zirconia/alumina samples using UVAG process by measuring cutting force. The following conclusions can be drawn from the study:

1) Ultrasonic vibration assisted grinding can be feasible technique for machining of Zirconia/Alumina composites for applications requiring drilling of holes.
2) From the comparison of the cutting forces when using UVAG to machine the 5 different Ziiconia/alumina composite samples, the cutting forces can be compared as following: #5 < #1 < #4 <#2 <#3.
3) UVAG is promising process to machine sample #1 (100% Alumina), and sample #5 (100% Zirconia) with cutting forces less than 500 N.
4) As for sample #4 (25% Alumina + 75% Zirconia), UVAG could be applied to machine it with cutting force less than 500N. But, further comparison between diamond drilling and UVAG need to be investigated. For Sample #2 (75% Alumina + 25% Zirconia) and sample #3 (50% Alumina + 50% Zirconia), more UVAG experiments are needed for further investigation.

## 9.2 Contributions of This Research

The contributions of this research are:

1) For the first time in the public domain, this research has established a mathematical model that reveals the relationship between the grinding marks and SDSG parameters like wheel rotation speed, wafer rotation speed, and wheel diameter.
2) For the first time in the public domain, this research has established a mathematical model that reveals the relationship between the wafer shape and SDSG parameters like wheel “roll” angle, wheel “pitch” angle, and wheel diameter.

3) For the first time in the public domain, this research has established a 3-D FEA model to analyze the edge chipping phenomenon in UVAG of ceramics.
4) For the first time in the public domain, this research has investigated a novel coolant system for the UVAG process.
5) For the first time in the public domain, the research has investigated the possibility of machining fiber-reinforced ceramic matrix composites and zirconia/alumina composites using UVAG.

# Appendix A - References


Abe, K. et al., 2000, Double side grinding apparatus and double side polishing apparatus, US Patent 6,165,054.

Abe, K., 1997, Double surface grinding-polishing machine of sheetlike workpiece, Japanese Patent JP09-249687.

Ahejew, A., 1984, Simultaneous double-acting split abrasive wheel for peripheral sharpening of helix tools and use thereof, US Patent 4,442,637.

Akio, I., Yasushi, O, Kiyohiro, O., 2004, Grinding device, Japanese Patent JP2004-098197.

Akira, I. et al., 2003, Wafer support member and double-ended grinding device using the same, Japanese Patent JP2003-124167.

Anantha Ramu, B.L., Krishnamurthy, R., and Gokularathnam, C.V., 1989, Machining performance of toughened zirconia ceramic and cold compact alumina ceramic in ultrasonic drilling, Journal of mechanical working technology, Vol. 20, pp. 365-375.

Anonymous, 1966, An improved ultrasonic machine tool for glass and ceramics, Industry Diamond Review, Vol. 26, No. 308, pp. 274-278.

Anonymous, 1973, Drilling deep holes in glass, Ultrasonic, (May), pp. 103-106.

Anonymous, 2000, Market survey report of ceramic matrix composites, Business Communications Company, Inc.

Bawa, M.S., Petro, E.F., and Grimes, H.M., 1995, Fracture strength of large diameter silicon wafers, Semiconductor International, Vol. 18, No. 11, pp. 115-118.

Bowan, G.J., 1997, Specifying air-operated double diaphragm pumps, World pumps, Jan, pp.38-39.

Butcher, C., 1990, Air-operated diaphragm pumps, Chemical Engineer (London), No.487, Dec, pp. 62-67.

Cao, Y.Q., 2001, Failure analysis of exit edges in ceramic machining using finite element analysis, Engineering Failure Analysis 8 (4) pp. 325-338.

Carlson, J.A., Bathrick, V.H., and Morse, A.J., 1953, Grinding of irregular shaped work, US Patent 2,636,322.

Carroll, J.W., Todd, J.A., Ellingson, W.A., and Polzin, B.J., 2000, Laser machining of ceramic matrix composites, Ceramic Engineering and Science Proceedings, Vol. 21, No. 3, pp. 323-330.

Chatterjee, S., Basu, D., Das R., and Guha, S.K., 1989, Evaluation of Mechanical Properties of Sintered Zirconia Toughened Alumina Ceramics, Transactions of the Indian Ceramic Society, Vol. 48, No. 4, pp. 68-72.

Chidambaram, S., Pei, Z.J., and Kassir, S., 2003, Fine grinding of silicon wafers: a mathematical model for grinding marks, International Journal of Machine Tools and Manufacture, Vol. 43, No. 15, pp. 1595-1602.

Chiu, W.C., Thouless, M.D., Endres, W.J., 1998, An analysis of chipping in brittle materials, International Journal of Fracture 90 (4) pp. 287-298.

Claussen, N., 1976, Fracture Toughness of $Al_2O_3$ with an Unstable $ZrO_2$ Dispersed Second Phase, Journal of American Ceramics Society, Vol. 61, pp. 49-51.

Cleave, D. V., 1970, Ultrasonics Gets Bigger Jobs in Machining and Welding, Iron Age, Vol. 218, No. 11, pp. 69-72.

Cleave, D.V., 1976, Ultrasonic gets bigger jobs in machining and welding, Iron Age, Sep, pp. 69-72.

Cook, R.L., 1976, Apparatus for cleaning thin, fragile wafers of a material, US Patent 3,939,514.

Dam, H., Quist, P., and Schreiber, M.P., 1995, Productivity, surface quality and tolerances in ultrasonic machining of ceramics, Journal of Materials Processing Technology, Vol. 51, Nos. 1-4, pp. 358-368.

Deng, G.P., Li, S.Z., Wu, S.Q., Yang, X.G., 1993, Ultrasonic vibration drilling of small-diameter deep holes of difficult-to-machine stainless steel: theoretical analysis and comparative experimental research, American Society of Mechanical Engineers, Production Engineering Division (Publication) PED, Manufacturing Science and Engineering, Vol. 64, pp. 835-839.

DeVor, R.E., Chang, T.H., and Sutherlan, J.W., Statistical Quality Design and Control: Contemporary Concepts and Methods, Macmillan, New York, 1992.

Doubman, J.R., and Cox, C., 1997, Double disc grinding in automotive parts manufacturing, Automotive Manufacturing & Production Oct 60-63.

Dudley, J.A., 1986, Abrasive technology for wafer lapping, Microelectronic Manufacturing and Testing 4 (4) 1-6.

Dunn, E.R., 1984, Headsetting structure for double disc grinding machine, US Patent 4,462,187.

Dunn, E.R., 1980, Double disk grinding doubles productivity, Tooling & Production 46 (2) 98-103.

Eade, R., 1988, Grinding both sides at the same time, Modern Machine Shop 61 (7) 84-89.

Evans, A.G., 1990, Perspective on the Development of High Toughness Ceramics, Journal of American Ceramics Society, Vol. 73, pp. 187-206.

Fetouh, M.A., and Malarz, A.J., 1988, Adjustable double end grinding machine, US Patent 4,753,045.

Freitag, D.W., Richerson, D.W., 1998, Ceramic matrix composites in opportunities for advanced ceramics to meet the needs of the industries of the future, Advanced Ceramic Association and Oak Ridge National Laboratory, Oak Ridge, Tennessee.

Fukami, T., Masumura, H., Suzuki, K., and Kudo, H., 1997, Method of manufacturing semiconductor mirror wafers, European Patent Application EP0782179A2.

Goldman, R., 1962, Ultrasonic technology, Reinhold Publishing Corporation, London.

Garcia, M. A., Paje, S.E., and Llopis, J., 2002, Relationship between mechanical grinding and photoluminescence of zirconia toughened alumina ceramics, Materials Science and Engineering A, Vol. 325, No. 1-2, pp. 302-306.

Graff, K.F., 1975, Ultrasonic machining, Ultrasonic, May, pp. 103-109.

Hamatani, G., Ramulu, M., 1990, Machinability of high temperature composites by abrasive water jet, Transactions of ASME, Journal of Engineering Materials and Technology, Vol. 112, No. 4, pp. 381-386.

Hannon, W.F., 1965, Apparatus for grinding a bevel on circular objects, US Patent 3,182,428.

Hasegawa, F., and Kobayashi, M., 1997, Method of manufacturing semiconductor wafers and process of and apparatus for grinding used for the same method of manufacture, US Patent 5,700,179.

Hashii, T., and Watanabe, T., 2004, Method of manufacturing semiconductor wafer, US Patent 6,753,256.

Hashii, T., Onizaki, K., and Masuda, S., 2002, Semiconductor wafer manufacturing method, US Patent 6,465,328.

Hocheng, H., Kuo, K.L., Lin, J.T., 1999, Machinability of zirconia ceramics in ultrasonic drilling, Materials and Manufacturing Processes, Vol. 14, No. 5, pp. 713-724.

Hocheng, H., Tai, N.H., and Liu, C.S., 2000, Assessment of ultrasonic drilling of C/SiC composite material, Composite: Part A, Vol. 31, pp. 133-142.

Hu, P., Zhang, J.M., Pei, Z.J., 2003, Experimental investigation on coolant effect in rotary ultrasonic machining, Proceedings of the NSF workshop on research needs in Thermal aspects of material removal processes. Stillwater. OK, pp. 340-345.

Hu, P., Zhang, J.M., Pei, Z.J., and Treadwell, C., 2003, Modeling of material removal rate in rotary ultrasonic machining: designed experiments, Journal of Material Processing Technology, Vol. 129, Nos. 1-3, pp. 339-344.

Ikeda, J., Sasakura, T., Yoshimura, Y., and Ueda, K., 1999, Double side grinding apparatus for plate disklike work, US Patent 5,989,108.

Ikeda, S., Okabe, K., Okuni, S., Kato, T., and Oshima, H., 2000, Semiconductor wafer and production method thereof, European Patent Application EP1049145.

Ikeda, S., Okuni, S., and Kato, T., 2003, Double-sided simultaneous grinding method, double-sided simultaneous grinding machine, double-sided simultaneous lapping method, and double-sided simultaneous lapping machine, US Patent 6,652,358.

Inasaki, I. and Nakayama, K., 1986, High Efficiency Grinding of Advanced Ceramics, Annals of the CIRP, Vol. 35, No.1, pp. 211-214.

Jana, J. K., and Satyanarayana, A., 1973, Production of fine diameter holes on ultrasonic drilling marching, Journal of the Institution of Engineers (India), Part MC: Mechanical Engineering Division, Vol. 54, No. Part ME 1, pp. 36-40.

Jiao, Y., Hu, P., Pei, Z.J., and Treadwell, C., 2005, Rotary ultrasonic machining of ceramics: design of experiments, International Journal of Manufacturing Technology and Management, Vol. 7, Nos. 2-4, pp. 192-206.

Jiao, Y., Liu, W.J., Pei, Z.J., Xin, X.J., Treadwell, C., 2005, Study on edge chipping in rotary ultrasonic machining on ceramics: an integration of designed experiment and FEM analysis, Journal of Manufacturing Science and Engineering, Vol. 127, No. 4, pp. 752-758.

Junker, E., 1936, Machine for plane grinding piston rings, US Patent 2,034,621.

Kassir, S.M., and Walsh, T.A., 1999, Grinding process and apparatus for planarizing sawed wafers, US Patent 5,964,646.

Kato, T., Masumura, H., Okuni, S., and Kudo, H., 1997, Method of manufacturing semiconductor wafers, European Patent Application EP0798405A2.

Kato, T., Okuni, S., and Okabe, K., 2001, Manufacturing process for semiconductor wafer, US Patent 6,284,658.

Kato, T., Ikeda, S., and Ohkura, K., 2004, Method and device for grinding double sides of thin disk work, European Patent Application EP1193029A1.

Kerstan, M., and Peitsch, G.J., 2000, Silicon wafer substrate planarization using simultaneous double-disk grinding: impact on wafer surface, geometry, morphology and subsurface crystal damage, Proceedings of the 3rd International Symposium on Advances in Abrasive Technology (ISAAT'2000), Hawaii, USA, Oct 30-Nov 2, pp. 211-218.

Khanna, N., Pei, Z.J., P. and Ferreira, M., 1995, Experimental investigation of rotary ultrasonic grinding of ceramic disks, Proceedings of the NAMRC XXIII Conference, Vol. MR, pp 67-72.

Koichi, U., and Yasuto, T., 1999, Double side grinding and cross section measuring device for thin plate disk workpiece, Japanese Patent JP11-198009.

Kubota, M., Tamura, Y., and Shimamura, N., 1977, Ultrasonic machining with a diamond impregnated tool, Bull. Japan. Soc. of Prec. Eng., Vol. 11, No. 3, pp. 127-132.

Kuroki, H., and Maeda, M., 2000, Method of manufacturing a semiconductor wafer, US Patent 6,066,565.

Lange, F. F., 1982, Transformation Toughening 4, Fabrication, Fracture Toughness and Strength of $Al_2O_3$-$ZrO_2$ Composites, Journal Materials Science, Vol. 17, pp. 247-254.

Legge, P., 1964, Ultrasonic drilling of ceramics' Industrial diamond review, Vol. 24 No. 278, pp. 20-24.

Legge, P., 1966, Machining without abrasive slurry, Ultrasonics, July, pp. 157-162.

Li, Z.C., Jiao, Y., Deines, T.W., Pei, Z.J., and Treadwell, C., 2004, Experimental study on rotary ultrasonic machining (RUM) of poly crystalline diamond compacts (PDC), CD-ROM Proceedings of the 13th Annual Industrial Engineering Research Conference (IERC-2004).

Li, Z.C., Cai, Liang-wu, Pei, Z.J., Treadwell, C., 2004, Finite element simulation of rotary ultrasonic machining for advanced ceramics, in: CD-ROM Proceedings of ASME International Mechanical Engineering Congress and Exposition, Anaheim, CA, USA, Nov 13-19.

Liu, W.J., Pei Z.J., and Xin X.J., 2002, Finite element analysis for grinding and lapping of wire-sawn silicon wafers, Journal Materials Processing Technology, Vol. 129, No. 1-3, pp. 2-9.

Lunzer, J.P., 1973, Diamond Drilling in Glass, Proceedings of the 18th Symposium on the Art of Glassblowing, Machine design, pp. 21-25.

Malkin, S., 1989, Grinding Technology: Theory and Applications of Machining with Abrasives, John Wiley & Sons, New York.

Marinescu, I.D., Shoutak, A., and Spanu, C.E., 2002, Technological assessment of double side lapping of silicon, Abrasive Magazine December/January 5-9.

Markov A.I., et al., 1977, Ultrasonic drilling and milling of hard non-metallic materials with diamond tool, Machine & tooling, Vol. 48, No. 9, pp.45-47.

Markov, A.I., and Ustinov, I.D., 1973, A study of the ultrasonic diamond drilling of nonmetallic materials, Industrial diamond review, March, pp. 97-99.

Merchant, M.E., 1998, Interpretive look at 20th centry research on modeling of machining, Machining Science and Technology, Vol. 2, No. 2, pp. 157-163.

Mondal, B., Chattopadhyay, A.B., Virkar A., and Paul, A., 1992, Development and Performance of Zirconia-Toughened Alumina Ceramic Tools, Wear, Vol. 156, pp. 365-383.

Ng, S., Le, D., Tucker, S., Zhang, G., 1996, Control of machining induced edge chipping on glass ceramics, in: Proceedings of the 1996 ASME International Mechanical Engineering Congress and Exposition, Manufacturing Engineering Division, MED(4), Atlanta, GA, USA, Nov 17-22, pp. 229-236.

Nishi, K., Nukui, M., Murai, S., Nakajim, K., and Wada, T., 2001, Grinding method, surface grinder, workpiece support, mechanism and work rest, US Patent 6,296,553.

Nishio, K., 1988, Double-end surface grinding machine, US Patent 4,782,631.

Nobuto, S., and Akihide, T., 1997, Double grinding device for high brittle material, Japanese Patent JP09-262747.

Ogawa, I., Sato, M., Morita, N., and Kobayashi, T., 1984, Double spindle grinding machine, US Patent 4,471,577.

Okamura, K., 1995, Ceramic matrix composites (CMC), Journal of the Japan Society of Composite Materials, Vol. 4, No. 3, pp. 247-259.

Okura, K., 2002, Both face grinding method for thin plate disclike workpiece and device thereof, Japanese Patent 2002-307303A.

Online Staff, 2005 Market share: silicon wafer, worldwide, 2005, 6/9/2006, available: http://www.gartner.com/DisplayDocument?doc_cd=141221

Online Staff, 2000 machining technical ceramics: the cost factor, ceramic industry , 8/6/2000, available:http://www.ceramicindustry.com/CDA/Archives/5d187dbb0b9c7010VgnVCM100000f932a8c0

Oppelt, P., 1984, Grinding machine, US Patent 4,439,951.

Paquin, M., 1995, Double-disc grinding on the move, Modern Machine Shop 68 (7) 66-73.

Pei, Z.J., Ferreira, P.M., and Haselkorn, M., 1995, Plastic flow in rotary ultrasonic machining of ceramics, Journal of Material Processing Technology, Vol. 48, No. 1-4, pp. 771-777.

Pei, Z.J., Prabhakar, D., Ferreira, P.M., Haselkorn, M., 1995[a], Ultrasonic drilling and milling of ceramics, Ceramic Transactions, Vol. 49, pp. 185-190.

Pei, Z.J., Prabhakar, D., Ferreira, P.M, and Haselkorn, M., 1995[b], A Mechanistic approach to the prediction of material removal rates in rotary ultrasonic machining, Journal of Engineering for Industry, Transactions of the ASME, Vol. 117, No. 2, pp. 142-151.

Pei, Z.J., Khanna, N., and Ferreira, P.M., 1995[c], Rotary ultrasonic machining of structural ceramics-a review, Ceramic Engineering and Science Proceedings, Vol. 16, No. 1, pp. 259-278.

Pei, Z.J., 1995, Rotary Ultrasonic machining of Ceramics, PhD thesis, University of Illinois at Urbana-Champaign.

Pei, Z.J., and Ferreira, P.M., 1998, Modeling of ductile-mode material removal in rotary ultrasonic machining, International Journal of Machine Tools and Manufacture, Vol. 38, Nos. 10-11, pp. 1399-1418.

Pei, Z.J., and Billingsley, S.R., and Miura, S., 1999, Grinding-induced subsurface cracks in silicon wafers, International Journal of Machine Tools and Manufacture, Vol. 39, No. 7, pp. 1103-1116.

Pei, Z.J., Xin, X.J., and Liu, W.J., 2003, Finite element analysis for grinding of wire-sawn silicon wafers: a designed experiment, International Journal of Machine Tools and Manufacture, Vol. 43, No. 1, pp. 7-16.

Pei, Z.J., and Strasbaugh, A., 2001, Fine grinding of silicon wafers, International Journal of Machine Tools and Manufacture, Vol. 41, No. 5, pp. 659-672.

Pei, Z.J., 2002, A study on surface grinding of 300 mm silicon wafers, International Journal of Machine Tools and Manufacture, Vol. 42, No. 3, pp. 385-393.

Pei, Z. J., and Ferreira, P.M., 1999, An experimental investigation of rotary ultrasonic face milling, International Journal of Machine Tools and Manufacture, Vol. 39, No. 8, pp. 1327-1344.

Petrukha P.G., et al, 1970, Ultrasonic diamond drilling of deep hole in brittle materials, Russian Engineering Journal, Vol. 50, No. 10, pp.70-74.

Pietsch, G.J., and Kerstan, M., 2001, Simultaneous double-disk grinding machining process for flat, low-damage and material-saving silicon wafer substrate manufacturing, in: Proceeding of the 2nd Euspen International Conference, Turin, Italy, May 27-31, 2001, pp. 644-648.

Pietsch, G.J., and Kerstan, M., 2005, Understanding simultaneous double disk grinding: opearation principle and material removal kinematics in silicon wafer planarization, Precision Engineering 29 (2) 189-196.

Prabhakar, P.D., 1992, Machining advanced ceramic materials using rotary ultrasonic machining process, M.S. Thesis, University of Illinois at Urbana-Champaign.

Prabhakar, P.D., Ferreira, P.M., and Haselkorn, M., 1992, An experimental investigation of material removal rate in rotary ultrasonic machining, Transactions of the North American Manufacturing Research Institution of SME, Vol. 20, pp. 211-218.

Prabhakar, D., Pei, Z.J., and Ferreira, P.M., 1993, Mechanistic approach to the prediction of material removal rates in rotary ultrasonic machining, Manufacturing Society Engineering, ASME PED, Vol. 64, pp. 771-784.

Quirk M., and Serda J., 2001, Semiconductor manufacturing technology, Prentice Hall, New Jersey, p. 2.

Ramulu, M., See, H.W., and Wang, D.H., 1990, Machining of ceramic composite $TiB_2$/SiC by spark erosion, ASME Manufacturing Review, Vol. 3, No. 2, pp. 123-129.

Rebro, P. A., Pfefferkron, F. E., Shin, Y. C., and Incropera, F. P., 2002, Comparative assessment of laser-assisted machining for various ceramics, Transactions of NAMRI of SME, Vol. 30, pp 153-160.

Richerson, D.W., 1997, Ceramic matrix composites, Composite Engineering Handbook, Marcel Dekker Inc., New York.

Rimmer, S.M. et al., 1968, Spring grinding machine, US Patent 3,393,473.

Ritchie, R.O., Knott, J.F., Rice, J.R., 1973, On the relationship between critical tensile stress and fracture toughness in mild steel, Journal of the Mechanics and Physics of Solids 21 (6) pp. 395-410.

Rodemeyer, H., 1930, Grinding apparatus and method, US Patent 1,763,820.

Rupp, W.E., 1977, Air-operated diaphragm pumps, Plant Engineering (Barrington, Illinois), Vol.31, No.1, Jan, pp. 69-72.

Saitoh, A., and Masahiko, H., 2004, Grinding method of vertical type double-head surface grinding machine for machining brake disk, Japanese Patent JP2004-066392.

Shaw, M.C., 1996, Principles of abrasive processing, Clarendon Press, Oxford.

Shih, A.J., and Lee, N.L., 1999, Precision cylindrical face grinding, Precision Engineering, Vol. 23, No. 3, pp. 177-184.

Shinetsu, H.K., 1997, Semiconductor wafer surface grinding method-involves reducing suction pressure of semiconductor wafer to base plate during generation of spark during grinding process, Japanese Patent JP09-9248758A.

Shizuki, S., Yasuo, Y., and Koichi, U., 2002, Double face grinding device for disk work, Japanese Patent JP2002-036078.

Sornakumar, T., 2001, CBN Wheel Grinding of ZTA, Proceedings from Processing and Fabrication of advanced materials X, ASM International, pp. 592-600.

Spur, G., Uhlmann, E., Holl, S.E., Daus, N.A., 1997, Influences on surface and subsurface during ultrasonic assisted grinding of advanced ceramics, in: Proceedings of the 14th Annual Meeting, the American Society for Precision Engineering, Monterey, CA, USA, Oct 31-Nov 5, pp.481-484.

Spur, G., Holl, S.E., 1997, Material removal mechanisms during ultrasonic assisted grinding, Production Engineering 4 (2) pp.9-14.

Sun, W.P., Z.J. Pei, and G.R. Fisher, 2004, Fine grinding of silicon wafers: a mathematical model for the wafer shape, International Journal of Machine Tools and Manufacture 44 (7-8) 707-716.

Tameyoshi, H., 1999, Double-face machining method and device for wafer, Japanese Patent JP11-090801.

Toshio, I., 1998, Double face grinding device for thin disk-shaped workpiece, Japanese Patent JP10-156681.

Treadwell, C., and Pei, Z.J., 2003, Machining Ceramics with Rotary Ultrasonic Machining, Ceramic Industry (June), pp. 39-42.

Tricard, M., Kassir, S., Herron, P., and Pei, Z.J., 1998, New abrasive trends in manufacturing of silicon wafers, Silicon Machining Symposium, American Society For Precision Engineering, April, St. Louis, MO.

Tso, P.L., and Teng, C.C., 2001, A study of the total thickness variation in the grinding of ultra-precision substrates, Journal of Materials Processing Technology, Vol. 116, pp. 182-188.

Tuersley, I.P., Hoult, A.P., and Pashby, I.R., 1996, Processing of a magnesium-alumina-silicate matrix, SiC fibre glass-ceramic matrix composite using a pulsed Nd-YAG laser Part I optimization of pulse parameters, Journal of Materials Science, Vol. 31, No. 15, pp. 4111-4119.

Tuersley, I.P., Hoult, T.P., and Pashby, I.R., 1998, Processing of SiC/SiC ceramic matrix composites using a pulsed Nd-YAG laser Part II The effect of process variables, Journal of Materials Science, Vol. 33, No. 4, pp. 963-967.

Ueda, M., 1982, Double-head automatic grinding machine, US Patent 4,322,917.

Uhlmann, E., Spur, G., Holl, S.E., 1999, Machining of complex contours by ultrasonic assisted grinding, Technical Paper of Society of Manufacturing Engineers MR99-284 pp.1-13.

Van Zant, P., 2000, Microchip fabrication: a practical guide to semiconductor processing, 4th edition, McGraw-Hill, New York, p. 37.

Vandamme, R., Xin, Y., and Pei, Z.J., Method of processing semi-conductor wafers, US Patent 6,114,245, 2001.

Walter, D., 1997, Pilkey Peterson's stress concentration factors, Second edition, John Wiley & Sons, Inc., New York, NY.

Wang, C., 1990, Vertical/horizontal double-way grinding type abrasive belt grinder, US Patent 4,939,870.

Watanabe, T., 2003, Epitaxial semiconductor wafer manufacturing method, US Patent 6,599,760, 2003.

Whitney, J.M. and Nuismer, R.J., 1974, Stress fracture criteria for laminated composites containing stress concentration, Journal of Composite Materials 8 (3) pp. 253-265.

Wolf, S., and Tauber, R.N., Silicon Processing for the VLSI Era Vo1ume 1: Process Technology, Lattice Press, Sunset Beach, California, 2000.

Xin, X.J., Liu, W.J., and Pei, Z.J., 2002, Modeling of waviness reduction in silicon wafer grinding by finite element method, in: Proceedings of the International Conference on Modeling and Analysis of Semiconductor Manufacturing, Tempe, AZ, USA, April 10-12, 2002, pp. 24-29.

Ya, G., Qin, H.W., Yang, S.C., Xu, Y.W., 2002, Analysis of the rotary ultrasonic machining mechanism, Journal of Materials Processing Technology, Vol. 129, pp. 182-185.

Yasunaga, N., Takashina, M., and Itoh, T., 1997, Development of sequential grinding-polishing process applicable to large-size Si wafer finishing, in: Proceedings of the 1st International Symposium on Advances in Abrasive technology (ISAAT'1997), Sydney, Australia, July 8-10, pp. 96-100.

Yoshifumi, O., Tetsuo, M., Minoru, S., 1995, Chipping in high precision slot grinding of Mn-Zn ferrite, Annals of the CIRP, Vol. 44, No. 1, pp.273-277.

Yu, M. Q. et al., 2003, Toughening and strengthening mechanism of zirconia-alumina multiphase ceramics, Key Engineering Materials, Vol. 249, No. Composites III, pp. 167-170.

Yutaka, I., Moritoshi, A., and Hideki, I., 2003, Sheet type double face machining device, Japanese Patent JP2003-103441.

Zeng, W.M., Li, Z.C., Pei, Z.J., and Treadwell, C., Experimental investigation into rotary ultrasonic machining of alumina, 2004, CD-ROM Proceedings of the International Mechanical Engineering Congress and Exposition 2004 (IMECE 2004) Anaheim, CA.

Zerbola, G., 1975, Method and device for grinding the end faces of cylindrical bodies, particularly of rollers for rolling bearings, US Patent 3,859,756.

Zhang, Q.H., Wu, C.L., Sun, J.L., and Jia, Z.X., 1995, The mechanism of material removal in ultrasonic drilling of engineering ceramics, Proceedings of the Institution of Mechanical Engineers, Part B, Journal of Engineering manufacture, Vol. 214, Issue. 9, pp. 805-810.

Zhang, Q.H., Zhang, J.H., Jia, Z.X., and Ai, X., 1998, Fracture at the exit of the hole during the ultrasonic drilling of engineering ceramics, Journal of Materials Processing Technology, Vol. 84, No. 1-3, pp. 20-24.

Zhang, Q.H., Wu, C.L., Sun, J.L., and Jia, Z.X., 2000, Mechanism of material removal in ultrasonic drilling of engineering ceramics, Proceedings of the Institution of Mechanical Engineers, PartB: Journal of Engineering Manufacture, Vol. 214, No. 9, pp. 805-810.

Zhou, L., Shimizu, J., Shinohara, K., and Eda, H., 2003, Three-dimensional kinematical analyses for surface grinding of large scale substrate, Precision Engineering, Vol. 27, No. 2, pp. 175-184.

# Appendix B - List of Publications during Ph.D. Study

## Journal Papers

1. **Li, Z.C.**, Jiao, Y., Deines, T.W., Pei, Z.J., and Treadwell, C., 2005, Development of an innovative coolant system for rotary ultrasonic machining, International Journal of Manufacturing Technology and Management, Vol. 7, Nos. 2-4, pp. 318-328.
2. **Li, Z.C**., Jiao, Y., Deines, T.W., Pei, Z.J., and Treadwell, C., 2005, Rotary ultrasonic machining of ceramic matrix composites: feasibility study and designed experiments, International Journal of Machine Tools and Manufacture, Vol. 45, Nos. 12-13, pp. 1402-1411.
3. Zeng, W.M., **Li, Z.C.**, Pei, Z.J., and Treadwell, C., 2005, Experimental observation of tool wear in rotary ultrasonic machining of advanced ceramics, International Journal of Machine Tools and Manufacture, Vol. 45, Nos. 12-13, pp. 1468-1473.
4. **Li, Z.C.**, Pei, Z.J., Zeng, W.M., Kwon, P., and Treadwell, C., 2005, Preliminary experimental study of rotary ultrasonic machining on zirconia toughened alumina, Transactions of the North American Manufacturing Research Institution of SME, Vol. 33, pp. 89–96.
5. **Li, Z.C.**, Cai, Liang-wu, Pei, Z.J., and Treadwell, C., 2006, Edge-chipping reduction in rotary ultrasonic machining of ceramics: finite element analysis and experimental verification, International Journal of Machine Tools and Manufacture, Vol. 46, Nos. 12-13, pp. 1469-1477.
6. **Li, Z.C.**, Pei, Z.J., and Fisher, G.R., 2006, Simultaneous double side grinding of silicon wafers: a literature review, International Journal of Machine Tools and Manufacture, Vol. 46, Nos. 12-13, pp. 1449-1458.
7. **Li, Z.C.**, Pei, Z.J., and Fisher, G.R., Simultaneous double side grinding of silicon wafers: a mathematical study on grinding marks, submitted to ASME Journal of Manufacturing Science and Engineering.

8. **Li, Z.C.,** Pei, Z.J., and Fisher, G.R., Simultaneous double side grinding of silicon wafers: a mathematical model of the wafer shape, submitted to International Journal of Machine Tools and Manufacture.

## Conference Papers

1. **Li, Z.C.**, Treadwell, C., and Pei, Z.J.**,** 2004, Drilling small holes in hard–to–machine materials by rotary ultrasonic machining, CD–ROM Proceedings of WESTEC Conference–New Frontiers in Manufacturing Technology, Los Angeles, CA, March 22–25, also SME Technical Paper TP04PUB137, Society of Manufacturing Engineers, Dearborn, MI.
2. Zeng, W.M., **Li, Z.C.**, Pei, Z.J.**,** and Treadwell, C., 2004, Rotary ultrasonic machining of advanced ceramics: effects of coolant, Proceedings of the 6th International Conference on Frontiers of Design and Manufacturing, Xi'an, China, June 21–23.
3. **Li, Z.C.**, Jiao, Y., Deines, T.W., Pei, Z.J., and Treadwell, C., 2004, Rotary ultrasonic machining (RUM) on ceramic matrix composites (CMC): Designed experiments, Proceedings of the Fifth International Conference on High Temperature Ceramic Matrix Composites (HTCMC–5), Seattle, WA, September 12–16.
4. **Li, Z.C.**, Jiao, Y., Deines, T.W., Pei, Z.J.**,** and Treadwell, C., 2004, Experimental study on rotary ultrasonic machining (RUM) of poly crystalline diamond compacts (PDC), CD–ROM Proceedings of the 13th Annual Industrial Engineering Research Conference (IERC–2004), Houston, TX, May 15–19.
5. Zeng, W.M., **Li, Z.C.**, Pei, Z.J.**,** and Treadwell, C., 2004, Experimental investigation into rotary ultrasonic machining of alumina, CD–ROM Proceedings of the International Mechanical Engineering Congress and Exposition 2004 (IMECE 2004), Anaheim, CA, November 13–19.
6. **Li, Z.C.**, Cai, Liang-wu., Pei, Z.J.**,** and Treadwell, C., 2004, Finite element simulation of rotary ultrasonic machining for advanced ceramics, CD–ROM Proceedings of the International Mechanical Engineering Congress and Exposition 2004 (IMECE 2004), Anaheim, CA, November 13–19.
7. Zeng, W.M., **Li, Z.C.**, Pei, Z.J.**,** and Treadwell, C., 2004, Tool wear in rotary ultrasonic machining of advanced ceramics, Progress of Machining Technology – Proceedings of the

Seventh International Conference on Progress of Machining Technology, ICPMT'2004, Suzhou, China, December 8–11, pp. 392–397.

8. Churi, N.J., **Li, Z.C.**, Pei, Z.J., and Treadwell, C., 2005, Rotary ultrasonic machining of titanium alloy: a feasibility study, CD–ROM Proceedings of the International Mechanical Engineering Congress and Exposition 2005 (IMECE 2005), Orlando, FL, November 6–11.